Reservoir characterization using laboratory ultrasonic rock physics: understanding pore fluid effects on elastic properties

by

Ganiyat Oluwaseun Shodunke

B.S., Kansas State University, 2018

A THESIS

submitted in partial fulfillment of the requirements for the degree

MASTER OF SCIENCE

Department of Geology
College of Arts and Sciences

KANSAS STATE UNIVERSITY
Manhattan, Kansas

2021

Approved by:

Co-Major Professor
Dr. Matthew Totten

Approved by:

Co-Major Professor
Dr. Abdelmoneam Raef

Copyright

Abstract

The quantity of hydrocarbon recovered from a carbonate reservoir varies depending on the quality (i.e., porosity, permeability, reservoir volume) of that reservoir, indirectly characterized from the elastic properties encoded in the seismic reflection data. Due to the complexity of carbonates, they require repeated updating of characterization and modeling during production. This creates added cost to well drilling but provides significant return in terms of decisive field development plans and knowledge of productive and nonproductive hydrocarbon zones. The purpose of this study is to understand the effects of pore-fluid composition on the elastic properties of the Viola formation reservoir found in Kansas, Oklahoma, and Texas, and implications for utilization of seismic data attributes in optimizing reservoir studies and guiding field development efforts. Rock physics experiments such as lab ultrasonic experiments and fluid replacement experiments integrated with seismic fluid replacement modeling were used to pursue a thorough understanding of the carbonate reservoir properties. Brine, oil, and water were injected into the carbonate rock during the fluid replacement experiment and ultrasonic waves were propagated through the rock to obtain Primary P wave velocity, Secondary S wave velocity, and elastic parameters such as Young's modulus, Shear (Rigidity) modulus, Bulk modulus, and Poisson's ratio. These parameters were also recorded for the rock under dry conditions, and they provided useful information about the seismic wave's response to fluids and lithofacies changes in the Viola carbonate rock. There was a noticeable response change in amplitude and some change in velocity and impedance of the wave traveling through the Viola limestone formation with the presence of and type of fluid present. Higher amplitudes and faster velocities were observed for dry rock wave signals, while lower amplitudes and slower velocities were recorded for brine and oil-saturated rock wave signals. The recorded results on the Viola cores were in accordance with previously observed Gassmann fluid replacement modeling results (Cimino, 2020) from the Viola well log data and seismic amplitude analysis (Vohs, 2016) from the Viola seismic data.

Table of Contents

List of Figures

List of Tables

Acknowledgements

First, I am grateful to my parents for this opportunity and their encouragement throughout the process of my master's degree. I am also thankful for my brother's unofficial advising.

I would like to thank my advisors, Dr. Raef and Dr. Totten for their constant encouragement and guidance throughout this entire process. I would also like to thank my thesis-committee member Dr. Adam for her guidance and input.

I would like to thank the geology department for monetary support in the form of graduate student scholarships and assistantships which reduced the financial burden associated with obtaining my degree. I am thankful for my undergraduate and graduate geology professors in the geology department at Kansas State University (K-State). I am also especially grateful to my professors Dr. Kirk, Dr. Ghanbarian, and Dr. Adam for being one of my first introductions to research and supporting me.

I am grateful for the fellow graduate students who encouraged me and supported me through this process: KayLeigh Rogers, Zach Van Ornam, Luke Rijfkogel, Iffat Azmi, and other graduate students in the department. I am also grateful for Taiwo Bamidele, Tomiwa Shodipe, Olalekan Sipasi, the Nigerian students' group, African Students Union at K-State, and everyone who has been left a positive impact on my time at K-State.

Dedication

I dedicate this thesis to my family.

Chapter 1 - Introduction

1.1 Introduction to the Study

According to the Schlumberger Oilfield Glossary online (2020), reservoir characterization is a model of a reservoir that incorporates all characteristics of a reservoir which are important to its ability to store and produce hydrocarbons. It is also defined as a process that simulates the behavior of fluids within reservoirs under different sets of circumstances to determine optimal ways to maximize production. By having a better understanding of a reservoir, a detailed field development plan can be created which reduces drilling risks and money loss from drilling non-producing wells. Reservoir characterization, although multifaceted in its approach, provides a useful way to better understand reservoirs.

Accurate petrophysical interpretation is one technique in reservoir characterization. It involves analyzing mineral content, porosity, and water saturation determined from log suites to describe the property and quality of a reservoir (Simm and Bacon, 2014, p. 150). Another involves analyzing log data such as sonic logs, density logs, and neutron logs to obtain important information about a reservoir.

Rock physics is one aspect of reservoir characterization which has grown in recent years and has become a key component in most studies focused on reservoir characterization. (Wang, 2001; Sayers & Chopra, 2009). Rock physics addresses the relationship between measurements of elastic parameters made from the surface, well, and lab equipment; and intrinsic properties of rocks such as mineralogy, porosity, and pore shapes; pore fluids; pore pressures; permeability; viscosity; stress; and overall architecture such as laminations and fractures (Sayers & Chopra, 2009). In short, it is a combination of petrophysics and geophysics and it serves as an important tool because it bridges reservoir properties and seismic data (Besheli et al., 1998). Part of rock physics analysis involves carrying out laboratory ultrasonic velocity experiments, fluid replacement experiments, and performing fluid replacement modeling, in order to understand velocity changes in rocks as a result of seismic waves traveling through and interacting with fluid presence in that rock. Rock physics analysis can also be performed by thoroughly analyzing and interpreting seismic data. This is because seismic data provides information about lithology, porosity, pore fluid content, and saturation (Besheli et al., 1998). All of which help in making educated guesses in hydrocarbon exploration.

In the past, core and log measurements have been used to establish a calibrated Rock Physics Model for seismic interpretation (Besheli et al., 1998). For accurate results, the data needs to be good quality data that has been interpreted and processed sufficiently. The rock formation data being analyzed needs to show a good relationship between some seismic attributes and rock properties. Also, there has to be coherency among the data acquired at the core, log, and seismic scales. The relationship between seismic attributes and rock properties can be obtained from both detailed laboratory analysis and detailed analysis of well log data.

The Middle and Upper Ordovician rocks of the Sedgewick basin in south-central Kansas contain hydrocarbon-bearing rocks (Adkison, 1972). These rocks are assigned to three units which are the Simpson Group, the Viola Limestone formation, and Sylvan Shale (Adkison, 1972). The Simpson Group shale and the Sylvan shale both serve as potential source rocks in this area (Henry & Hester, 1995), while the Viola limestone formation serves as the reservoir rock in this assemblage. The Viola has largely been neglected in production due to a focus on the Mississippian-aged rocks above it and a quest for operators to control pressures in the active water-drive reservoirs in the past (Raef, 2019). The accidental discovery of production from the Viola formation at the Box Ranch field in 1988 and an even greater discovery of the Viola pay in

Herd field in central Comanche County, Kansas established this formation as one with great potential (Raef, 2019). This reservoir consists mainly of carbonates, dolomites, and cherty dolomite (Adkison, 1972; Bornemann, 1982; Henry & Hester, 1995). Subsequent studies have shown that the Viola production is controlled by the selective preservation of dolomite porosity beneath an erosional unconformity, and production is associated with topographic highs (Linares, 2016; Hagood, 2019). These producing areas have distinct signatures in seismic data (Vohs, 2016; Raef et al., 2017) and petrographic and geophysical well-log analyses (Raef et al., 2019).

The purpose of this study is to expand on previous research (Raef et al., 2017, Hagood, 2019; Raef et al. 2019; Cimino, 2020) on the Viola limestone formation in Kansas that explores the relationship between elasticity, porosity, and velocity. Using rock physics, this study examines the effects of pore-fluid composition on the elastic properties of the Viola formation reservoir. Velocity and amplitude dependence on frequency is also examined. This study takes Cimino's (2020) research (where he examined the Gassmann fluid replacement model in understanding elastic properties of the Viola formation) further by performing actual fluid replacement experiments on rock from the Viola limestone formation and examines attributes in explaining dry rock and fluid-saturated rock conditions. Porosity and pore type play an important role in seismic velocity response from reservoir or non-reservoir facies, so petrophysical interpretation (pore structure and types) is also considered here using the Viola limestone formation as the basis for this study. Additionally, because integrating lab-tested ultrasonic frequency and geophysical data provides both valuable information and enhances exploration technique (Grochau & Gurevich, 2009), laboratory ultrasonic experiment results are compared with geophysical well logs (sonic logs).

For this study, we focus on data obtained from the Rich C 7 well in the Herd field in Comanche County, Kansas; a county in southern Kansas with a lot of producing oil and gas fields. The producing formations include the Viola, the Morrow, and the Mississippian. According to the Kansas Geological Survey (KGS, 2020), 18,099,451 barrels of oil and 464,241,552 million cubic feet of gas have been produced from Comanche county from 1995 to 2020. The availability of core data, production history, and location in terms of surrounding structural features makes this location suitable for analyzing Viola data.

1.2 Research Significance

This study takes a novel approach to understand the effect of seismic wave propagation on the elastic properties of a carbonate rock at different fluid conditions, through laboratory experiments. This is a novel study because of the limited number of fluid replacement experiments and ultrasonic velocity testing that has been performed on carbonate rocks, especially the Viola formation in Kansas.

Results from this study will help reduce the uncertainty during hydrocarbon exploration and development targeting the Viola limestone formation in Kansas. While there is a scale difference between high-frequency lab experiments on cores and field well logs collected at lower frequency, both types of data collection have been shown to correlate well in terms of describing the Viola formation.

1.3 Prior Research

Most of the focus for prior research studies on the Viola formation has been on the upper zones in the Viola. This is because primary hydrocarbon production was found to occur just at “paleotopographic highs” above the Viola C zone (Richardson, 2013). Furthermore, Vohs (2016) and Raef et al. (2017) observed that the Viola displays distinct seismic signatures associated with producing areas.

To provide a geological and geophysical framework for the study of zones with higher productivity in the Viola, Vohs (2016) examined 3D seismic attributes from this formation, while, Linares (2016) described petrophysical properties of samples from the Viola formation in the Morrison Northeast field in Clark county. Seismic attributes are useful for identifying the presence and absence of hydrocarbons and characterize structures within a rock. Information from Vohs (2016) research guides the attributes examined in this study. The data analyzed by Vohs (2016) comes from a 3D seismic survey in the Morrison Northeast field and the Morrison field of Clark County, KS, which is just west of Comanche county. Vohs (2016) found that the seismic attribute: instantaneous frequency, amplitude anomalies, and velocity anomalies successfully distinguished productive zones in the Viola. Lower amplitude anomalies were associated with producing wells, while higher amplitudes were associated with dry holes. Velocity anomalies were also consistent with the top of the Viola, indicating either the presence of hydrocarbons or more porous rock, or a combination of both. Linares (2016) found that production from the Viola was higher in areas with dolomitization and predominantly intercrystalline and fracture porosity type (Linares, 2016).

A coarse description of the Viola zones has been in use for a long time, but in order to better understand the rock property of the Viola, some researchers like Hagood (2019) performed detailed petrographic and well log analysis of the Viola limestone cores of the Rich C 7 well. Hagood (2019) defined five distinct lithofacies in the Viola: Cherty dolomite, intraclastic breccia, intraclastic rudstone, bioclastic grainstone, and muddy dolomite and provided more detailed information on the cores which were used in this study.

Primary P waves and Secondary S waves, which are components of elastic waves that can be obtained from ultrasonic lab experiments or fluid replacement models like Gassmann, have shown statistical and analytical correlation with sonic and density logs of the same location. This was noticed by Grochau & Gurevich (2009) for studies on turbidite sandstones of Campos Basin at offshore Brazil. Studies by Cimino (2020) and Hagood et al. (2018) confirmed this for density, neutron, and sonic logs of the Viola Rich C 7 well (Figure 1.1). The different zones can easily be distinguished based on P wave and porosity values. Change in lithology and porosity can also be seen across the different zones of the Viola limestone formation.

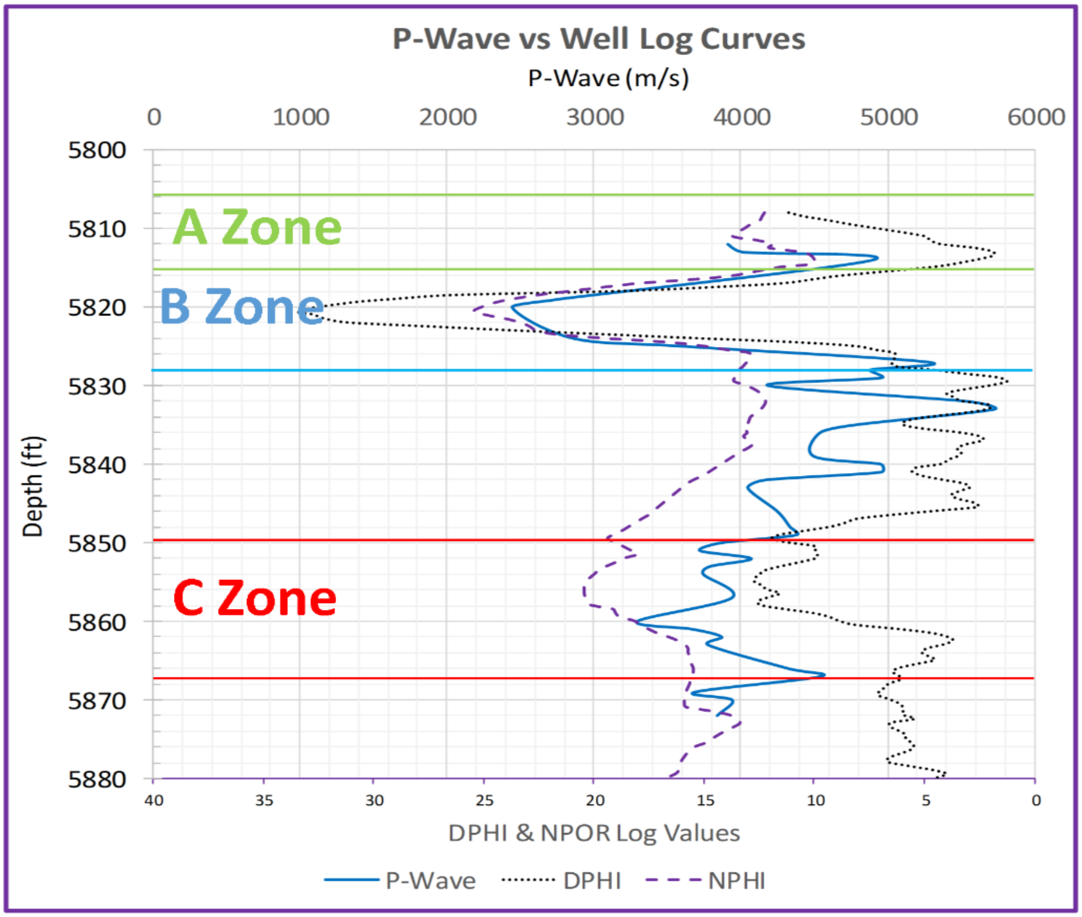

Figure 1.1 P wave velocity changes with depth which was obtained from ultrasonic lab experiments plotted against neutron and density porosity logs. Ultrasonic P wave matches well log curves. Figure from Hagood et al. (2018).

Cimino (2020) carried out experiments on the Viola limestone cores taken from the Rich C 7 well using ultrasonic lab measurements to better understand the relationship between the elastic parameters and the rock properties. The reservoir quality of the Viola limestone formation has been found to be largely based on dolomitization-induced porosity after the development of the Herd field (Raef et al. 2019). This conclusion was achieved by comparing best-fit trends on density-porosity well logs with typical model-trends of limestone and dolomite density-porosity (Raef et al. 2019).

Chapter 2 - Background

2.1 Study Area

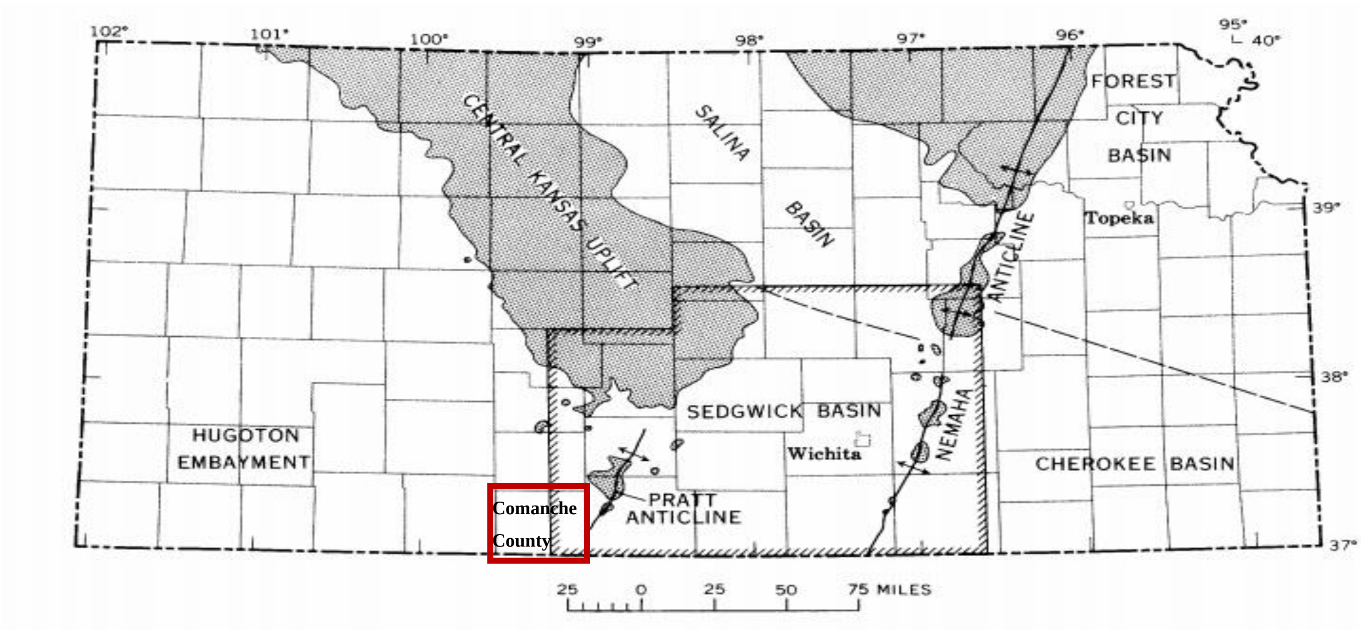

Figure 2.1 Study area showing area of focus which is Comanche county.

The study area for this research is the south-central part of Kansas in Comanche county. Comanche county is in a prime location that straddles the Pratt Anticline, which separates the Hugoton Embayment to the west from the Sedgewick Basin to the east, with the Central Kansas Uplift north of it. This area has extensive oil exploration and a high density of well control (Bornemann et al., 1982).

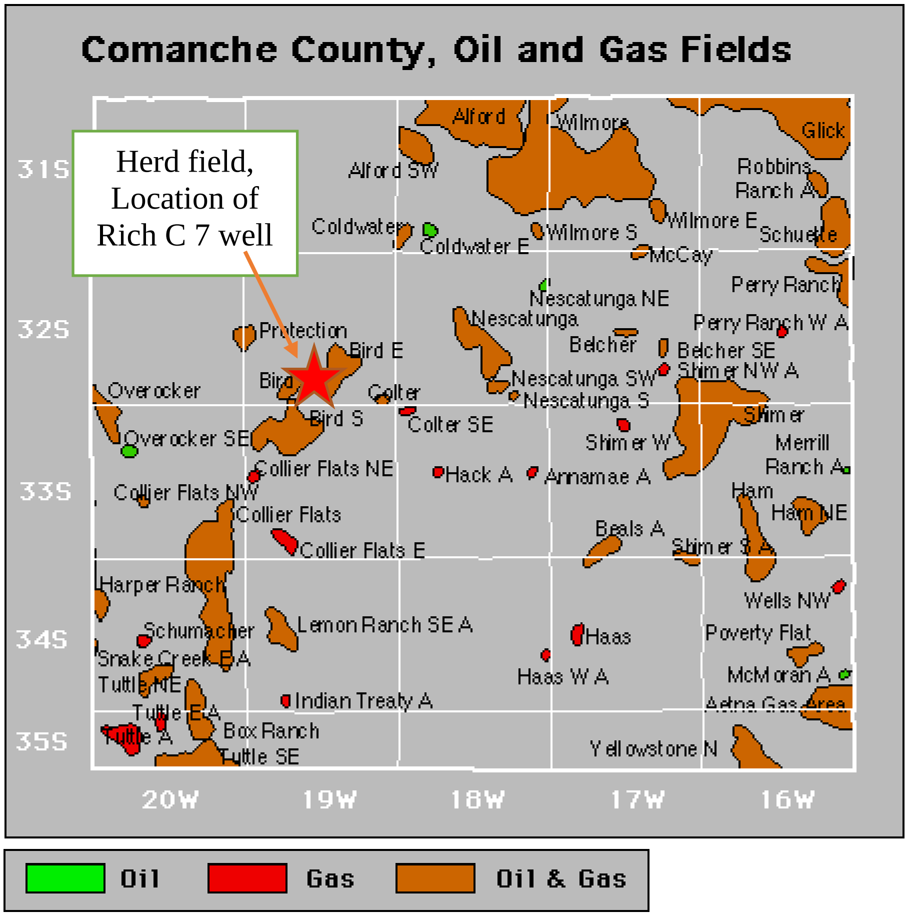

Figure 2.2 Oil fields in Comanche county**.**

The formation of study is the Viola formation. The Viola cores were obtained from the Kansas Geological Survey core library. These cores had been taken from the Rich C 7 well, API no: 15-033-21305 in Herd field in Comanche County, Kansas. The cored interval ranges from a depth of 5808 feet to 5868 feet. The Rich C 7 well was specifically chosen for this study because of the availability of core and its proximity to Clark county where the previous petrographic study by Linares (2016) and the 3D seismic attribute analysis by Vohs (2016) had been conducted. This well has currently produced up to 364,038 barrels of oil from 2002 to present (2019) and 7504mcf of gas from 2007 to 2009, from the Viola formation, according to the Kansas Geological Survey, KGS (2019), making it a good well to use for the study. Comanche county is highlighted in the red box in Figure 2.1 and the oil and gas fields map showing Herd field and the location of Rich C 7 well can be seen in Figure 2.2.

Comanche county has produced 76,196bbls (barrels) of oil and 1,173,028mcf (1000 cubic feet) in 2020 alone. Since production began in 1995, 18,099,451bbls of oil and 464,241,554mcf of gas have been produced from the 179 wells drilled up till June 2020 this year. Since a peak in 2013, production has slowed (Table 2.1). Having a better understanding of the rock property might help to reduce this downturn.

Year	Oil			Gas		
	Production (bbls)	Wells	Cumulative (bbls)	Production (mcf)	Wells	Cumulative (mcf)
2010	286,539	259	14,200,054	5,459,025	419	403,428,286
2011	328,899	267	14,528,953	5,040,263	414	408,468,549
2012	562,137	278	15,091,090	7,812,291	467	416,280,840
2013	800,867	342	15,891,957	12,508,579	497	428,789,419
2014	660,867	341	16,552,824	9,753,243	486	438,542,662
2015	486,320	329	17,039,144	8,040,637	460	446,583,299
2016	330,592	289	17,369,736	5,475,051	422	452,058,350
2017	256,355	268	17,626,091	4,443,874	392	456,502,224
2018	208,214	227	17,834,305	3,585,874	360	460,088,098
2019	188,950	206	18,023,255	2,980,428	328	463,068,526
2020	76,196	179	18,099,451	1,173,028	300	464,241,554

Table 2.1 Production data in Comanche county in the last decade. Modified from http://www.kgs.ku.edu/PRS/County/abc/comanche.html

2.2 Geologic History

The Viola limestone formation, an important petroleum reservoir in the midcontinent, was deposited during the middle to late Ordovician period during the acme of a shallow epicontinental sea that covered North America (Figure 2.3) (Witzke, 1980; Bornemann et al., 1982; Newell, 1996; Barnes, 2004).

Figure 2.3 Illustration of inland sea which covered most of the North American craton during the Middle Ordovician. The entire state of Kansas was inundated as seen here (Blakey, 2016)

This limestone formation is the northern portion of the Anadarko basin, and the Anadarko basin is a prolific reservoir that spans across five states: Kansas, Oklahoma, Texas, Colorado, and New Mexico; the Viola in Kansas also correlates with other stratigraphic equivalents like the Kimmswick limestone of Missouri (Adkison, 1972).

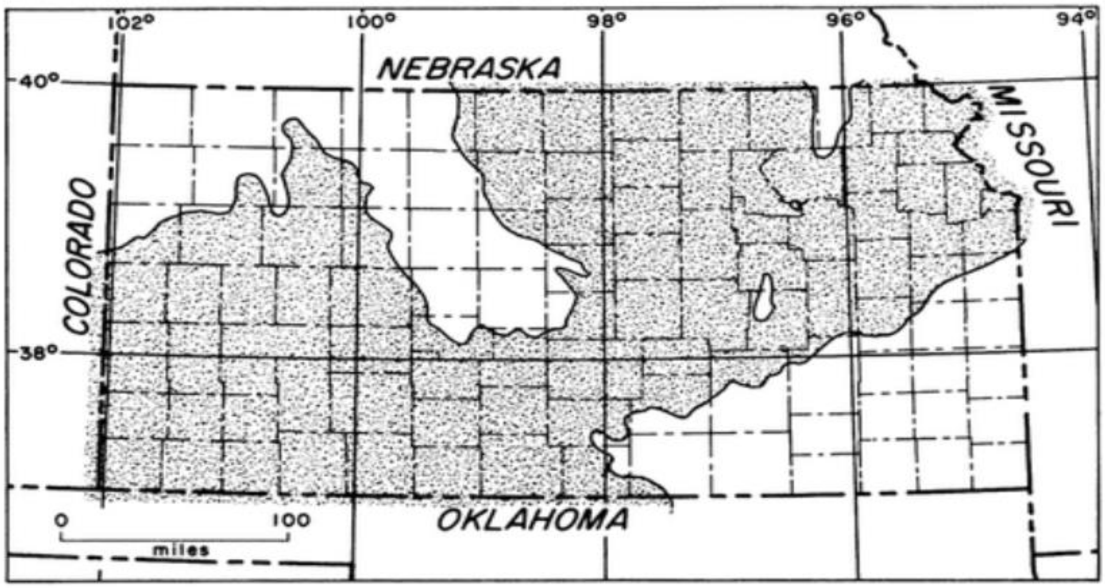

Figure 2.4 Illustration of the lateral extent of the Viola limestone beneath Kansas (Merriam, 1963)

2.3 Stratigraphy

The Viola formation is present only in the subsurface in Kansas (Figure 2.4) but outcrops in the Arbuckle mountains of southern Oklahoma with stratigraphic equivalents also outcropping in neighboring states: the northeastern flank of the Ozark uplift in eastern Missouri, where they are known as Kimmswick limestone, and in palisades in the Upper Mississippi Valley in northeastern Iowa and southeastern Minnesota where they are known as Galena formation (Newell, 1996). This formation consists of limestone, dolomites, and cherty dolomitic limestone which are a product of variation in depositional environments and diagenetic histories (Adkison, 1972; Bornemann et al., 1982).

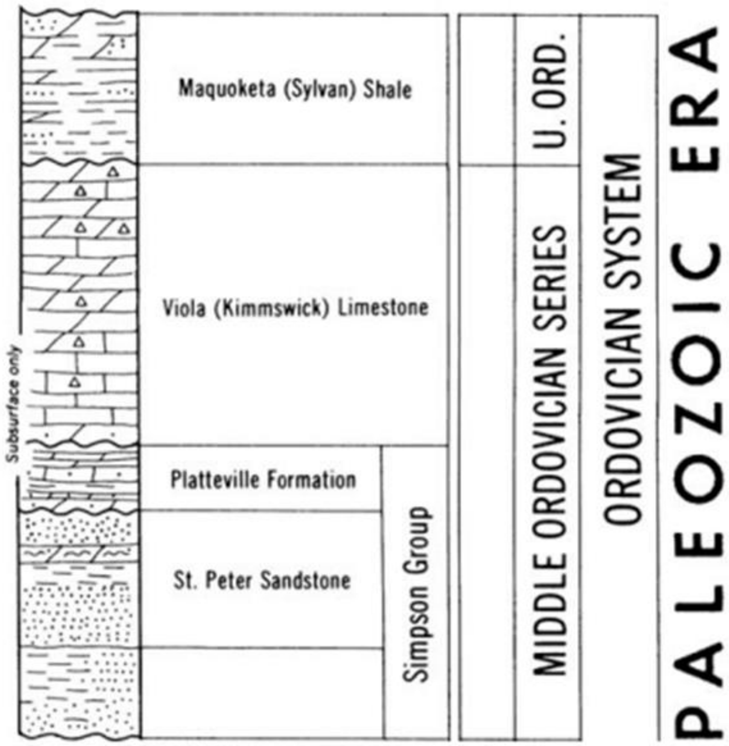

Figure 2.5 Stratigraphy of the Middle and Upper Ordovician Series (modified from Zeller, 1968)

The Viola formation lies above the Arbuckle formation, along with the Simpson group which comprises the St. Peter Sandstone, the Platteville formation, and an unnamed sandstone and shale bed (Figure 2.5) (Jensik, 2007). The Viola occurs throughout the state except in places on the Central Kansas uplift, in northwest Kansas, on the Chautauqua arch, and the northern end of the Nemaha anticline (Figure 2.6) (Zeller et al, 1968).

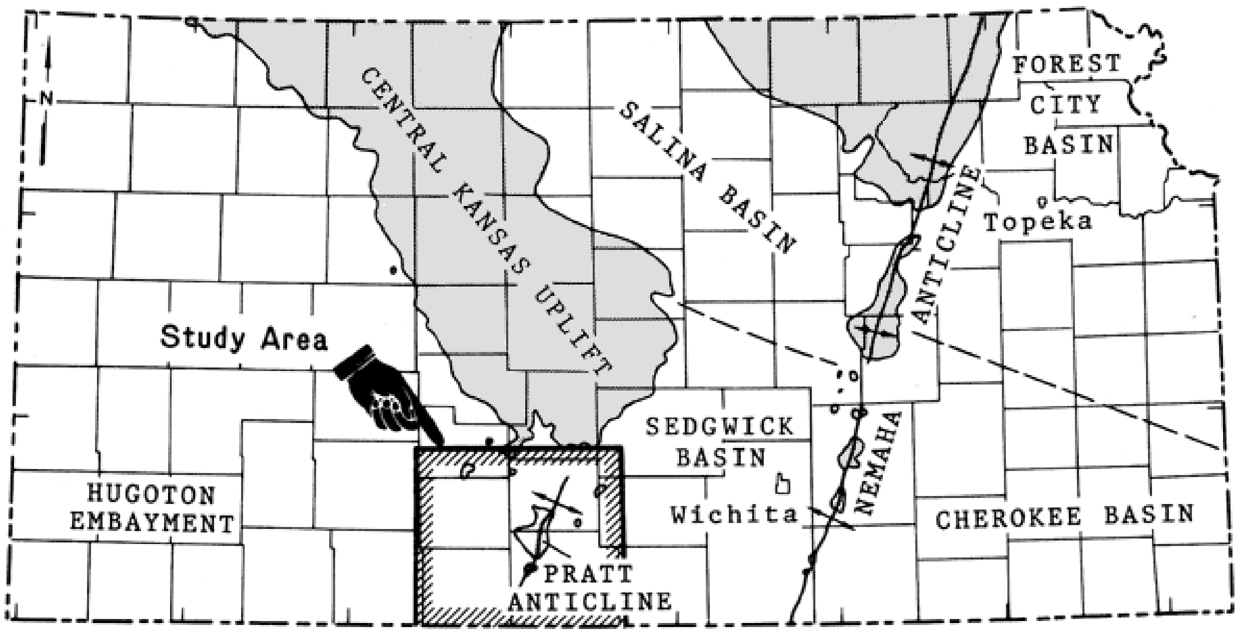

Figure 2.6 Structural features in Kansas Extracted from (Bornemann et al, 1982)

The Viola is characterized by several periods of subaerial erosion and underground drainage which has reduced its thickness and areal extent. This differential erosion of the Viola occurred during the Devonian and Pennsylvanian times (Bornemann et al, 1982). As a result, unconformities can be found in most sub-areal exposures of the Viola at the top and bottom of the beds (Zeller et al. 1968) with progressive thinning of the formation towards the east of Kansas and the removal of upper Viola subdivisions ((Bornemann et al, 1982). The Viola beds are also absent in all the structural highs in Kansas, and this accounts for about 30% of the state (Newell, 2000, Lee, 1943). The Viola limestone has had as much as 239ft of carbonate.

2.4 Hydrocarbon Production

Hydrocarbon production from the Viola is not only associated with structural features as for most hydrocarbon reservoirs, but production is also controlled by the process of dolomitization (Richardson, 2013; Linares, 2016) and the presence of secondary porosity that developed after its deposition (Saberi, 2020). Due to the initial deposition of some of the Viola on higher arches and some of the Viola in deeper valleys, subsequent erosion led to an erosional unconformity between the Maquoketa Shale above and the Viola formation below. This impermeable shale layer created paleotopographic traps where the generated hydrocarbons could be stored within the pores of the dolomite facies (dolomitization induced porosity) of the Viola (Linares, 2016; Hagood, 2019). Therefore, most producing areas in the Viola are associated with areas with topographic highs. As a result of the differential erosion of the Viola, it is difficult to accurately characterize the Viola into zones regionally (Lee, 1956), but four zones are usually identified, with each zone displaying distinct characteristics. The presence of vugs in the upper zone of the Viola makes it suitable for the storage of hydrocarbons and increases its reservoir quality (Bornemann et al., 1982). Typically, production does not occur below Zone C because of the absence of vugs below that zone (Richardson, 2013). Most Viola oil fields are found in eastern Kansas in a generalized alignment due to the presence of the upper sections of the Viola that were not removed by erosion (Bornemann et al, 1982).

2.5 Lithofacies Zones

Four major facies arrangements have been consistently observed within the Viola formation (Figure 2.7) (Adkison, 1972; Cole, 1975; Bornemann et al, 1982). The Kansas Geological Survey describes them as: Zone A – the basal limestone, Zone B – the lower cherty dolomitic limestone, Zone C – upper limestone, the upper part of the Viola limestone, Zone D – the upper cherty dolomitic limestone (Bornemann et al, 1982).

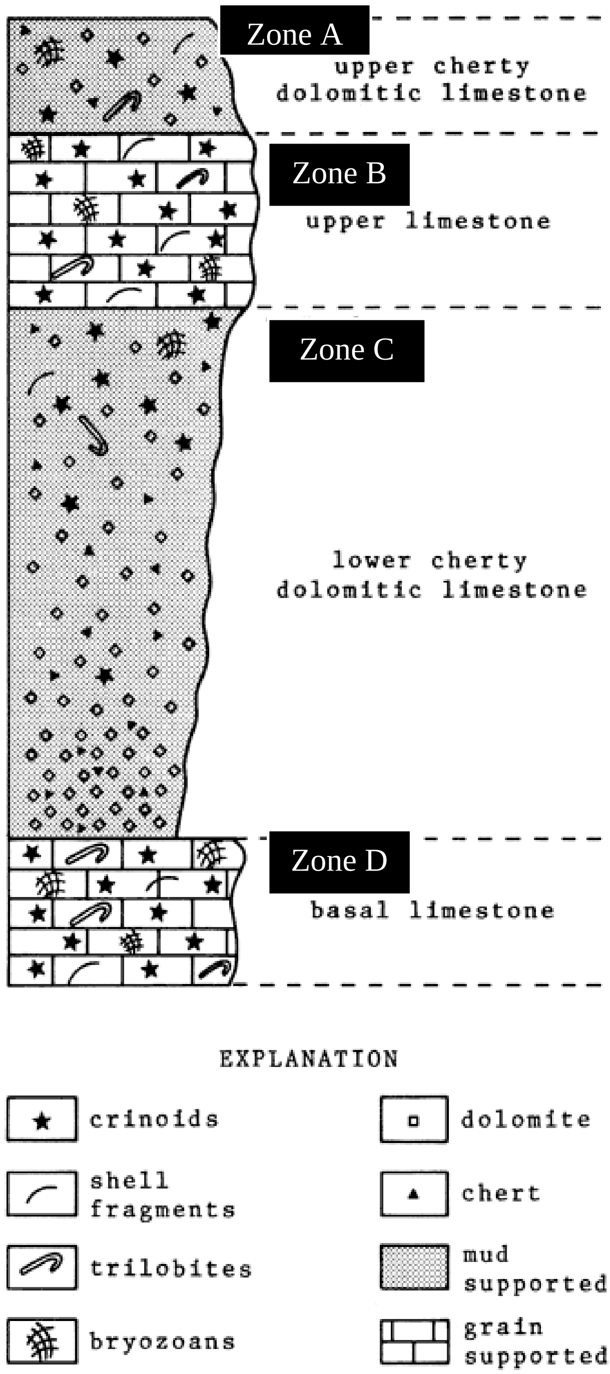

Figure 2.7 Generalized stratigraphic section of the Viola limestone in south-central Kansas. Modified from Bornemann et al., 1982

Looking at each zone in more detail, each zone differs slightly from the other. In Zone D (the basal limestone), it consists of light gray to buff, medium to coarsely crystalline crinoidal limestone that is about 5 feet to 30 feet thick (Adkison, 1972). This limestone is mostly free of chert (Adkison, 1972). Abundant crinoid fragments, absence of chert, and the relatively large grain size make this zone distinct, although its distinctiveness is destroyed by dolomitization in most places (Adkison, 1972). This layer forms an almost continuous sheet across the study area and has a characteristic tight-lime (low porosity) log response, which is useful for locating the boundary between the Viola and the underlying Simpson Group (Bornemann et al., 1982).

Zone C (the lower cherty dolomitic limestone) overlies the basal crinoidal limestone zone in southmost Kansas. It is gray to brownish-gray in color, very fine to fine-grained, and very silty. It has a thickness of between 15 feet and 60 feet (Adkison, 1972). It consists of light gray to buff finely to medium crystalline limestone and dolomite. These beds are partly cherty or silty with crinoid fragments abundant in some locations. Glauconite is present in the upper part of the formation (Adkison, 1972)

Zone B (the upper Limestone) ranges in thickness from 4 feet to 32 feet and consists of crinoid packstones and grainstones. In almost all aspects, the petrographic characteristics of the upper limestone are similar to those of the basal limestone (Bornemann et al., 1982).

Zone A (the upper cherty dolomitic limestone) ranges in thickness from 4 feet to 48 feet and consists of mixed-skeletal wackestones, with some dolomitic intraclast wackestones and dolomitic mudstones over the Pratt Anticline (Bornemann et al., 1982). The dolomite matrix consists of micritic to very fine-grained anhedral crystals and fine-grained clear rhombic crystals Ferroan dolomite occurs only as a very coarse-grained, void-filling, saddle dolomite cement (Bornemann et al., 1982). The most common fossils found in this zone are crinoids, trilobites, and ostracodes, all composed of calcite (Bornemann et al., 1982). The degree of dolomitization in the original matrix increases as the number of fossils decreases, probably due to a sharp increase or decrease in salinity (Bornemann et al., 1982).

2.6 Facies found in Rich C 7 well

Viola cores obtained for this study from the Rich C 7 well include facies from Zones B to parts of Zone D. Each of the different zones have variable percentages as they occur through the Rich C 7 well cored interval. Figure 2.8 shows that a large percentage of the lithofacies in the cores available are muddy dolomite, with only 14% being the cherty dolomite that displays dolomitization induced porosity. The rest of the core consists of lithofacies that display less than 20% porosity. This makes it extremely important to know where the cherty dolomite, which contains most of the potential hydrocarbon fluids, is present. For a more detailed breakdown of the facies present in the cored section, Figure 2.9 displays this better.

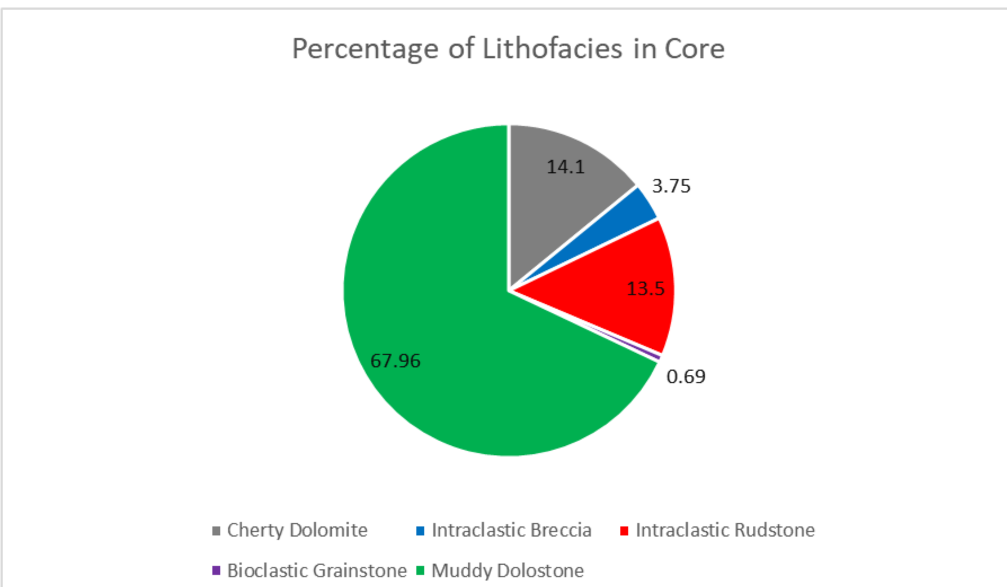

Figure 2.8 Pie chart showing the percentage of different lithofacies inside the Rich C 7 core. Extracted from Hagood (2019).

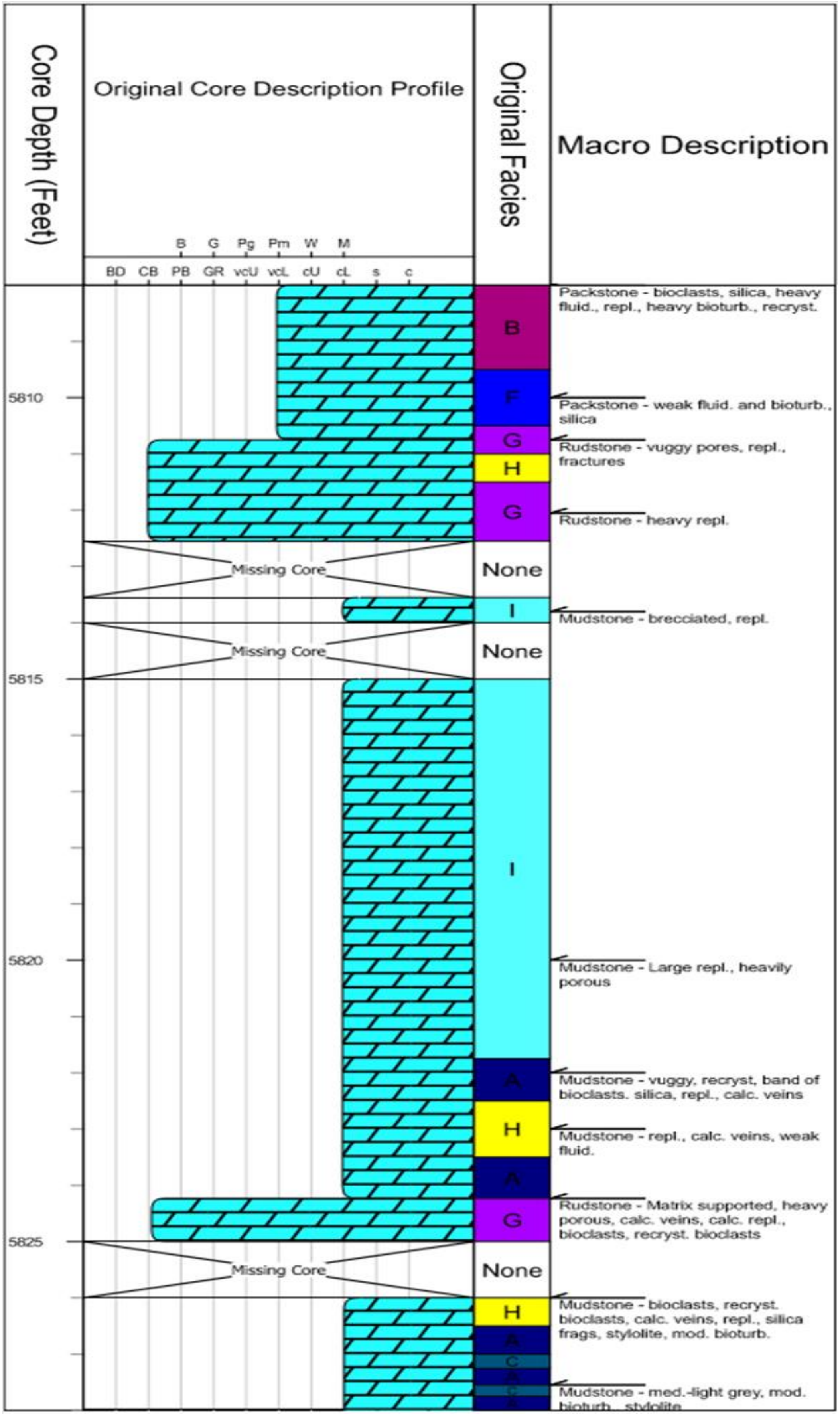

Core Depth (Feet)
Original Core Description Profile
B G Pg Pm W M
BD CB PB GR vcU vcL cU cL s c
Original Facies
Macro Description
5810
5815
5820
5825
Missing Core
Missing Core
Missing Core
B
F
G
H
G
None
I
None
I
A
H
A
G
None
H
A
C
A
C
Packstone - bioclasts, silica, heavy fluid., repl., heavy bioturb., recryst.
Packstone - weak fluid. and bioturb., silica
Rudstone - vuggy pores, repl., fractures
Rudstone - heavy repl.
Mudstone - brecciated, repl.
Mudstone - Large repl., heavily porous
Mudstone - vuggy, recryst, band of bioclasts. silica, repl., calc. veins
Mudstone - repl., calc. veins, weak fluid.
Rudstone - Matrix supported, heavy porous, calc. veins, calc. repl., bioclasts, recryst. bioclasts
Mudstone - bioclasts, recryst. bioclasts, calc. veins, repl., silica frags, stylolite, mod. bioturb.
Mudstone - med.-light grey, mod. bioturb., stylolite

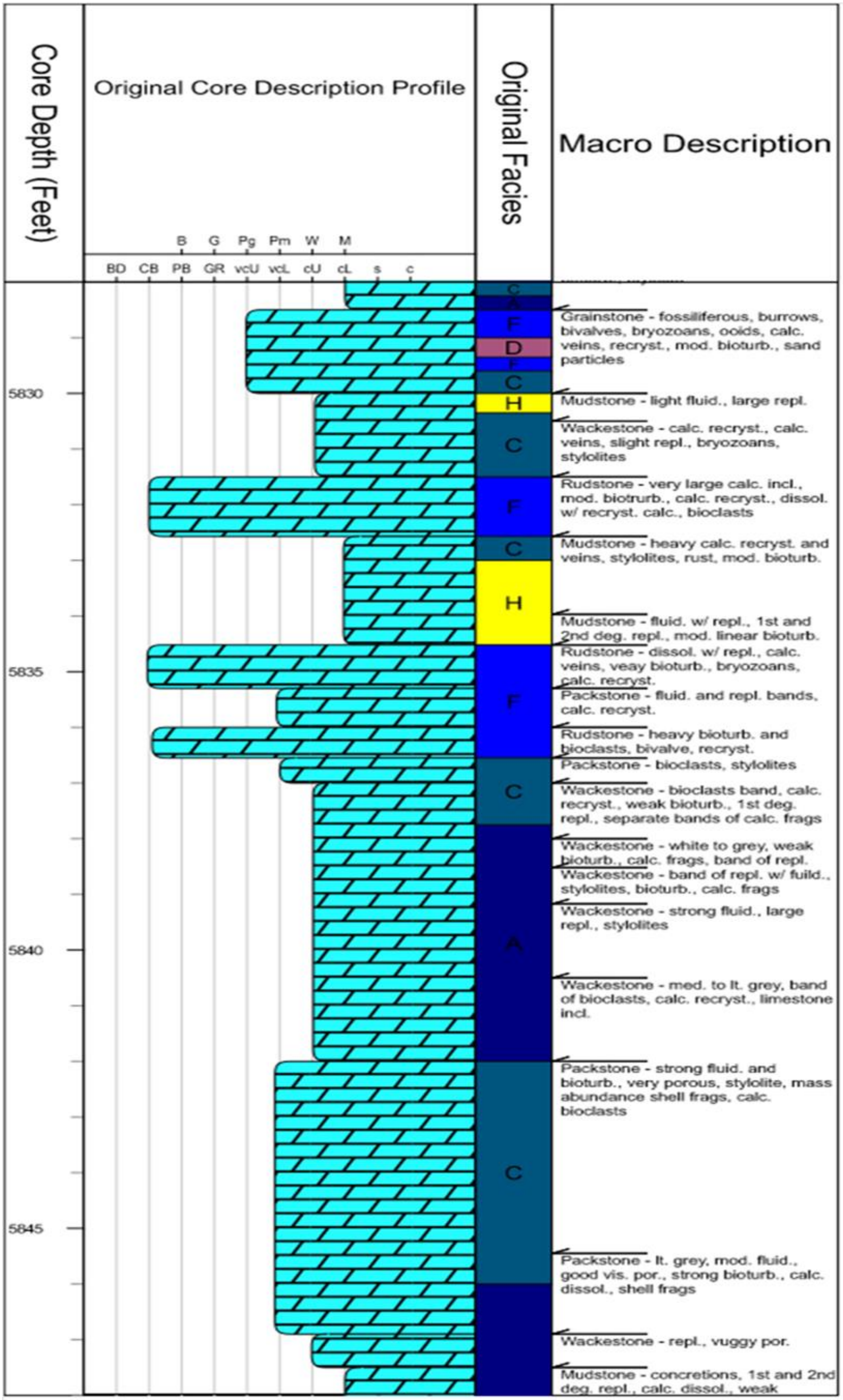

Core Depth (Feet)
Original Core Description Profile
B G Pg Pm W M
BD CB PB GR vcU vcL cU cL s c
Original Facies
Macro Description
5830
5835
5840
5845
C
A
F
D
F
C
H
C
F
C
H
F
C
A
C
Grainstone - fossilliferous, burrows, bivalves, bryozoans, ooids, calc. veins, recryst., mod. bioturb., sand particles
Mudstone - light fluid., large repl.
Wackestone - calc. recryst., calc. veins, slight repl., bryozoans, stylolites
Rudstone - very large calc. incl., mod. biotrurb., calc. recryst., dissol. w/ recryst. calc., bioclasts
Mudstone - heavy calc. recryst. and veins, stylolites, rust, mod. bioturb.
Mudstone - fluid. w/ repl., 1st and 2nd deg. repl., mod. linear bioturb.
Rudstone - dissol. w/ repl., calc. veins, veay bioturb., bryozoans, calc. recryst.
Packstone - fluid. and repl. bands, calc. recryst.
Rudstone - heavy bioturb. and bioclasts, bivalve, recryst.
Packstone - bioclasts, stylolites
Wackestone - bioclasts band, calc. recryst., weak bioturb., 1st deg. repl., separate bands of calc. frags
Wackestone - white to grey, weak bioturb., calc. frags, band of repl.
Wackestone - band of repl. w/ fuild., stylolites, bioturb., calc. frags
Wackestone - strong fluid., large repl., stylolites
Wackestone - med. to lt. grey, band of bioclasts, calc. recryst., limestone incl.
Packstone - strong fluid. and bioturb., very porous, stylolite, mass abundance shell frags, calc. bioclasts
Packstone - lt. grey, mod. fluid., good vis. por., strong bioturb., calc. dissol., shell frags
Wackestone - repl., vuggy por.
Mudstone - concretions, 1st and 2nd deg. repl., calc. dissol., weak

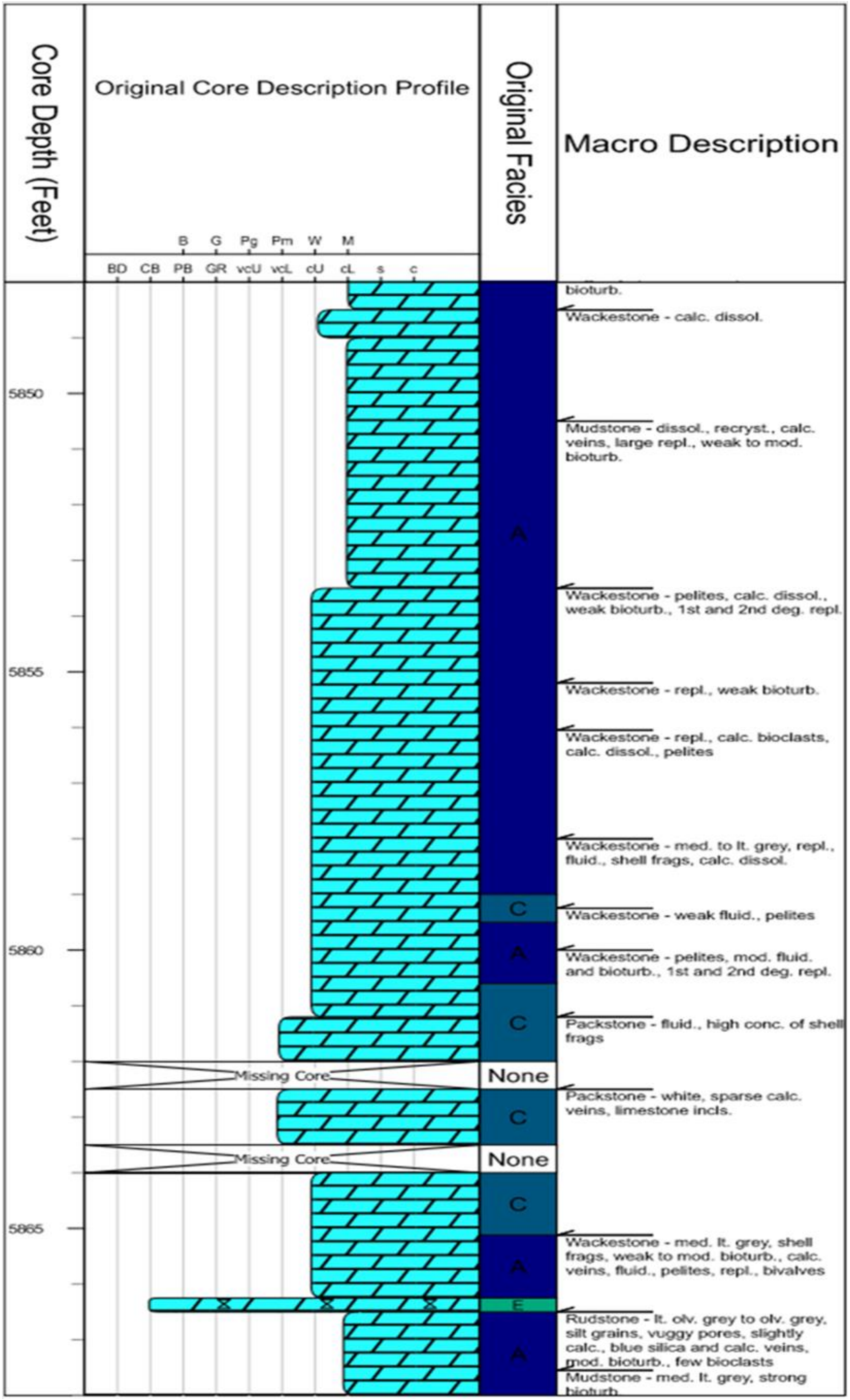

Core Depth (Feet)
Original Core Description Profile
B G Pg Pm W M
BD CB PB GR vcU vcL cU cL s c
Original Facies
Macro Description
5850
5855
5860
5865
A
C
A
C
None
C
None
C
A
E
A
Missing Core
Missing Core
bioturb.
Wackestone - calc. dissol.
Mudstone - dissol., recryst., calc. veins, large repl., weak to mod. bioturb.
Wackestone - pelites, calc. dissol., weak bioturb., 1st and 2nd deg. repl.
Wackestone - repl., weak bioturb.
Wackestone - repl., calc. bioclasts, calc. dissol., pelites
Wackestone - med. to lt. grey, repl., fluid., shell frags, calc. dissol.
Wackestone - weak fluid., pelites
Wackestone - pelites, mod. fluid. and bioturb., 1st and 2nd deg. repl.
Packstone - fluid., high conc. of shell frags
Packstone - white, sparse calc. veins, limestone incls.
Wackestone - med. lt. grey, shell frags, weak to mod. bioturb., calc. veins, fluid., pelites, repl., bivalves
Rudstone - lt. olv. grey to olv. grey, silt grains, vuggy pores, slightly calc., blue silica and calc. veins, mod. bioturb., few bioclasts
Mudstone - med. lt. grey, strong

Figure 2.9 Macro description of core facies labels and descriptions. Categorization is made based on the Dunham and Modified Dunham classification profiles. Meaning of abbreviations: B (boundstone), G (grainstone), Pg/Pm (packstone), W (wackestone), M (mudstone). Figure from Hagood (2019).

Below are the lithofacies observed in the Rich C 7 well.

1. Muddy dolostone: This facies ranges in thickness from a few inches to almost 17 feet (5.18m) in the Rich C 7 well, occupying approximately 68% of the cored interval (Hagood, 2019). It is characterized as being a medium to light gray dolostone with micritic mud that is replaced by fine-crystalline to medium-crystalline dolomite (Hagood, 2019). It has vuggy porosity, with some vugs filled with calcite, coarse dolomite, or silica, and others left unfilled (Hagood, 2019). This facies most commonly occurs between the B and C zones and below Zone C, the non-productive zone (Hagood, 2019).
2. Cherty dolomite (main reservoir facies of Zone B): Hagood (2019) describes this section as having a thickness of about 8ft in the Rich C 7 core, which represents about 14% of the total cored interval. It comprises most of the B zone and isn't found anywhere else along the cored interval. This facies is observed only once in the cored interval (Hagood, 2019). It is characterized by white to light gray chert composed of sponge spicules and exhibits laminations and modern bioturbations. This facies is the most porous compared to the other facies in the Rich C 7 well, with a porosity of about 34%. Some of the vuggy pores which formed from the dissolution of chert are filled in with dolomite (Figure 2.10). Hydrocarbons are contained in the pores between the chert grains and dolomite rhombs. (Hagood, 2019).

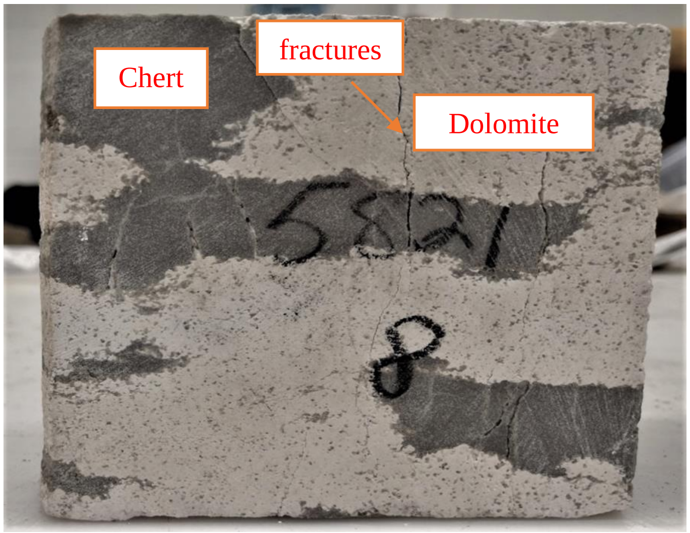

Figure 2.10 Cherty dolomite from 5821feet of Rich C 7 well. You can notice from the rock sample, the very visible pores and some fractures incurred from the rock physics experiments that were carried out later in this project. The chert can be seen being replaced by dolomite.

3. Intraclastic Breccia: This facies is observed in parts of the A and B zones and occupies less than a foot (about 4%) of the cored interval in the Rich C 7 well. It has good intragranular porosity and the fractures and vugs are filled with coarsely crystalline calcite. It consists of white to gray breccia composed of angular intraclasts of dolomite and chert that range from 2 cm to 6 cm in length, with a mud matrix that later became dolomitized (Figure 2.11).

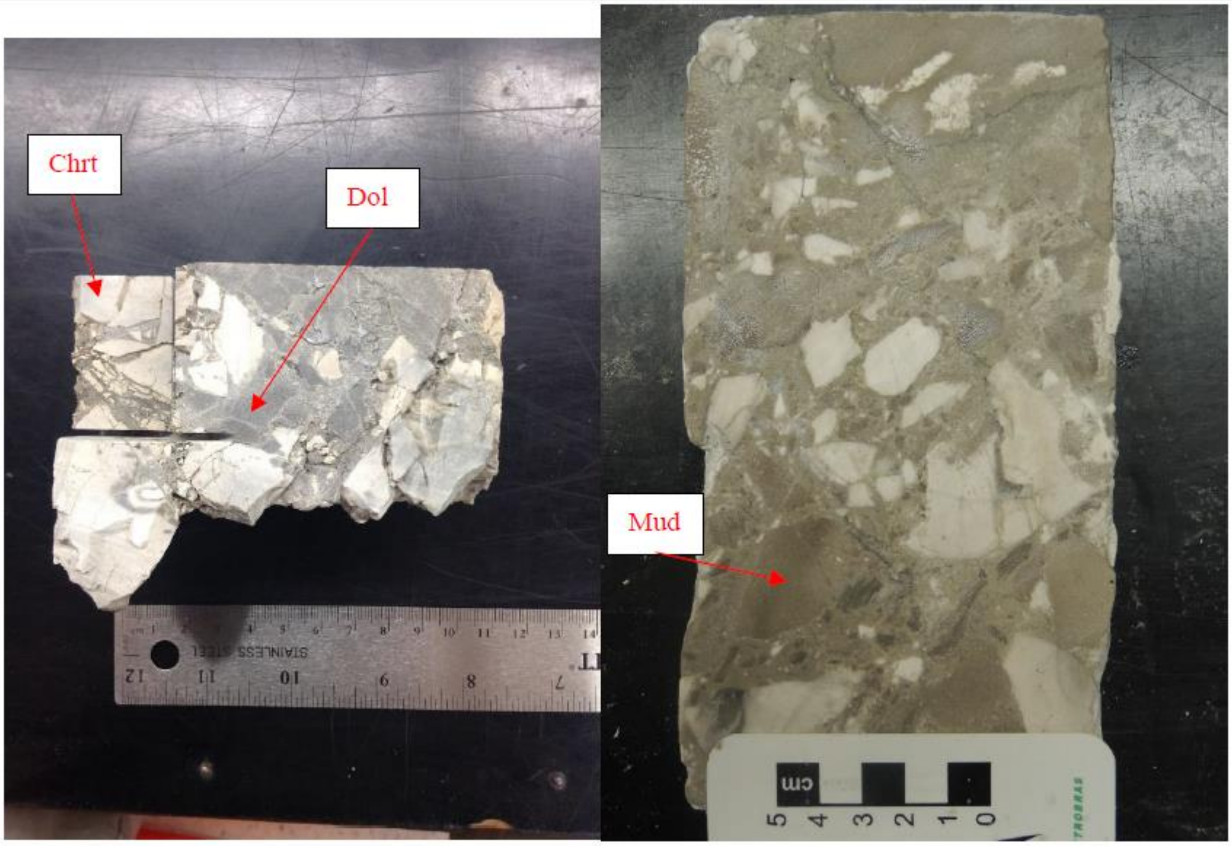

Figure 2.11 Intraclastic breccia from depths 5811.66 feet (left) and 5812 feet (right) of Rich C 7 well. Dolomite, chert, and mud intraclasts can be seen in the cored sections. Abbreviations: Dol (dolomite), Chrt (chert), Mud, (mud). Figure from Hagood, 2019.

4. Intraclastic Rudstone: Observed between the A and B zones with some sporadic occurrence below the B zone. This zone is about 2 feet thick (13% of the cored interval) in the Rich C 7 well. It contains interparticle and vuggy porosity that is locally replaced by silica and dolomite nodules. The rudstone contains calcite veins. It is light to olive-gray in color and consists of dolomite, mud, with some chert intraclasts and bioclasts.
5. Bioclastic Grainstone: This facies is characterized as a white to light gray, horizontally laminated grainstone with some silicified index fossils and dolomite intraclasts. It covers a

very small zone of less than 1% of the cored interval and it is observed in only two intervals throughout the core.

2.7 Carbonate Pore Classification and Velocity Interaction

Pores are the void spaces present in a rock. They can either be filled with air or fluids such as oil, gas, or water. The volume measurement of pores (voids) in a rock to the bulk volume is termed porosity. The total porosity of a rock includes all void spaces regardless of whether the pores are interconnected or isolated. Meanwhile, effective porosity includes pores that are interconnected in the rock and the pores that contribute to the volume of fluid that can be extracted from that rock.

Classification of Pore Types

According to Choquette and Pray (1970), pores found in carbonates are classified into 15 different types and then subclassified based on whether they are fabric selective, non-fabric selective, or fit into neither category. Porosity in most carbonate facies, including most carbonate petroleum reservoir rocks, is largely fabric selective. Attributes used in the classification include size, shape, origin, and position with respect to fabric elements of the rock.

Fabric selective porosity involves the relationship between pore space and other constituents of the rock. In this case, the configuration of the pore boundary and the position of the pore are relative to the fabric elements in the rock and are determined completely by the fabric elements. An example is the selective removal of aragonite ooliths or gastropod shells from a calcite rock. The pore space that is left will take the shape of the removed oolith or shell. The pore types interparticle, intercrystal, moldic, and fenestral pores have both their positions and boundaries determined by the fabric elements and are fabric selective. Some fabric selective elements form during the process of deposition while others form during the process of diagenesis. The intercrystal porosity of dolomites is one of the porosity types that forms after the process of diagenesis but before cementation. This is because their position does not coincide with recognizable primary elements in the sediment (Figure 2.12).

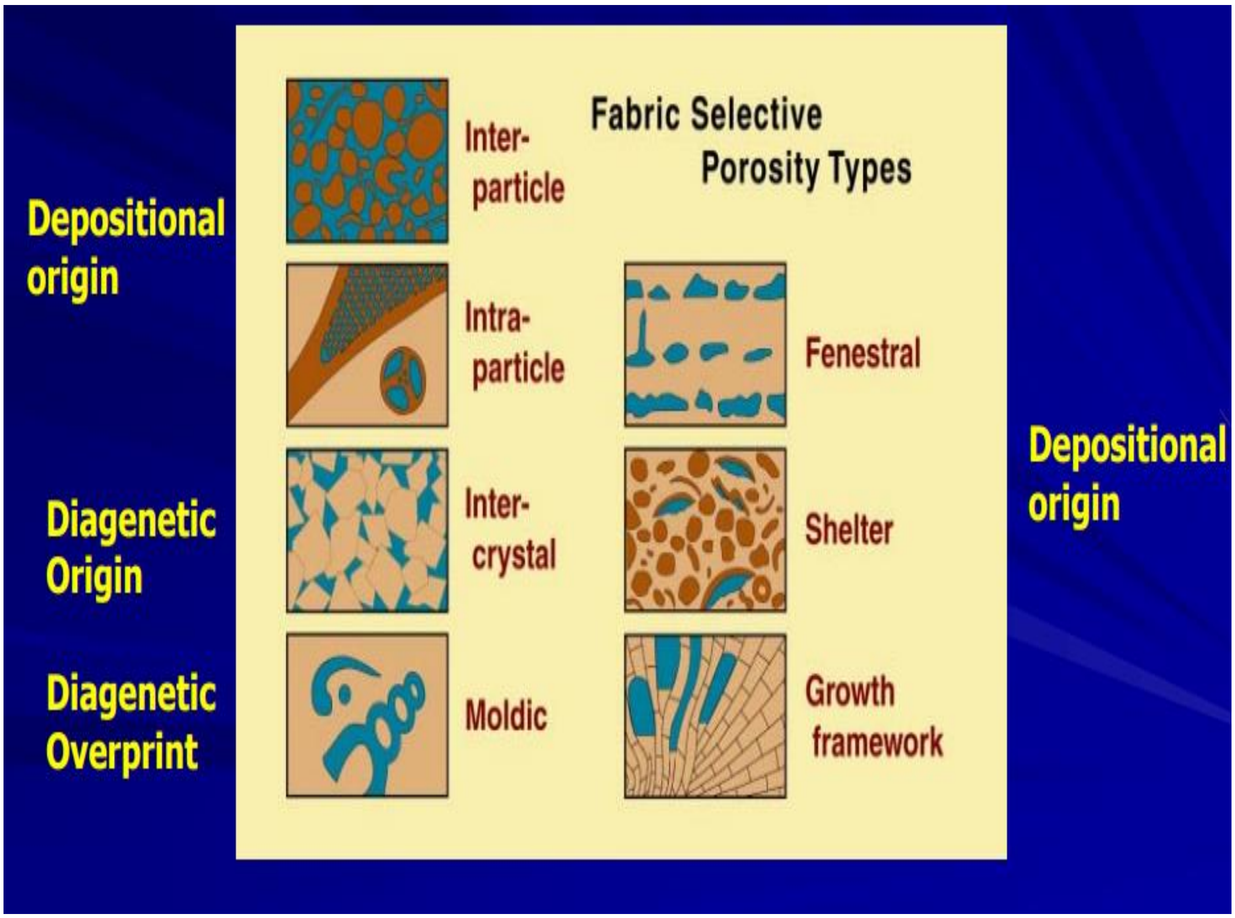

Figure 2.12 These are some of the 15 different classification of pores developed by Choquette and Pray (1970). Image shows fabric-selective pore type. Modified from Ahr, W.M., 2008. http://www.searchanddiscovery.com/documents/2008/08177ahr/ahr-40308.pdf

Non-fabric selective porosity refers to pores that do not show any positional relation to the depositional or diagenetic fabric elements of the rock (Figure 2.13).

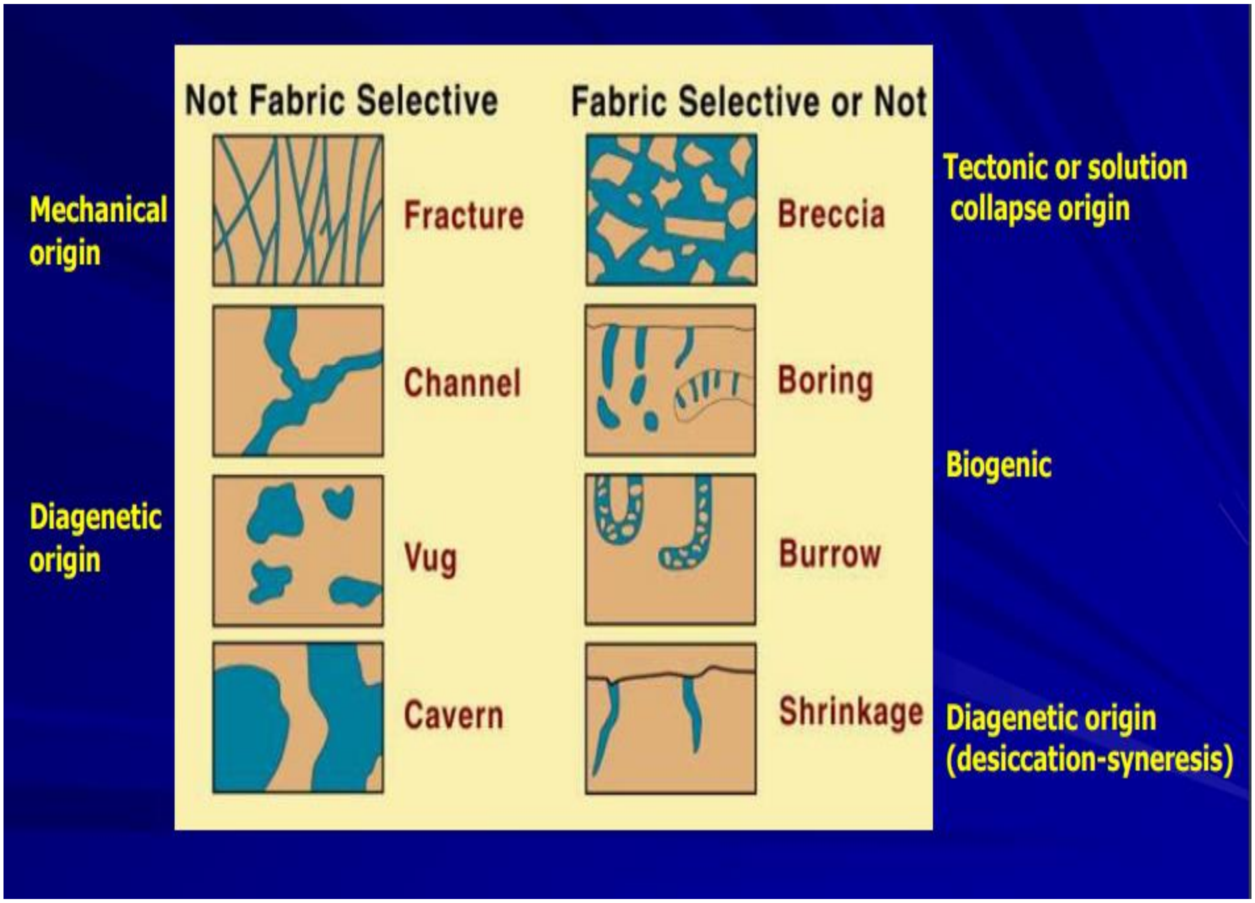

Figure 2.13 These are some of the 15 different classification of pores developed by Choquette and Pray (1970). Image shows not fabric selective pore types and pores that fit into neither category. Modified from Ahr, W. M. ,2008. http://www.searchanddiscovery.com/documents/2008/08177ahr/ahr-40308.pdf.

Seven of these pore types are common and volumetrically important because they form the bulk of pore spaces in carbonate rocks. They are the interparticle, intraparticle, intercrystal, moldic, fenestral, fracture, and vuggy porosity (Choquette and Pray, 1970; Misaghi, 2010). The most common pore type associated with the Viola formation is vuggy porosity. **Vugs** refer to pores that are somewhat equant or markedly elongate, large enough to be visible with the unaided eye (diameter greater than 1/16mm), and do not specifically conform in position, shape or boundaries to particular fabric elements of the host rock (i.e. not fabric selective) (Choquette & Pray, 1970). Vuggy porosity occurs after the dissolution of pre-existing rock (secondary porosity). The presence of vugs strongly influences the velocity-porosity behavior of P and S waves (Besheli, 1998). According to Choquette & Pray (1970), it is more common to see modern carbonates with porosities ranging from 40% to 70%, whereas ancient carbonates have much less porosity up to 5% and 15% found in reservoir facies. Since the Viola limestone formation is an ancient carbonate that formed during the Ordovician, the porosity range observed is between 0% and ~35% (Hagood, 2019).

Correlation between velocity and porosity or density in carbonate rocks is normally highly scattered (Saberi, 2020). This gives an indication of the high degree of petrophysical heterogeneity within the mineral matrix and makes it difficult to model the acoustic behavior in carbonates when compared to siliciclastics (Saberi, 2020).

Pores and Velocity Interaction

Seismic velocity in carbonate rocks is controlled by two main factors: petrology of the sediments and diagenetic processes like cementation and partial dissolution (Misaghi et al, 2010). Carbonate rocks are typically monomineralic, comprised of about 95% calcite, aragonite or dolomite, resulting in similar densities and seismic velocities (Misaghi et al., 2010). As a result, velocity variation is not affected by the mineralogy. The velocity variation in carbonates is a complex function of two main parameters: (i) internal parameters such as porosity, pore type, pore shape, and physical properties due to the fabric of the rock; and (ii) external parameters including induced pressures due to overburden or tectonic stress and physical characteristics of passing waves (Misaghi et al., 2010).

2.8 Well Logs

Well logs are borehole logs used for understanding the lithology and porosity of rock formations. Well logs commonly employed for measuring porosity include neutron logs, density logs, and sonic logs. None of these logs measure porosity directly. Instead, they measure certain properties of the rock that can be interpreted in terms of porosity.

Neutron logs measure the hydrogen content in a formation. The neutrons are released from a chemical source and in collision with nuclei in a rock, they are scattered and lose energy. The energy (loss) can then be recorded to indicate the proportion of water- or hydrocarbon-filled pores in a formation.

Sonic logs are acoustic logs that display P wave travel time versus depth (Schlumberger oilfield glossary online, 2020) and usually have the units of microsecs/ft (Figure 2.14). Sonic logs record sound waves that have propagated through a rock formation, similar to an ultrasonic velocity lab experiment. The major difference between the two is the frequency at which both are collected. Ultrasonic lab experiments data collection occurs at high frequency. Sonic logs record data at lower frequencies than ultrasonic velocity experiments.

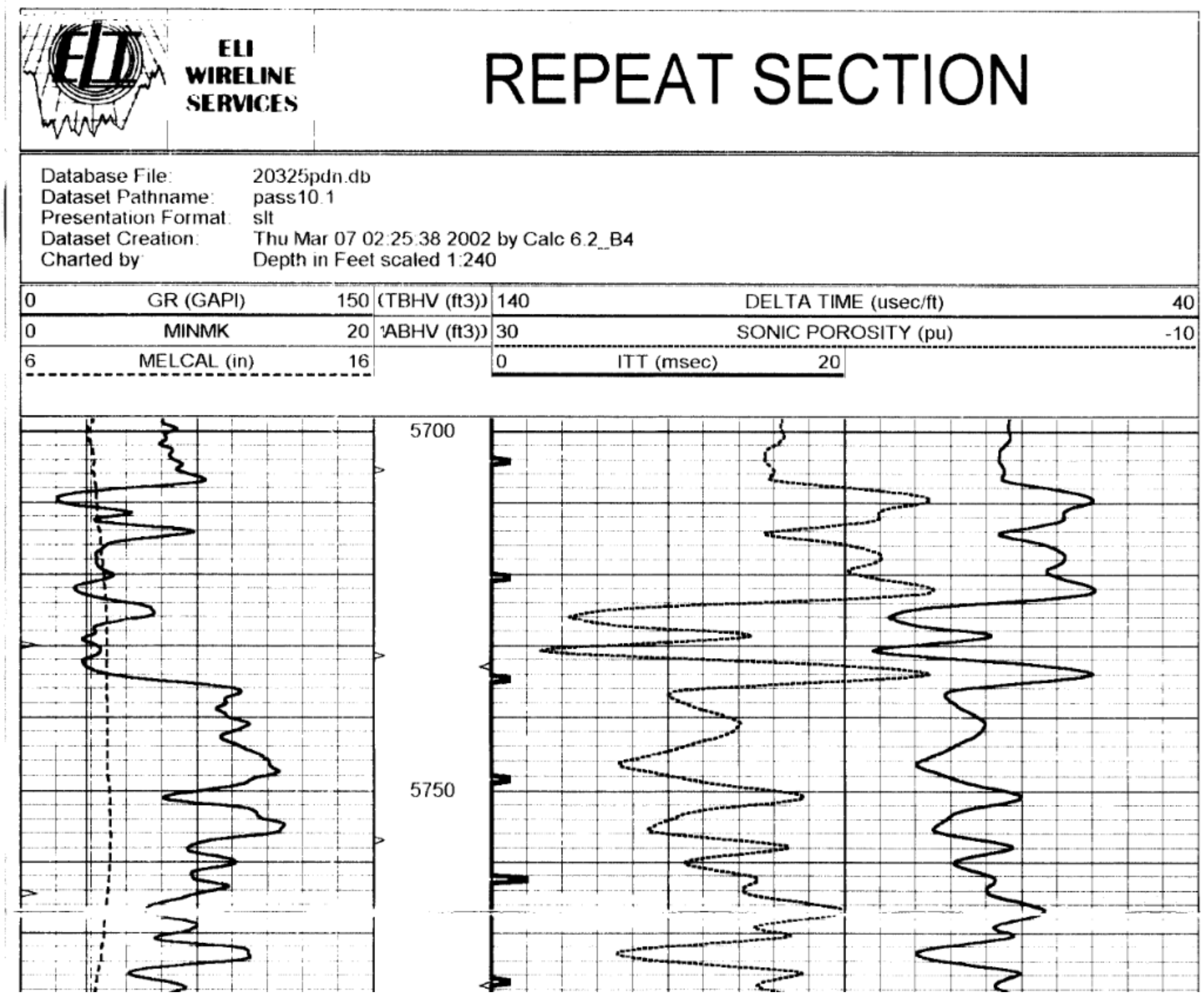

Figure 2.14 Extract of a small section of the sonic log from 5700 feet to ~5780 feet, collected in the Rich C 7 well, Kansas

Comparing both the sonic log and calculated P wave graph shows that there is a relationship between both parameters, one collected from ultrasonic velocity lab measurements on dry rock and the other from sonic borehole logging out in the field (Refer back to Figure 1.1)

2.9 Seismic Data Attributes

A seismic attribute is any characteristic, measurement, or property that can be observed or derived from seismic data (Mukerji et al., 2001). These seismic attributes can be used in understanding and explaining rock properties observed in seismic data (Vernengo et al., 2017).

Some attributes which have been proven to indicate either hydrocarbon presence or porosity in the Viola are amplitude, acoustic impedance, instantaneous frequency, instantaneous phase, normalized amplitude, and thin bed indicator (Vohs, 2016). This study examines amplitude and acoustic impedance change based on ultrasonic velocity lab experiments.

Amplitude

Amplitude analysis is a useful attribute in hydrocarbon reservoir characterization. It measures the height of a peak or trough on a wave. A peak is a positive amplitude while a trough shows a negative amplitude. This is the most common attribute and it is often compared with porosity and liquid saturation (Vohs, 2016).

Instantaneous frequency

Instantaneous frequency is the rate of change of phase over time. It can be useful for indicating low impedance thin beds and relating those thin beds to tuning the thickness of a seismic wave (IHS Global Inc., 2012). Tuning thickness is the vertical resolution of seismic data, and it is the vertical distance of two pieces in a vertical object that can be distinguished by seismic waves.

$$Tuning\ thickness = \frac{1}{4}\lambda$$

Vohs (2016) found that zones with decreasing amplitude had instantaneous frequencies peak. A peak in instantaneous frequency indicates hydrocarbon saturation in the Viola (Raef, 2001).

$$Instantaneous\ frequency = \frac{d(\Phi(t))}{dt}$$

where Φ (t) is instantaneous phase and t is time (or depth).

Acoustic impedance

Acoustic impedance is the product of velocity and density. It is a useful attribute in indicating hydrocarbon presence. The acoustic impedance decreases as the porosity of a rock increases or fluid presence increases.

$$Z=\rho * \upsilon$$

Where Z = acoustic impedance, ρ = density of the rock under a certain condition (e.g. dry, fluid-saturated) and υ = velocity

Chapter 3 - Data and Methods

3.1 Rock Physics Measurements: Laboratory Ultrasonic measurements

Laboratory ultrasonic measurement is a useful tool to measure the elastic property of soil or rock samples, including providing information about various elastic parameters such as Young's modulus, Poisson's ratio, bulk modulus, and shear modulus. Simm and Bacon (2014) describe elastic moduli, bulk modulus, shear modulus, and Poisson's ratio as follows: elastic moduli describes the rock's response to different types of stress (force per unit area), bulk modulus is the rock's response to normal stress applied in all directions on a unit rock, which is an indicator of the extent to which a rock has been squashed, the shear modulus indicates the rigidity of the rock or the resistance of the rock to elastic shaking motion, and finally, Poisson's ratio is described as the ratio of the fractional change in width to the fractional change in length under uniaxial compression.

For this experiment, two main groups of experiments were carried out: one involving the Viola dry rock and another involving the Viola saturated with different fluids (water, oil, and brine). Experimental data were acquired using the GCTS CATS Ultrasonic Velocity Test System ULT 100 for both the dry rock and fluid-saturated rock experiments. To simulate external parameters which cause velocity variation in carbonate rocks, overburden pressures are applied to the cores in increments.

3.2 GCTS Ultrasonic Velocity Test System ULT 100 Test

The Ultrasonic Velocity Test System is provided by GCTS Testing Systems. The GCTS CATS Ultrasonics system consists of a ULT100 controller and a Graphical User Interface (GUI) called the CATS Ultrasonic software. The ULT100 controller acts as a microprocessor running the control program in the background of the operating system and runs the entire analysis and test, emitting the P and S waves, and saving the data files. The CATS Ultrasonics software on the other hand helps the user to interact with the controller and run the experiments. This also acts as the viewing platform to view the P and S wave graphs and a database for storing information for all the sensors, projects, samples, and specimens. The CATS Ultrasonics software can be installed on any Windows computer to be used with the controller.

The entire setup of the Ultrasonic Velocity lab experiment carried out consists of the GCTS CATS Ultrasonics system including both the controller and the CATS Ultrasonic 1.81 software for Windows, the controller comes with a compact box and two platens from which the P and S wave ultrasonic signals are transmitted from, a standard computer that runs Windows Operating System and which has the software already installed, and a hydraulic press by Carver Inc, to apply overburdening pressure. The setup is the same as that used by Cimino (2020), but with a different hydraulic press.

Figure 3.1 GCTS CATS Ultrasonics system including the two platens, the computer on which the software is installed and the hydraulic press with a pressure gauge for monitoring the pressure applied.

3.3 Rock Experiment Procedure

The procedure for carrying out the rock physics experiments involves the following:

1. Select rock cores to be used for testing. The cores are from the Viola Limestone formation from Comanche county in Kansas. For best results, cores selected for testing should include those that reflect reservoir and non-reservoir characteristics and without

cracks. The cracks weaken the sample and make the cores more susceptible to getting broken during the ultrasonic velocity testing.

2. Prepare the cores for testing by obtaining weight, height, and diameter/volume measurements for each core selected.
3. Apply pressures in increments of 2000lbf and simultaneously run signals of P wave and S wave through the core. These wave signals will be recorded, and the first-arrival time picked. By picking the first-arrival times on the ULT 100 system, the P wave and S wave velocities can automatically be calculated along with elastic parameters: Poisson's ratio, Young's modulus, bulk modulus, and shear modulus.

3.4 Core Measurements Procedure

The Viola limestone cores obtained from the Kansas Geological Survey (KGS) rock library was between 5808 feet and 5868 feet, which is 60 ft in total length. Unfortunately, facies A and part of facies B were missing from these depths, so only a small portion of the rocks available displayed reservoir properties. Rocks displaying reservoir characteristics and rocks displaying non-reservoir characteristics/facies were selected at random from between 5808 feet and 5868 feet. The cores are cylinders cut in halves, but not perfect halves. Unlike a similar research by Madonna et al. (2012), where rock cores were dried out before the ultrasonic velocity experiments were carried out, these Viola cores do not need to be dried out because they are not freshly procured cores, so they have had more time to dry out at room temperature. Some experiments prefer to dry out the samples before carrying out the ultrasonic measurements because ultrasonic measurements are prone to the effect of dispersion which can affect the ultrasonic velocities (Grochau & Gurevich, 2009). This is a result of fluid within the pores consuming and dampening the energy of the propagating wave thereby causing a lower than actual velocity to be recorded (Mavko et. al., 1995). This phenomenon is dependent on frequency and seems to decrease under higher compressive strengths or pressures (Mavko et al. 1995). If the samples need to be dried out, this would be done under controlled humidity drying (Smith et al., 2003). Caution would need to be taken not to completely dry out the rock because this could cause the obtained velocity values to be too fast (Smith et al., 2003)

The ULT-100 system requires weight, height, and diameter/volume measurements including the rock type. In this case, it is mostly limestone, so this is selected on the software interface as the rock type. Height is measured using a caliper and a ruler. The density is calculated by the software using the weight and diameter/volume based on the equation:

$$\text{Density } (\rho) = {}^{Mass\ (m)}\!\big/_{Volume\ (V)}$$

The weight is used as a measure of the rock mass using a scale balance (Figure 3.2). Since the cylinder is not perfectly halved, it is difficult to correctly estimate the diameter, in order to obtain a closer estimate of this, the volume estimate is used instead. Volume is measured using the displacement method. The rock sample is placed in a beaker of water and the initial and final volume of the water is recorded. The volume of the rock sample is the amount of water that was displaced by the rock or the difference between the initial and final water volume.

$$Rock\ Volume = Final\ volume\ of\ water\ in\ beaker\ after\ rock\ was\ added$$
$$-\ initial\ volume\ of\ water\ with\ rock\ sample$$

After these obtained values are entered into the GCTS CATS software user interface, the software automatically calculates the density based on the inputted values of weight and volume. These parameters are needed for the software to calculate the required results such as P wave velocity (Vp), S wave velocity (Vs), Poisson's ratio, Young's modulus, bulk modulus, and shear modulus (CATS Ultrasonics Manual, P. 32).

Figure 3.2 Scale balance used for taking weight readings

In order to calculate Vp, Vs, and subsequently, Poisson's ratio, bulk modulus, shear modulus, and Young's modulus, the first-arrival occurrence needs to be determined. The first-arrival time is the time it takes for the propagating wave to travel through the rock. The GCTS CATS software offers five methods in determining the first-arrival time: Absolute Threshold, Relative Threshold, Relative of First Peak, First Peak Time, Tangent of First Peak but none accurately estimate the first-arrival time of the Viola carbonates. Instead, the first-arrival time was manually determined because this has been shown to work better for the Viola data. The software calculates the Velocity based on the formula:

$$Velocity = \frac{specimen\ height}{arrival\ time - platen\ face\ to\ face\ arrival\ time}$$

The first-arrival time needs to be corrected for the time it takes for the wave signal to travel through the platen itself, so the formula takes this into account and removes this time from the first-arrival time calculation. By dividing the distance traveled by the wave by the corrected first-arrival time, the Vp and Vs values were calculated.

The next step involves applying pressures to the cores by placing between a hydraulic press, thereby simulating compressive stresses which the rock experienced in its environment of deposition. First, we calculate what pressure to apply to the rock.

The sensor measures the pressures in lbf, so to obtain pressures in lbf from psi (pounds per square inch) measured by the hydraulic pressure gauge, $psi\ (pounds\ per\ square\ inch) = \frac{force\ (pounds)}{area\ of\ platen\ (\pi r\text{^}2)}$, where r = radius of each sample in inches. The psi can be set equal to the depth at which the rock was taken based on the assumption that each foot of overburdening rock is equivalent to 1 pound per square inch (psi). Therefore, $Depth = \frac{Force\ (Pounds)}{Area\ of\ platen}$ and the pounds-force to apply based on a specific depth is the $depth\ x\ area\ of\ platen.$ For example, a rock taken at 5829 feet depth and area of platen of 2.12 inches (5.38 cm_ diameter would have pounds-force of 20,575.7 lbf from [5829 feet x (π x $(\frac{2.12\ inches}{2})^2$)] applied. Since this laboratory testing involves uniaxial shear testing with stress applied only in one axial direction, confining pressure cannot be completely achieved, and applying pressures this high could cause the rock sample to fail and break after reaching its elastic limit. We wanted to preserve the Viola rock samples as they were borrowed from the Kansas Geological survey core library, so any testing that would intentionally ruin the rock was avoided. As a result, slightly lower pressures were applied, and this was dependent on the lithofacies. Samples with more dolomite present in the rock (cherty dolomite facies) could only take lower pressures of up to ~8000lbfs, while samples with denser structures (muddy dolomite, intraclastic breccia, intraclastic rudstone, bioclastic grainstone) could withstand higher pressures of ~14,000lbfs without cracking. For the sample from 5829 feet depth, although the calculated lbf is 20,575.7 lbf, the maximum pressure applied to this rock was 14,000lbfs.

The Carver hydraulic press used can apply pressures up to 50,000lbf / 10,000psi, although the maximum that was applied to any of the cores did not exceed 14,000lbf. The aluminum test core provided by GCTS is used to test the strength of the ultrasonic waves signal before using the actual core. The core is placed on the hydraulic press with the two 2.12 inches cylindrical platens, which act as the ultrasonic wave transmitters, on either side of the core (Figure 3.3). A thin film of honey is spread between the face of contact of the platen and the core, to ensure good coupling and ensure that the waves being shot out from one side of the platen (the source) gets received by the receiver.

Once the rock along with the platens (which serve as piezoelectric transducers) are placed on the hydraulic press, the P and S wave signal buttons are clicked, which sends out a sinusoidal pulse of P and S wave signal through one end of the platen and then received on the other end of the platen (Figure 3.4). A central frequency of 1.25MHz was propagated through the sample. After the P and S wave signals are recorded, the pressure applied is cranked up by increasing the pressure on the hydraulic press in increments of 2000 pounds-force (2000lbf) starting with 0 and ending approximately at 8000lbf and sometimes up to 14000lbf in instances where the rock was non-reservoir rock with high density and very low porosity. The attached pressure gauge on the hydraulic press measures the pressure changes (Figure 3.5). For each step of incremental pressure, velocities were determined for the samples.

The rocks were tested both when dry and when saturated with fluids. For the dry rock experiment, the above protocol was followed with the core sample used in its natural state without adding additional water.

Figure 3.3 Ultrasonic wave transmitter cylindrical platen pair (left). Aluminum core used in initial test to ensure good signal and good signal to noise ratio placed between the ultrasonic wave transmitters (right).

Figure 3.4 Setup of core in hydraulic press. The core is placed between platens and then between the "jaws" of the hydraulic press. The setup is ready for compressive pressures to be able for the rock sample being tested.

Figure 3.5 Close-up of the pressure gauge attached to the hydraulic press showing psi from 0 psi to 10,000 psi, pounds force from 0 lbf to 50,000 lbf and metric tons from 0 metric tons to 22 metric tons.

Dry Rock Experiment

For the dry rock experiment, samples from depths 5809ft, 5815ft, 5820ft, 5825ft, 5838ft, 5839ft, 5846ft, 5848ft, 5862ft, 5865ft, 5866ft were used. Then the rock experiment procedure and the core measurement procedure were followed.

In the GCTS software, the items in the red boxes (Figure 3.6) were filled in depending on the rock property and the results from the rock experiment procedure. By selecting the “Type” of rock as limestone, the software automatically predicts a first-arrival time based on the information provided and the rock type (the blue bar in Figure 3.6). This prediction is close to the actual first-arrival time (the red bar in Figure 3.6) but the actual first-arrival time needs to be selected to obtain accurate velocity readings.

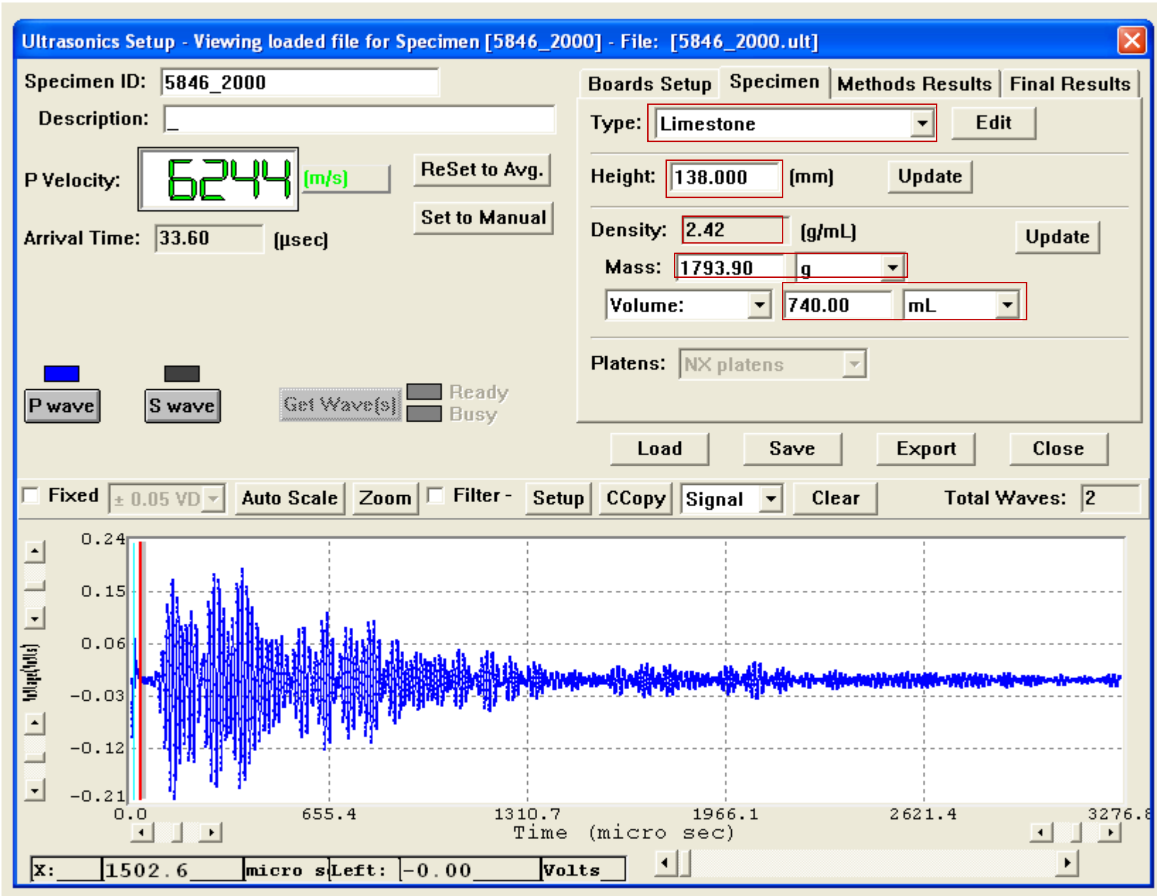

Figure 3.6 GCTS CATS software showing items that need to be filled out before running data collection.

Fluid Saturation Experiment

Physical and chemical fluid-rock interaction are important factors to consider in characterizing a reservoir due to their effect on a rock's microstructure (Mikhaltsevitch et al., 2016). This phenomenon can be observed either by carrying out fluid replacement experiments or by making use of replacement relation models which quantify changes in effective elastic properties of a rock when the pore-filling material is changed. This makes it possible to distinguish for example between an oil-saturated rock and a water-saturated rock.

There are several models in rock physics which estimate how P and S wave velocities change with fluid saturation. The low-frequency Gassmann's theory is a common theory used for fluid substitution models because of its simplicity and the few parameters it requires. Gassmann is also the most theoretically sound approach at seismic frequencies which relates the bulk modulus of a rock to its pore, frame, and fluid properties (Smith et al., 2003)

Some of the basic assumptions that need to be satisfied for the Gassmann model to work (Wang & Nur, 1992; Smith et al., 2003; Simm & Bacon, 2014, p. 159), are the following.

1. Gassmann's model assumes a homogenous and isotropic rock where all pore spaces are completely connected.
2. The model is valid only at low frequencies where pore pressures are equalized over a length scale much greater than a pore dimension and much less than the wavelength of the passing seismic wave.
3. Saturating fluid is frictionless (i.e. low viscosity)
4. No coupling between the solid and fluid phases.

Based on these assumptions, the Gassmann model works best with "clean" sandstones with moderate to high porosity and at seismic/low frequencies. Although, sometimes, by extending the Gassmann model with models such as those proposed by Biot (1962) and Mavko et al., (1998), the effectiveness in its use for carbonate rocks can be increased.

Meanwhile, even with this slight deficiency in the Gassmann model's use for carbonate rocks, it is generally held as an acceptable model for carbonate rocks with relatively homogenous pore systems (Wang & Nur, 1992; Wang et al., 2001; Grochau et al., 2009). The Gassmann model relates the saturated bulk modulus of the rock to its porosity, the bulk modulus of the porous rock frame, the bulk modulus of the mineral matrix, and the bulk modulus of the pore-filling fluids (Smith et al., 2003):

$$K_{sat} = K* + \frac{\left(1 - \frac{K*}{Ko}\right)^2}{\frac{ø}{K_{fl}} + \frac{(1-ø)}{Ko} - \frac{K*}{K_O^2}}$$

Ksat = saturated bulk modulus of rock

Ko = bulk modulus of the mineral matrix

K_{fl} = bulk modulus of the pore fluid used

K^* = bulk modulus of the porous rock frame (dry rock)

Ultrasonic P and S wave velocities have been noticed to change with fluid saturation (Misaghi et al, 2010). Therefore, for the same sample at dry conditions and at fluid-saturated conditions, we expected to notice a difference in the results. These new P and S wave velocities can either be obtained from lab ultrasonic experiments or by using one of the many fluid replacement models to obtain the new values. Elastic moduli like the bulk moduli is expected to change between the different fluid types, but the shear moduli should remain constant because the elastic modulus is independent of the type of fluid present. Models like Gassmann fluid substitution model are used to calculate the new values for the elastic moduli and the new values for the compressional wave and shear wave velocities after the substitution of fluid into a dry rock.

3.5 Fluid Replacement Procedure

To test for how the presence of fluids would affect the velocity variation in the rock, a sample of rock was injected with multiple fluid types until saturated. For the fluid-saturated aspect, the steps used in the dry rock experiment were used, in terms of taking the measurements, but some additional steps needed to be included before the rock was placed between the platens on the hydraulic press and compressive stress applied.

To test for change in P and S wave velocity depending on the fluid present in the rock, the Viola cores were injected with different types of fluids commonly found in the Viola. Water, brine, and oil were the different fluid types tested. Mineral oil which has a similar density to the crude oil from the Viola, was used in the place of crude oil. Mineral oil also does not stain the sample as much as crude oil would, making the sample available for possible further testing. Volume readings for the samples were taken using the fluid displacement technique and these volume readings were taken for the samples submerged in the different fluids. There was no significant difference in the volume displaced in the different fluids tested.

Most of the residual fluids from the volume measurement were ejected using the vacuum pump and left to dry out under room temperature. The samples were then injected with the different fluids and using the vacuum pump, air was removed to allow for the fluid to penetrate the sample. Most of the residual fluids from the volume measurement were ejected using the vacuum pump and left to dry out under room temperature. The samples were then injected with the different fluids and using the vacuum pump, air was removed to allow for the fluid to penetrate the sample (Figure 3.7). The vacuum pump is run until a vacuum is created within the glass container from all the air removed. The removal of air from the vacuum and the rock itself causes water to fill in the void spaces until saturation. The pump can be turned off when the water in the vacuum is still and no air bubbles can be seen escaping. The weight was immediately taken and then the ultrasonic velocity test was carried out on the hydraulic press to measure P and S waves. A few of the samples were jacketed with a thin plastic wrap similar to

Toksoz (1979), but there wasn't much of a difference. See **Appendix B** for a more detailed explanation of the preparation of the fluids and the injection process of the core.

Unfortunately, this test could only be performed on one good reservoir rock core sample because other reservoir rock cores which were about five, either got destroyed before the fluid replacement experiment could be carried out or while the fluid replacement experiment was ongoing. In order to ensure the one remaining sample left available did not get destroyed like the others, very little pressure was applied to the rock.

Figure 3.7 Setup of fluid injection process with a vacuum pump and desiccator container. The vacuum pump (left) is run until no bubbles can be seen escaping from the desiccator (right).

3.6 Rock Measurements at different Sampling Frequency

The ULT system has the option to collect the ultrasonic velocity at different sampling frequencies. The default sampling frequency for the experiment was set at 1.25MHz. We decided to test how much the different sampling frequencies would contribute to a change in the calculated velocities. This was carried out for both the dry rock and fluid-saturated rock scenarios. It was the main goal to use rocks with higher porosity values for this experiment, but due to the limited number of porous samples that were structurally fit for the remainder of the experiment, only sample 5820 which is a cherty dolomite was used to represent the porous samples. The remainder of the reservoir sample unfortunately got damaged during the experiment because of how fragile they were, or they previously had cracks on them which made them get easily destroyed. Therefore, the results for the fluid-saturated experiments at different frequencies did not exceed pressures of between 4000lbf and 5000lbf because lower pressures were used in order to conserve the Viola samples available. The sampling frequencies used include: 156.3kHz, 312.5kHz, 1.25MHz, 2.5MHz, 5.0MHz, 20MHz.

3.7 First-Arrival Time

Once each data is collected, it is saved as a ULT file which makes it easier to edit the data later. The data was also exported out as a text file to make picking of first-arrival time easier. Accurately picking the first-arrival time is important because it affects what the P and S wave velocity values you obtain will turn out to be. Previous research by Isham (2012), Lueck (2017), and Cimino (2020) employed the method of superimposing the different applied pressures and marking the point of deviation between those pressures as the start of the first-arrival time, and everything else as noise. This method made it easier to determine the first-arrival time compared with other methods described by the ULT 100 software. To achieve this, the exported text file containing information about Time, Raw signal, Energy, Frequency, and Frequency Spectrum for both the P wave and S wave signal was imported into an Excel spreadsheet. The raw signal in unit volts is plotted against the time and this generates the sinusoid graph. Once this is done for the first applied pressure on that sample (2000lbs), the next text file for that same sample is opened and the time and raw signal for the next pressure are plotted against the previous graph (Figures 3.8 & 3.9). A complete plot showing the superimposition of the different graphs is achieved and first-arrival time is estimated from this. Figures 3.8 & 3.9 show typical first-arrival time picks for the P wave and S wave signal. First arrival time is chosen at the point where cyclicity of the waveform begins and a regular pattern is noticed, or where the different compressive stresses show a divergence.

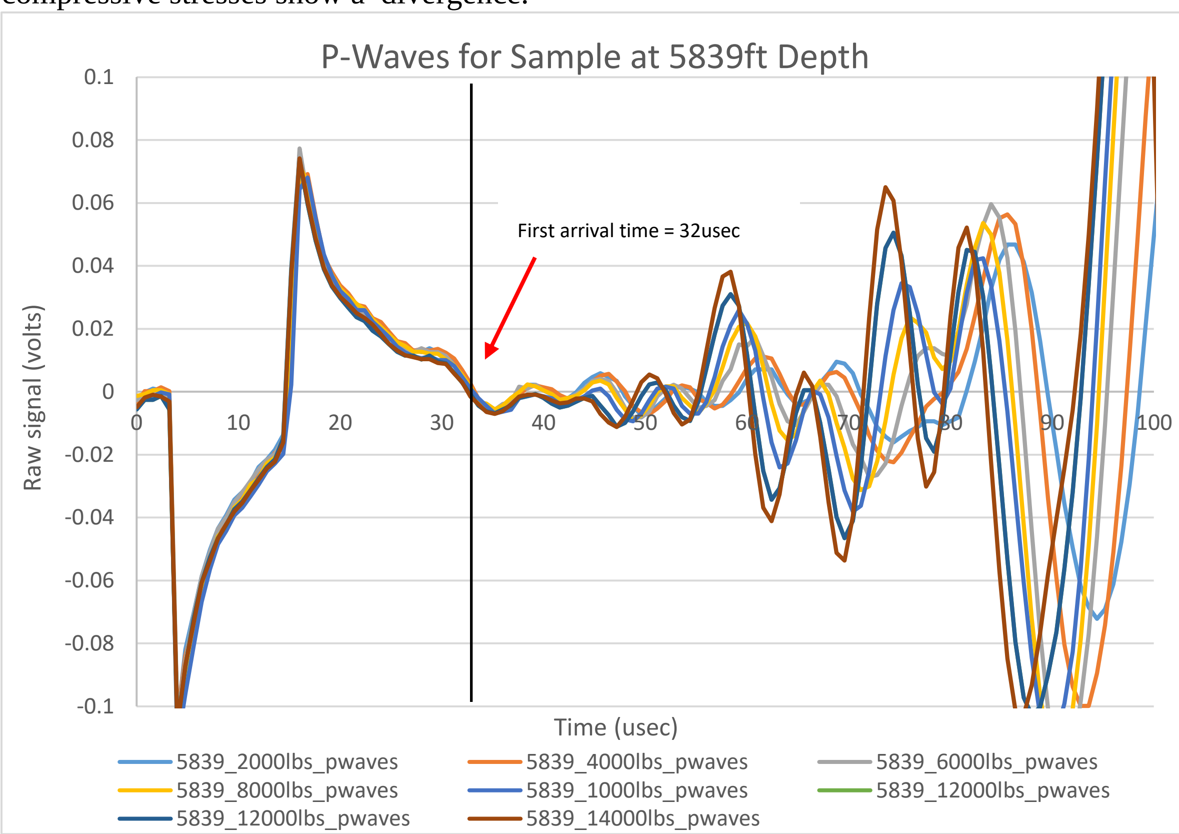

Figure 3.8 P wave velocities simulated at different in-situ pressures overlapped on top of each other to estimate arrival times. First arrival time for P wave is 32usec.

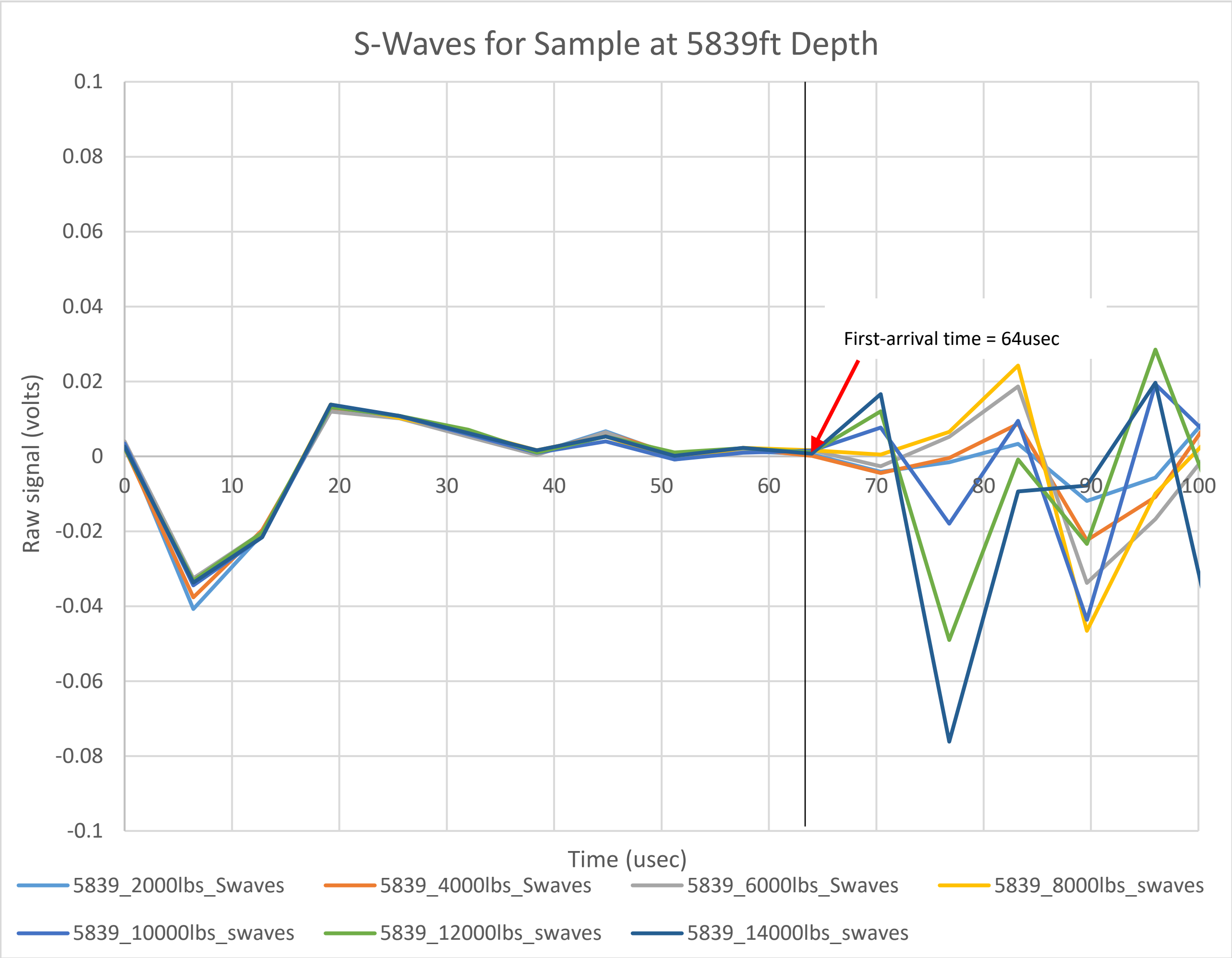

Figure 3.9 S Wave velocities simulated at different in-situ pressures overlapped on top of each other to estimate arrival times. 64usec for the first-arrival time of S wave graph.

3.8 Challenges

Before any data interpretation can be made, it is important to note some challenges faced during the experiment and picking of first-arrival times that could have contributed to some source of error. Some of these challenges were:

1. When wrong first-arrival time picks were made due to underestimation of first-arrival time. This means that noise was included in the P wave and S wave velocity calculations. This affected the Vs readings and made Vs either close to Vp or higher than Vp and

Poisson's ratio and bulk modulus could not be estimated as a result. To avoid this, the first-arrival times needed to be estimated as accurately as possible.

2. Vs first-arrival times are the more difficult to determine compared to Vp first-arrival times. Unfortunately, some of the S wave patterns did not show a regular pattern like the P wave pattern which contributed to the difficulty in estimating the S wave velocity values.
3. The ultrasonic experiments were carried out on Viola cores which were either half-cylinders or semi-half cylinders instead of full cylinders and with pressures applied only on the major axis of the cores (uniaxial compressive stress) and not enough compression along the sides of the cores. For better result, a triaxial shear stress test which was not readily available might provide better results in terms of the modeling.
4. Gassmann's model which is used as a comparison works better on siliciclastic rocks that have uniformity.
5. Not enough reservoir rock was available for the ultrasonic testing and with more rocks to compare this result to, a better model comparison could be made.
6. The platens got damaged due to continual use which had the wires twisted and led to some of the P and S wave cables getting damaged. This made it difficult to adequately obtain the rest of the fluid-saturated experiment data: oil and brine. This was eventually fixed. Care should be taken when handling the platens to ensure that the wear and tear do not limit further experiments. Figure 3.10 shows an instance when testing had to be stopped to fix the platen which had a cut in the wire.

Figure 3.10 Platen with cut wires. Both the external insulating material and the inner cable for the P wave signal showed a cut due to wear.

Chapter 4 - Results

Once the recorded text file from the methods section is imported into excel and the different compressive stresses plotted against each other, the resulting output was analyzed.

The results of the ultrasonic velocity experiments conducted on the Viola formation core samples are shown in Figures 4.1 to 4.10 below. These figures show the resulting output of the wave signal plotted against the arrival time of the wave. Results also include steps involved in first-arrival time picking, and the resulting P and S wave velocity (Vp and Vs) values calculated from the first-arrival time determination. Once Vp and Vs are calculated, the software uses that information in calculating the elastic parameters: Poisson’s ratio, Bulk modulus, Young’s modulus, and Shear modulus (Tables 4.1, 4.2, 4.3).

4.1 Dry Rock Results

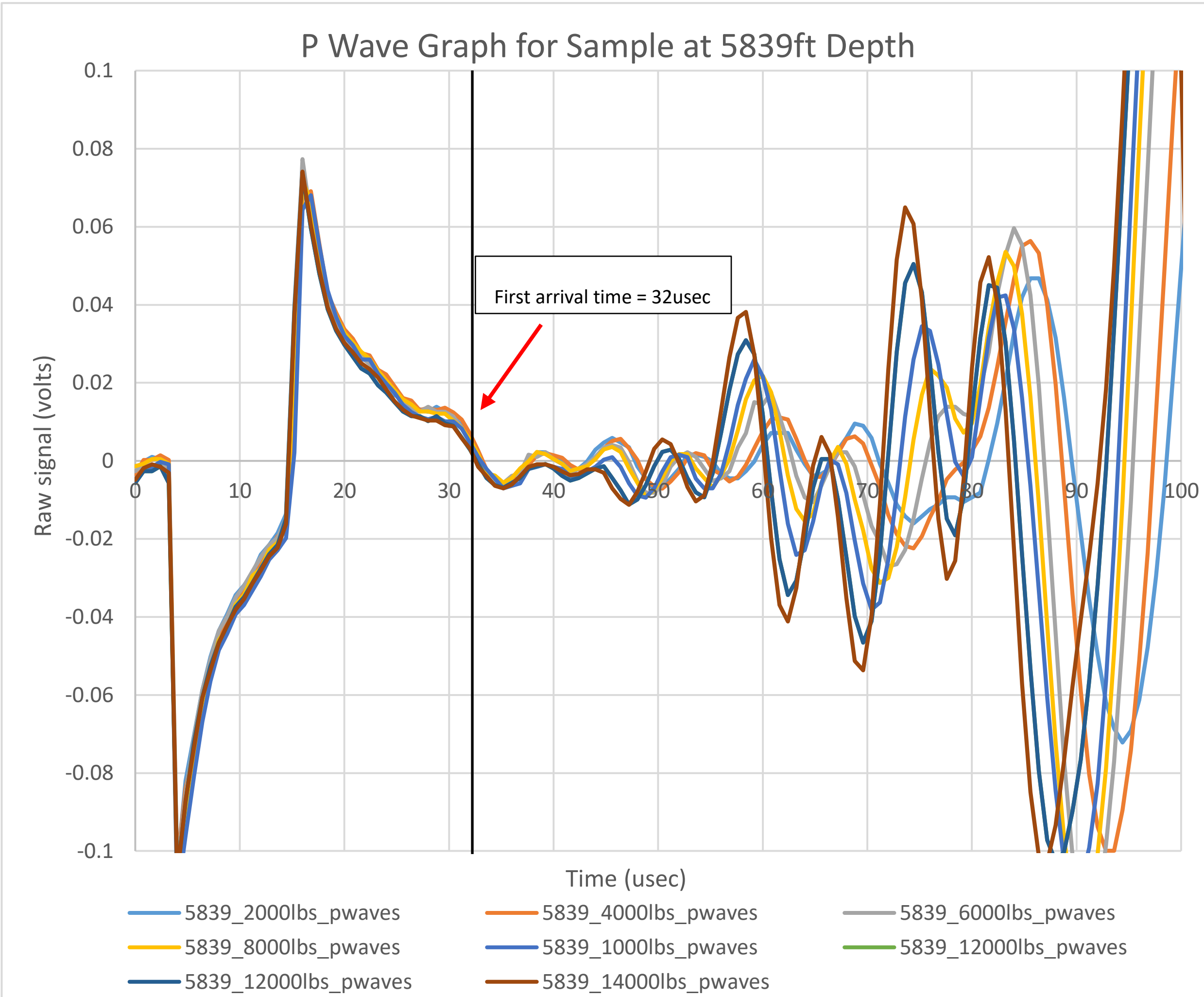

Figure 4.1 P wave graph showing wave raw signal versus time for different compressive stresses for sample taken at depth 5839 feet. Dry rock. First-arrival time = 34usec.

Figures 4.1 and 4.2 show the wave signals generated from ultrasonic velocity experiments on dry Viola rock taken from depth 5839 feet. Different compressive stresses applied on the rock from 2000lbfs to 14000lbfs superimposed against each other and raw signal (volts) plotted on the y-axis against arrival time (usec) on the x-axis. Pressures up to 14000lbfs could only be applied to non-reservoir Viola samples, which were denser and showed no evidence of the fragile cherty dolomite reservoir rock facies. The first arrival time is determined at 32usec for the P wave graph, while the first arrival time is determined at 64usec for the S wave graph. We notice higher amplitudes for each wave signal propagated at higher compressive stresses. The P wave signals show much higher amplitudes than S wave signals, and this is common for P waves. P waves which are the primary waves in general arrive faster than secondary S waves and this is noticed from the resulting graphs where the first arrival times for P waves are picked earlier than first-arrival times for S waves (Figures 4.1 and 4.2). The waveforms also become more cohesive due to traveling at faster velocities as pressures applied

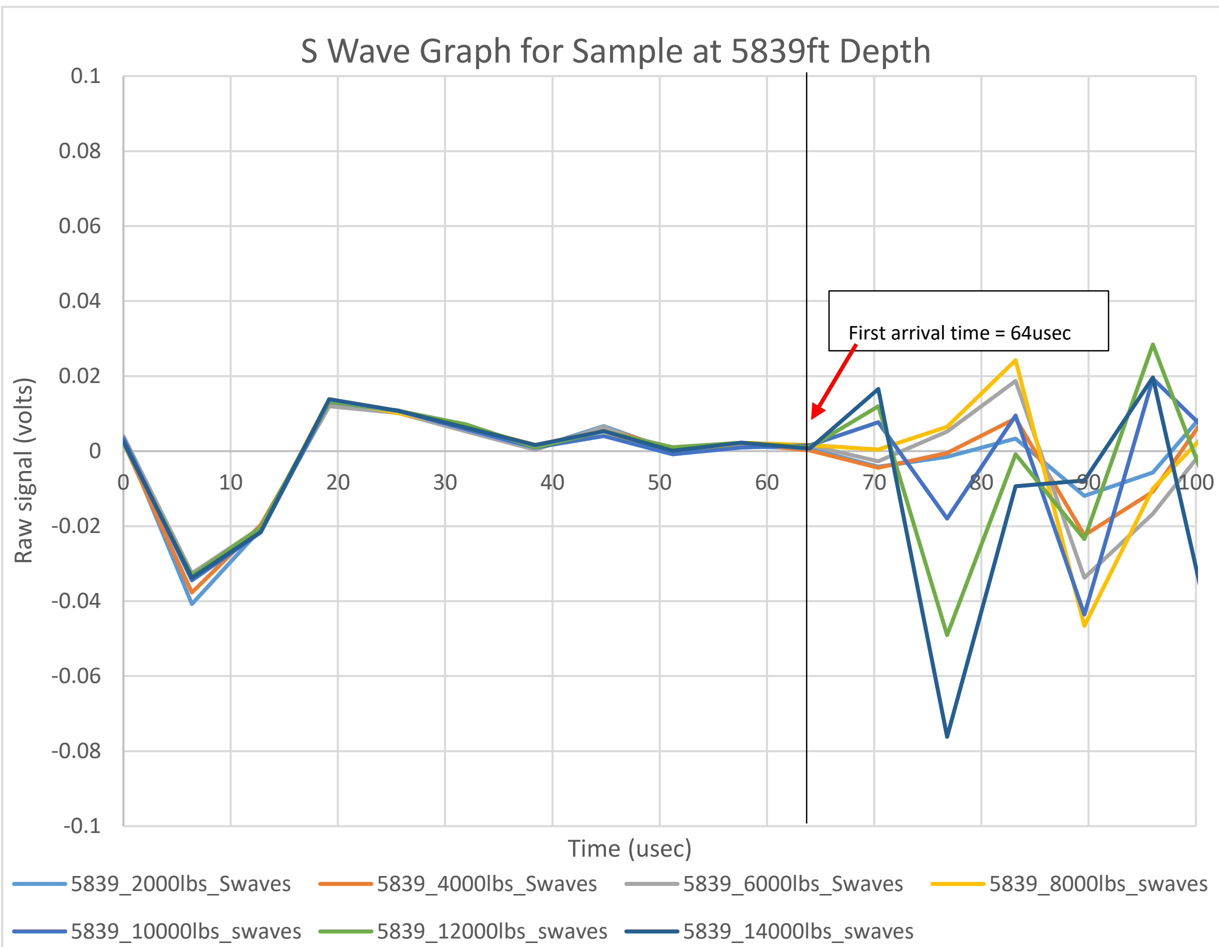

Figure 4.2 S wave graph showing wave raw signal versus time for different compressive stresses for sample taken at depth 5839ft. Dry rock. First-arrival time = 34usec.

to the rock increases.

Table 4.1 Vp, Vs , Poisson's ratio, Young's modulus, bulk modulus, and shear modulus values for dry rock cores from Rich C 7 well.

Sample Depth	Vp (m/s)	Vs (m/s)	Poisson's Ratio	Young's Modulus (kPa)	Bulk Modulus (kPa)	Shear Modulus (kPa)
5808	2217	5250	n/a	305,144,896	n/a	72,358,960
5809	5317	1829	0.43	24,724,382	61,419,444	8,627,342
5815	9718	4423	0.37	124,188,512	158,448,544	45,345,112
5820	8778	5706	0.13	163,451,952	74,472,184	72,056,104
5825	5446	1946	0.43	28,501,524	64,883,616	9,988,002
5838	6620	2650	0.4	51,538,788	89,991,328	18,347,100
5839	5510	2885	0.31	57,916,024	51,137,524	22,084,432
5846	6244	2949	0.36	57,185,268	66,419,332	21,078,172
5848	4615	3000	0.13	49,185,852	22,410,118	21,683,080
5862	7302	2949	0.4	62,583,820	107,050,024	22,310,518
5865	6923	2567	0.42	46,407,292	97,036,192	16,337,234
5866	5171	2624	0.33	45,739,380	43,967,500	17,239,110

Table 4.1 shows all Vp, Vs, Poisson's ratio, Young's modulus, Bulk modulus, and Shear modulus values calculated. All values were calculated from the first-arrival times obtained from the ultrasonic velocity experiment on dry rock, and height, weight, volume, and density readings taken from the Viola Rich C 7 well cores.

4.2 Data Collected at Different Sampling Frequency (dry rock)

Table 4.2 The table below shows the results for sample 5812, sample 5820, and sample 5834

Dry							
Sample Depth	**Frequency**	**Vp (m/s)**	**Vs (m/s)**	**Poisson's ratio**	**Young's modulus (kPa)**	**Bulk modulus (kPa)**	**Shear modulus (kPa)**
5812	156.3kHz	4537	2735	0.21	34981072	20414296	14402531
(4000lbfs)	312.5kHz	4537	2133	0.36	23789362	27939834	8758377
	1.25MHz	4061	2214	0.29	24322258	19164158	9438394
	2.5MHz	4366	2214	0.33	25047174	24113062	9438394
	5.0MHz	4061	2214	0.29	24322258	19164158	9438394
	20MHz	4115	2214	0.3	24468548	20012628	9438394
5820	156.3kHz	4244	1635	0.41	14555031	27822708	5151090
(5000lbfs)	312.5kHz	4244	1635	0.41	14555031	27822708	5151090
	1.25MHz	4085	2444	0.22	28095830	16796156	11503297
	2.5MHz	4085	2444	0.22	28092536	16798944	11501206
	5.0MHz	4416	1995	0.37	21040218	27339974	7669187
	20MHz	-	-	-	-	-	-
5834	156.3kHz	4397	2925	0.1	47349400	19897030	21456534
	312.5kHz	4397	2541	0.25	40472244	26908890	16197638
	1.25MHz	5299	3163	0.22	61410928	36976356	25102624
	2.5MHz	4397	2627	0.22	42331916	25419884	17314392
	5.0MHz	-	-	-	-	-	-
	20MHz	4092	2627	0.15	39806384	18929304	17314392

Table 4.2 shows different sampling frequencies (156.3kHz, 312.5kHz, 1.25kHz, 2.5MHz, 5.0MHz, 20MHz) at which ultrasonic velocity experiments were carried out on dry rock taken

from depth 5812 feet, 5820 feet, and 5834 feet. First arrival time was not picked for data collected at 20MHz for 5820 feet depth rock sample and data collected at 5.0MHz for 5834 feet depth rock sample. Therefore, these results are not shown in Table 4.2. The Vp, Vs values showed a slight change for the different sampling frequencies at which data were collected for each sample, but this might just be as a result of human error in having a few small differences in selection of first-arrival time for each data collection at the different frequencies.

4.3 Fluid Saturated Experiments Results (water-saturated experiment results only)

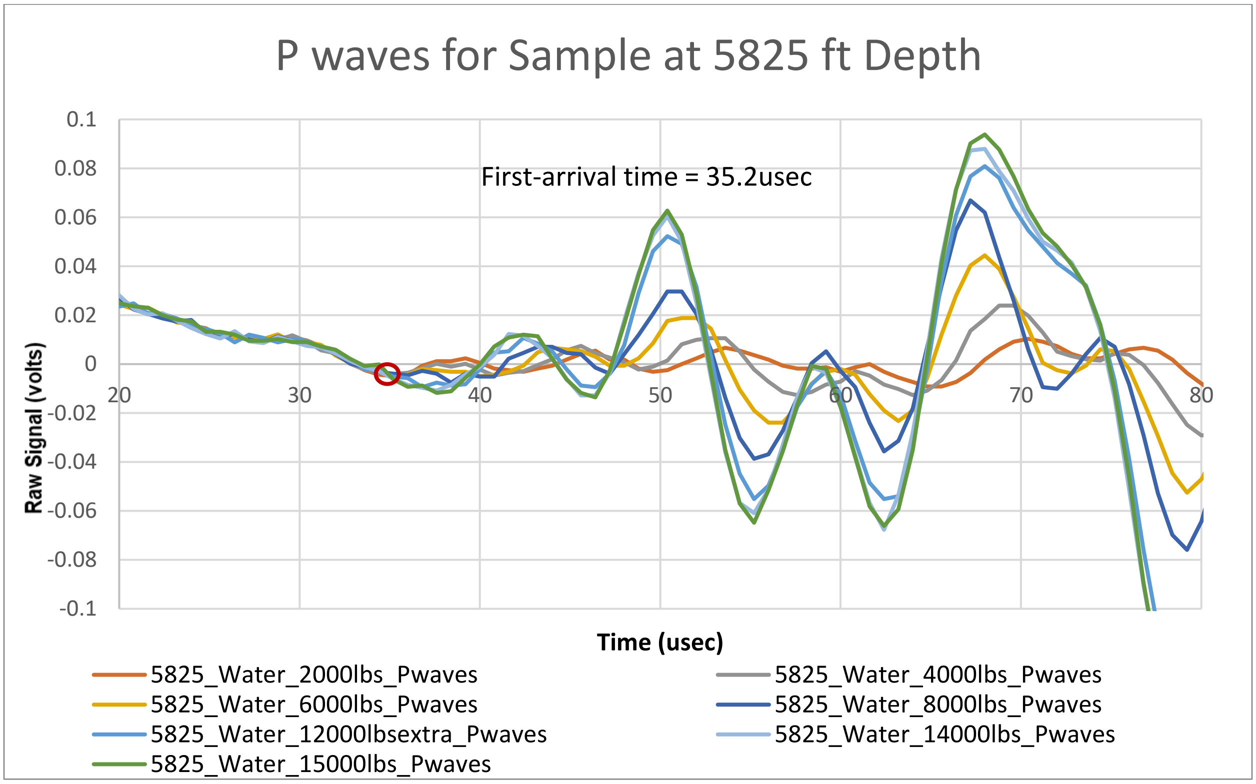

Figure 4.3 Primary P wave graph showing amplitude versus time for different confining pressures for the sample taken at depth 5825 ft. Water-saturated rock; higher effective stress is associated with higher velocity and less attenuation of the signal. The red circle represents the first arrival time pick. First-arrival time = 35.2usec.

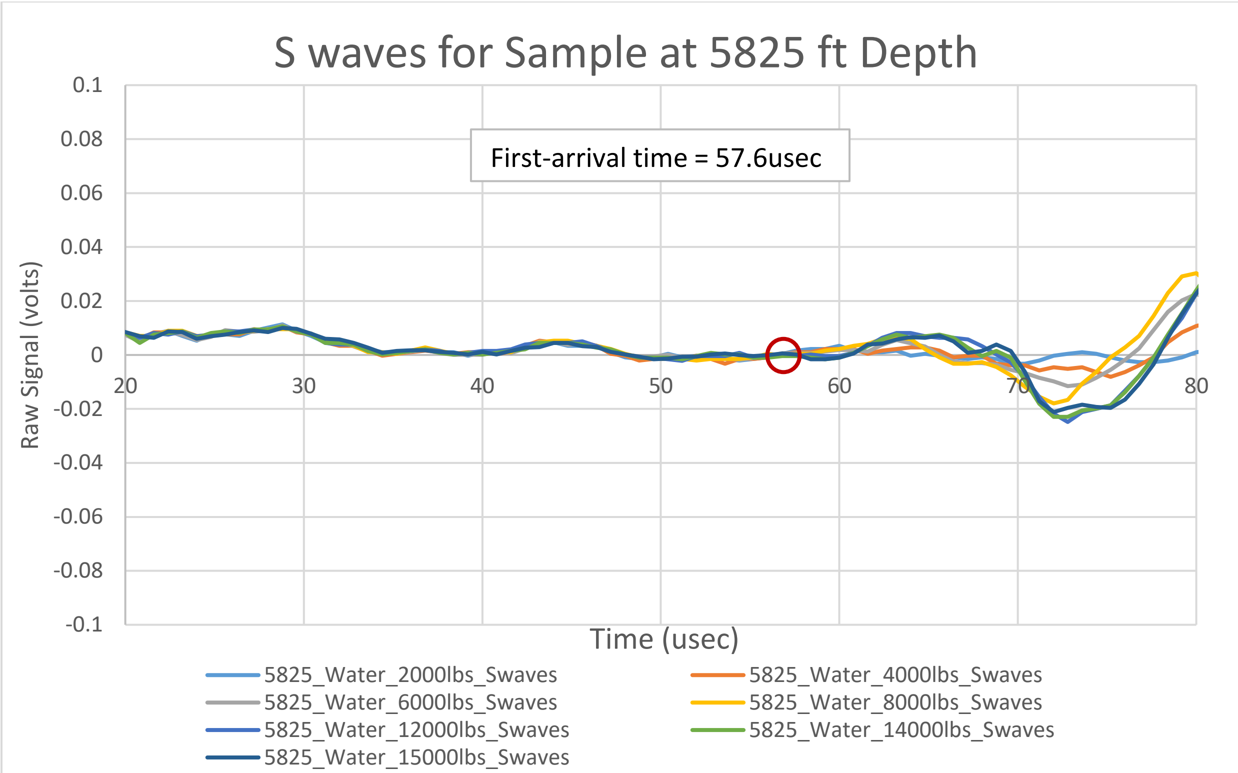

Figure 4.4 Secondary / Shear S wave graph showing amplitude versus time for different compressive stresses for the sample taken at depth 5825ft. Water-saturated rock; higher effective stress is associated with higher velocity and less attenuation of the signal. The red circle represents the first arrival time pick. First-arrival time = 57.6usec.

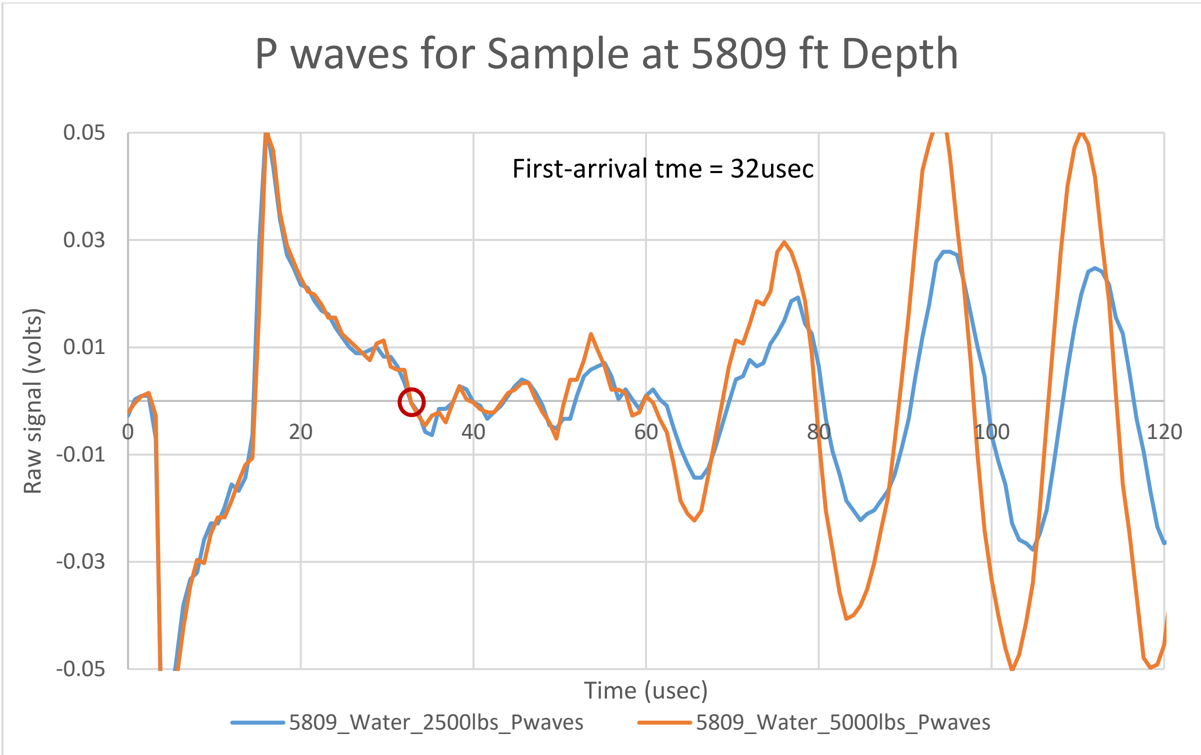

Figure 4.5 P wave graph showing amplitude versus time for different compressive stresses for a sample taken at depth 5809ft. Water-saturated rock; higher effective stress is associated with higher velocity and less attenuation of the signal. The red circle represents the first arrival time pick.

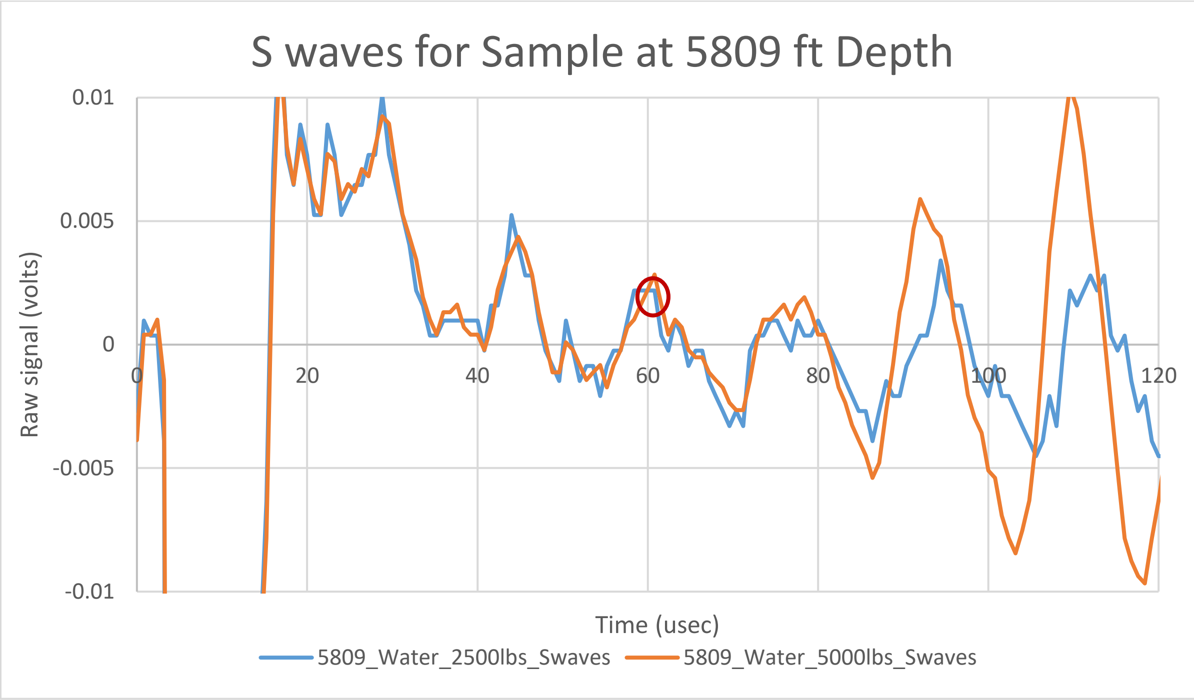

Figure 4.6 S wave graph showing amplitude versus time for different compressive stresses for a sample taken at depth 5809ft. Water-saturated rock; higher effective stress is associated with higher velocity and less attenuation of the signal. The red circle represents the first arrival time pick.

Figures 4.3 and 4.5 show P wave output signals for water-saturated rock ultrasonic velocity experiments conducted on Viola rock samples from depth 5825 feet and 5809 feet respectively. Meanwhile, Figures 4.4 and 4.6 show S wave output signals for water-saturated rock ultrasonic velocity experiments conducted on Viola rock samples from depth 5825 feet and 5809 feet respectively. Different compressive stresses are applied to the rock, up to 15,000lbfs for sample 5825, and up to 5000lbfs for sample 5809. Due to the dense structure of sample 5825 (Figure 4.7), it allows for high pressures to be applied on the rock without the sample becoming compromised. Sample 5825 is an intraclastic breccia which is a non-reservoir rock because it only has a porosity value of 3% (Hagood, 2019), so this sample is not used for further fluid saturation experiments (brine saturation and oil saturation). Sample 5809 is an intraclastic rudstone that has a porosity of 5% and is a non-reservoir rock and is not used for further fluid saturation experiments. This sample 5809 already had a crack running through the sample, so the maximum pressure applied to the rock was limited to 5000lbfs.

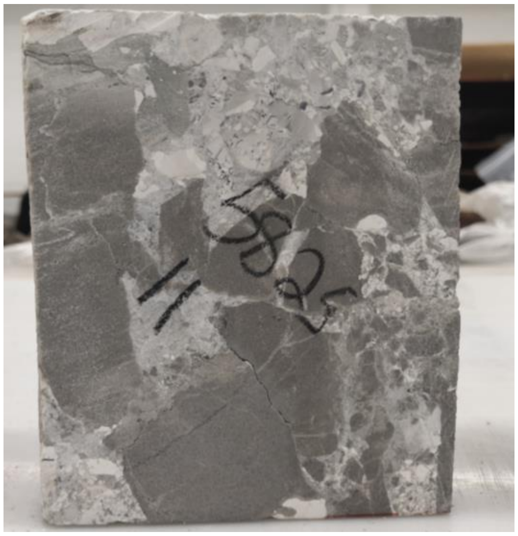

Figure 4.7 Viola core sample taken from depth 5825 feet. The lithofacies of this rock is an intraclastic breccia which consists of some angular dolomitic and siliceous intraclasts, and fragments of chert making it dense compared to the other rocks (Hagood, 2019). It also has a porosity of about 3%. The dense structure of the rock allows for higher pressures of up to 15,000lbfs to be applied on the rock.

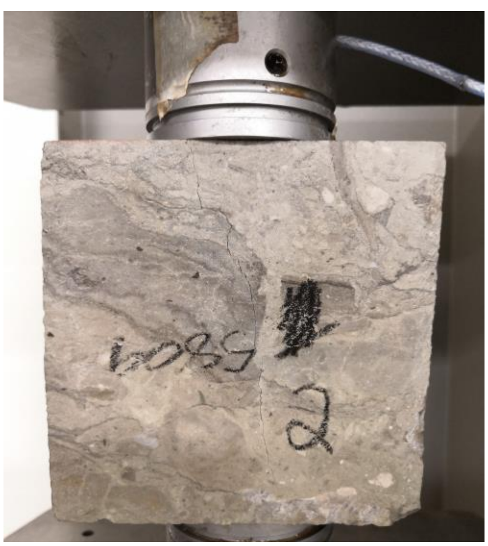

Figure 4.8 Viola core sample taken from depth 5809 feet. The lithofacies of this rock is an intraclastic breccia which consists of some dolomite and mud intraclasts. It has porosity of 5%. In order to protect the sample from getting destroyed, pressure applied on the rock did not go above 500lbfs.

Table 4.3 Vp, Vs, Poisson's ratio, Young's modulus, Bulk modulus, and Shear modulus values for fluid-saturated rock with water as saturating fluid with cores from the Viola Rich C 7 well.

WATER						
Sample Depth	**Vp (m/s)**	**Vs (m/s)**	**Poisson's Ratio**	**Young's modulus (kPa)**	**Bulk modulus (kPa)**	**Shear modulus (kPa)**
5809	5317	2500	0.36	44,886,316	52,717,528	16,525,510
5821	4072	2273	0.27	31,574,714	23,267,878	12,393,595
5825	3827	2086	0.29	24,658,780	19,457,478	9,566,710
5829	5610	3264	0.24	71,327,424	46,438,148	28,668,446
5839	5895	3553	0.21	83,167,496	48,613,364	34,229,036
5846	8790	1062	0.49	8,505,245	191,545,520	2,849,139
5848	6157	3561	0.25	78,934,704,128	52,368,752,640	31,604,584,448

Table 4.3 shows all Vp, Vs, Poisson's ratio, Young's modulus, Bulk modulus, and Shear modulus values calculated. All values were calculated from the first-arrival times obtained from the ultrasonic velocity experiment on the water-saturated rock, and height, weight, volume, and density readings taken from the Viola Rich C 7 well cores.

4.4 Data Collected at Different Sampling Frequencies (water, brine, and oil experiments)

The different sampling frequencies tested during the course of collecting ultrasonic velocity data at different sampling frequencies include: 156.3kHz, 312.5kHz, 1.25MHz, 2.5MHz, 5.0MHz, 20MHz, but not all listed frequencies were examined for each of the experiments. Apart from 1.25MHz which was used as the default initially due to this frequency, at least one other sampling frequency was examined for each sample. Due to the initial problem that the platen had with the twisted wires and infrequent recording of the P and S wave signals at this point in the experiment, it was essential to ensure that at least two different frequencies could be compared.

Table 4.4 Table showing the results for sample 5820 with cherty dolomite porosity and sample 5834 which has slight porosity. Water saturation experiment.

Water							
Sample Depth	Frequency	Vp (m/s)	Vs (m/s)	Poisson's ratio	Young's modulus (kPa)	Bulk modulus (kPa)	Shear modulus (kPa)
5820	156.3kHz	-	-	-	-	-	-
	312.5kHz	-	-	-	-	-	-
	1.25MHz	4085	2345	0.25	29,105,570	19,733,736	11,603,417
	2.5MHz	4085	2242	0.28	27,252,200	21,058,810	10,609,611
	5.0MHz	4085	2302	0.27	28,334,414	20,300,436	11,178,392
	20MHz	4085	2652	0.14	33,712,312	15,410,031	14,846,196
5834	156.3kHz	4397	2925	0.1	48,881,212	20,540,724	22,150,678
	312.5kHz	4397	2541	0.25	41,781,572	27,779,424	16,721,652
	1.25MHz	4662	2541	0.29	43,096,604	33,984,656	16,721,652
	2.5MHz	4276	2541	0.23	41,035,808	25,054,778	16,721,652
	5.0MHz	-	2541	-	-	-	16,721,652
	20MHz	4397	2541	0.25	41,781,572	27,779,424	16,721,652

Table 4.4 shows different sampling frequencies (156.3kHz, 312.5kHz, 1.25kHz, 2.5MHz, 5.0MHz, 20MHz) at which ultrasonic velocity experiments were carried out on water-saturated rock taken from depth 5820 feet and 5834 feet. Data was not collected at 156.3kHz, 312.5kHz for 5820 feet rock sample, and 5.0MHz for 5834 feet rock sample. Same as for the dry rock experiment, Vp, Vs values showed a slight change for the different sampling frequencies at which data was collected for each sample.

Table 4.5 Vp, Vs, Poisson's ratio, Young's modulus, Bulk modulus, and Shear modulus values for fluid-saturated rock with brine as saturating fluid with cores from the Viola Rich C 7 well. Brine saturation experiment.

Brine							
Sample Depth	Frequency	Vp (m/s)	Vs (m/s)	Poisson's ratio	Young's modulus (kPa)	Bulk modulus (kPa)	Shear modulus (kPa)
5820	156.3kHz	4713	2559	0.29	35,954,752	28,674,552	13,924,960
(4000lbs)	312.5kHz	4244	2339	0.28	29,823,734	22,794,252	11,632,309
	1.25MHz	4416	2339	0.31	30,363,276	25,968,394	11,632,309
	2.5MHz	4416	2339	0.31	30,363,276	25,968,394	11,632,309
	5.0MHz	4163	2164	0.31	26,193,052	23,570,618	9,960,924
	20MHz	4416	2164	0.34	26,734,652	28,196,908	9,960,924

Table 4.6 Vp, Vs, Poisson's ratio, Young's modulus, Bulk modulus, and Shear modulus values for fluid-saturated rock with oil as saturating fluid with cores from the Viola Rich C 7 well. Oil saturation experiment.

Oil							
Sample Depth	Frequency	Vp (m/s)	Vs (m/s)	Poisson's ratio	Young's modulus (kPa)	Bulk modulus (kPa)	Shear modulus (kPa)
5820	156.3kHz	-	1635	-	-	-	5612276
(2000lbs)	312.5kHz	-	2339	-	-	-	11478270
	1.25MHz	4244	2242	0.31	27567352	23728592	10551124
	2.5MHz	4328	2242	0.32	27783168	25247906	10551124
	5.0MHz	-	2289	-	-	-	11000058

Tables 4.5 and 4.6 show different sampling frequencies (156.3kHz, 312.5kHz, 1.25kHz, 2.5MHz, 5.0MHz, 20MHz) at which ultrasonic velocity experiments were carried out using brine as saturating fluid (Table 4.5) and oil as saturating fluid (Table 4.6). All sampling frequencies

were unable to be tested for oil-saturation experiment due to the damage to the platen wire (Figure 3.10) and limited access to the lab during the Covid-19 pandemic.

With the injection of fluids into the rock, there was a decrease in amplitude of the P and S wave velocity graphs with raw signal plotted against arrival time. The different sampling frequencies displayed attenuated peaks also. This is discussed in more detail in Chapter 5 and shows comparisons across the different frequencies for the same Viola core sample.

Results from acoustic impedance (density of rock with fluid type present x velocity) calculations on sample 5820 provide lower acoustic impedance for oil-saturated rock compared to brine saturated rock and water-saturated rock. This is because density values for brine saturated rock = 2.13g/ml (2.13kg/l) and density values for oil-saturated rock = 2.10g/ml (2.10kg/l). These values multiplied with velocity values from Table 4.5 and 4.6 provide higher acoustic impedance values for the oil-saturated rock compared to the brine saturated rock.

Chapter 5 - Discussion

Results from the ultrasonic velocity experiments carried out on dry rock experiment and fluid saturation rock show that seismic waves are affected during propagation through Viola carbonate rock at different fluid conditions. This suggests that fluid type in the pore space affects ultrasonic wave velocities, and amplitudes of propagating waves, porosity, and lithology affects elastic parameters. The following observations were made from the experiments.

In both dry rock and fluid-saturated rock ultrasonic velocity experiments, as compressive stresses applied on a rock increases, the ultrasonic wave traveling through the rock travels at a faster velocity than each preceding compressive stress. In Figures 4.1 to 4.6, the wave signal for ultrasonic velocity wave signal traveling under a compressive stress of 14,000lbfs differs from that of the wave signal for waves traveling under lower compressive stresses of 2000lbfs. This is consistent in other figures for both dry rock and fluid-saturated rock. Waves traveling through Viola carbonate rocks under high compressive stresses will travel at a faster velocity due to the structure becoming denser and more compact. This is as a result of a reduction in the effects of air or fluids within the rock causing dispersion of the wave (Grochau & Gurevich, 2009).

Primary P wave and Secondary S waves traveling through dry rock show much higher wave amplitudes compared to when the waves travel through fluid-saturated rock. This can be explained through the process of attenuation causing a reduction in the force of the wave traveling through any rock and in this case Viola carbonate rock. The presence of fluids in a rock will cause attenuation of waves propagating through that rock because the fluids present within the rock will absorb some of the energy of the propagating wave. We see that this is true in the case of the Viola carbonates from the ultrasonic velocity data.

The observed increase in amplitude and velocity of the ultrasonic P and S waves as compressive stress increases is probably due to the closure of pore spaces in the rock sample under pressure. Increasing compressive stress caused an increase in P and S wave velocity.

Distinguishing between the fluid types present in any rock is a major objective of most exploration projects due to the amount of capital that could be lost in drilling a dry hole or water-saturated borehole versus drilling a hydrocarbon well. To test to see if the change in elastic parameters of a rock can be used to identify the pore fluid type and presence in the Viola formation, we compared how ultrasonic wave signals change when propagated through oil-saturated rock, brine saturated rock, water-saturated rock, and dry rock. The raw signals (volts) for oil-saturated rock, brine saturated rock, water-saturated rock, and dry rock were plotted against time and overlapped for the sample taken from depth 5820ft on which all the experiments were carried out (Figures 5.1 to 5.8) to analyze for amplitude differences, velocity changes, and waveform changes. Water does not occur in the Viola without other compounds or constituents mixed in, and without the water naturally occurring as brine, so for the analysis, in Figures 5.1 to 5.8, water is not compared with the remaining results. Two frequency readings are compared: 1.25MHz and 2.5MHz.

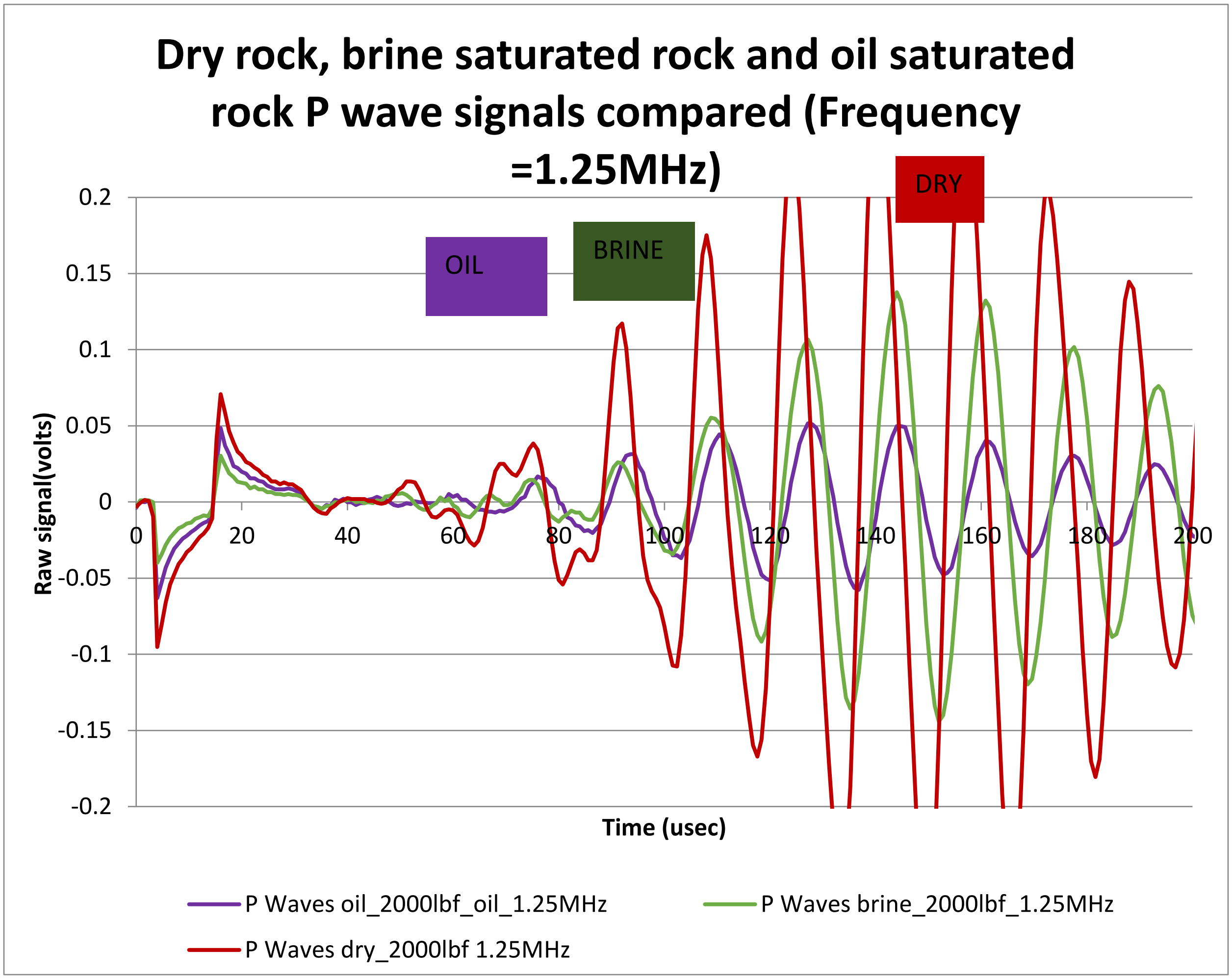

Figure 5.1 Comparison between P wave velocity for sample from depth 5820ft against arrival time, Dry rock is shown in red, oil is represented in purple, and brine is shown in green. Readings were taken at 1.25MHz frequency. All at 2000lbs compressive stress**.**

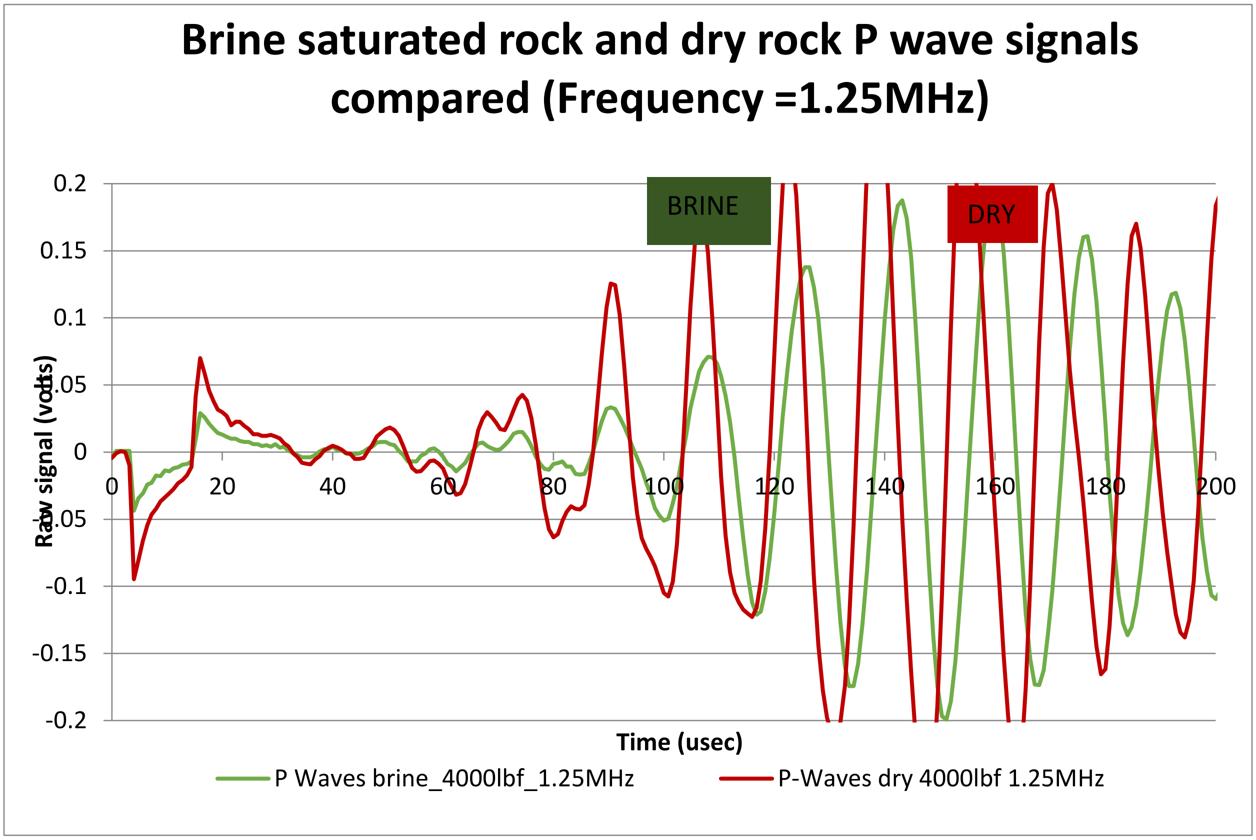

Figure 5.2 Comparison between P wave velocity for sample from depth 5820ft against arrival time, Dry rock is shown in red, brine is shown in green.. Readings taken at 1.25MHz frequency. All at 4000lbf compressive stress.

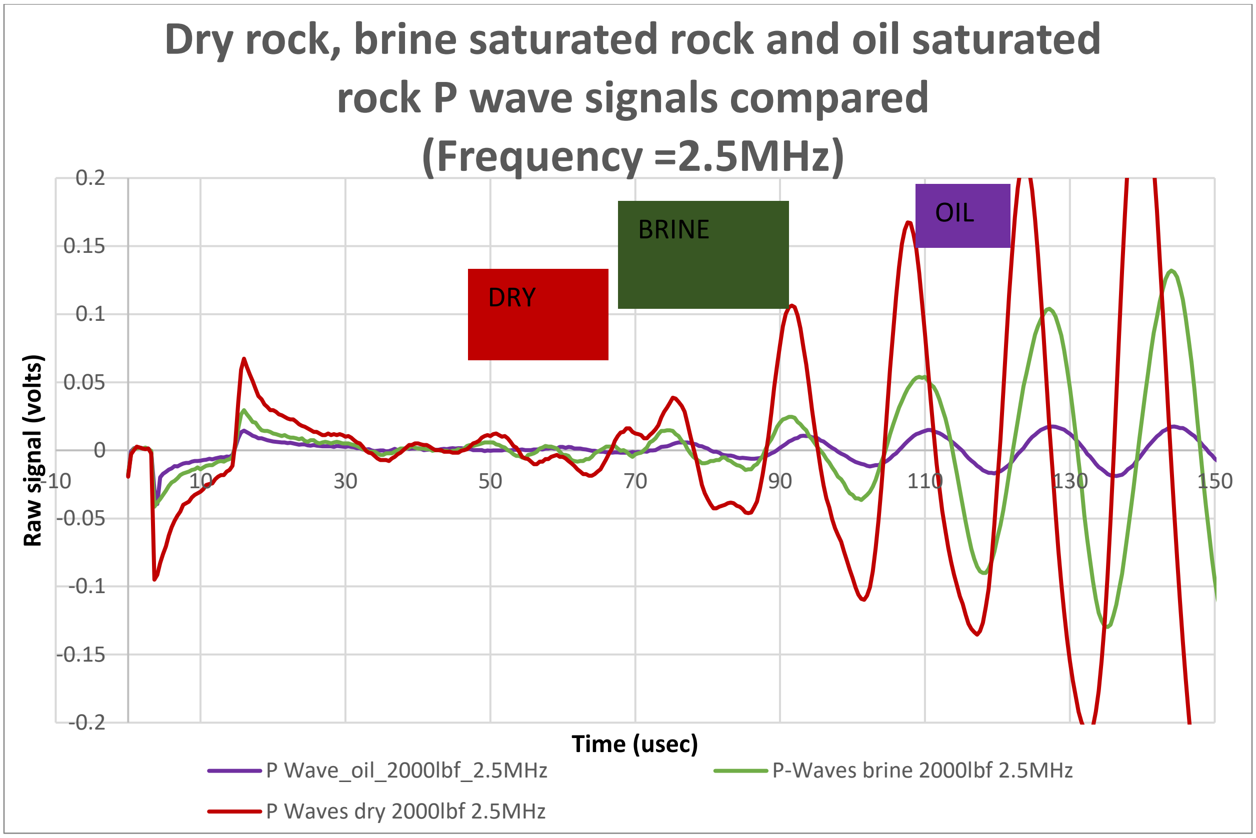

Figure 5.3 Comparison between P wave velocity for sample from depth 5820ft against arrival time, dry rock is shown in red, oil is represented in purple, and brine is shown in green. Readings were taken at 2.5MHz frequency. All at 2000lbs compressive stress.

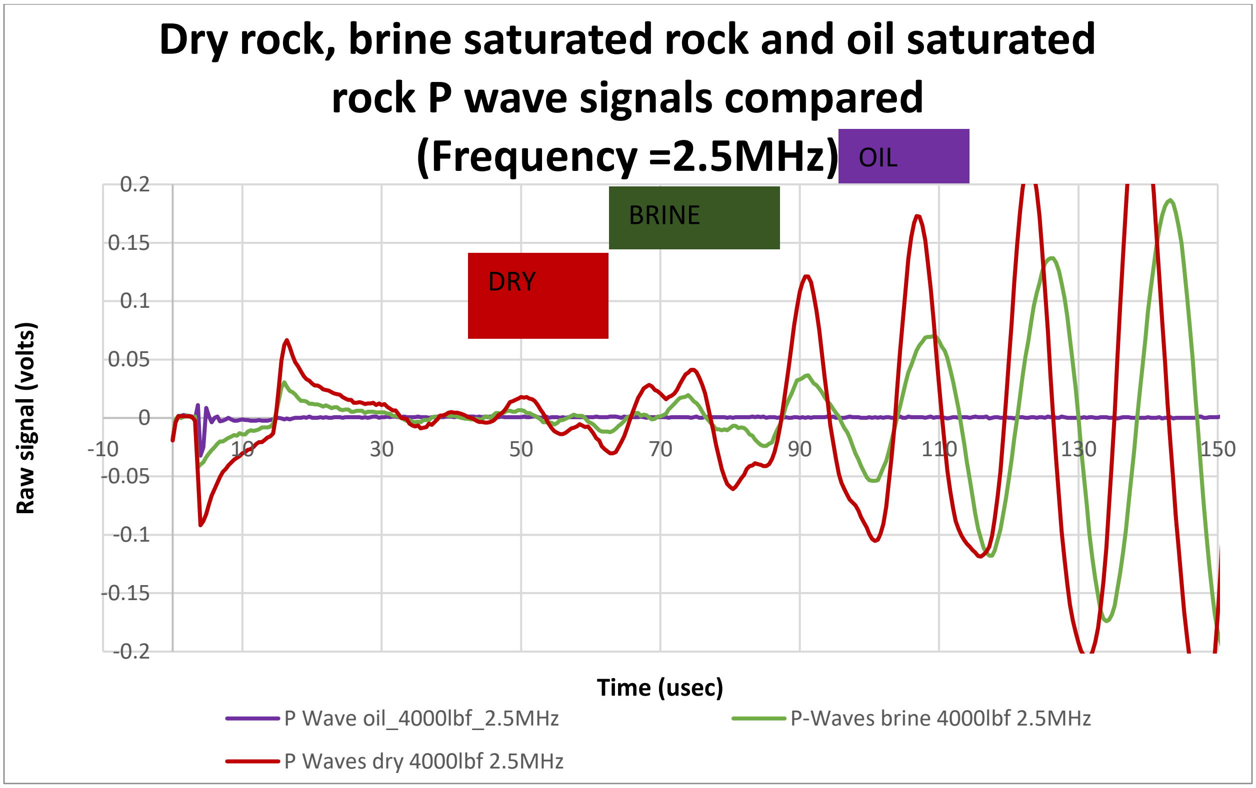

Figure 5.4 Comparison between P wave velocity for sample from depth 5820ft against arrival time, Dry rock is shown in red, oil is represented in purple, and brine is shown in green. Oil is missing from this experiment. Readings were taken at 2.5MHz frequency. All at 4000lbs compressive stress.

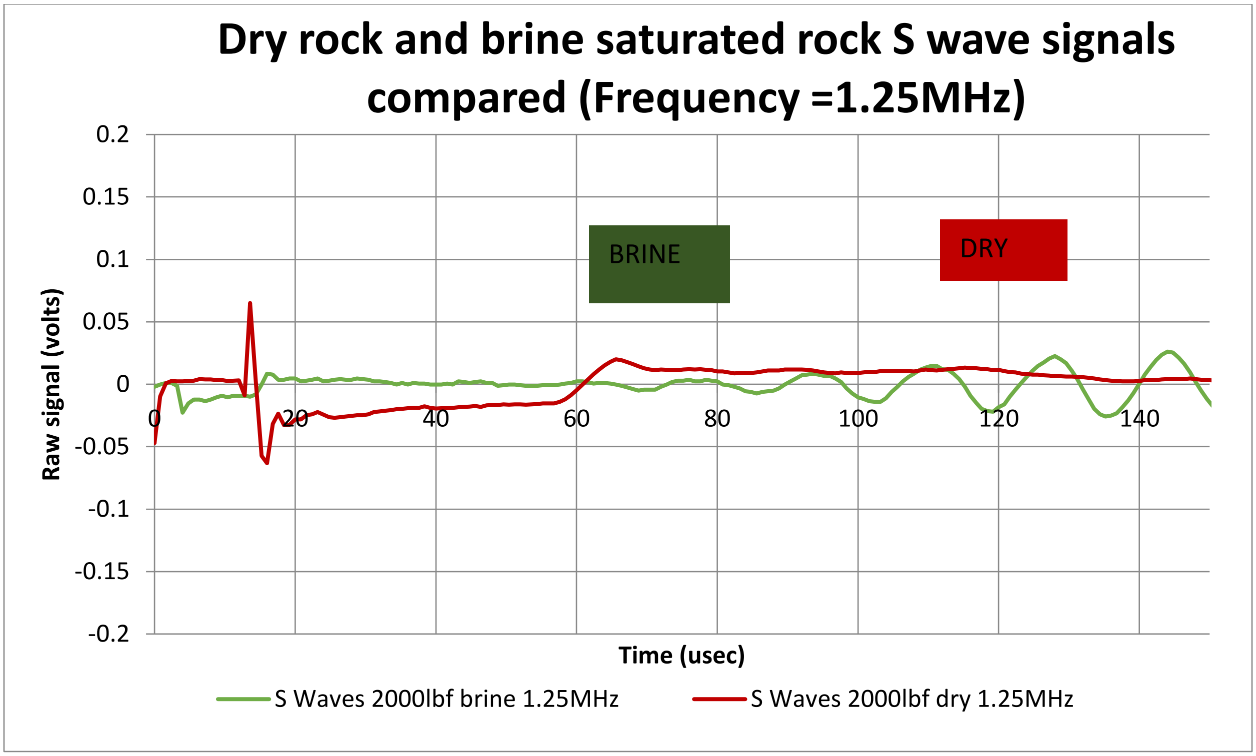

Figure 5.5 Comparison between S wave velocity for sample from depth 5820ft against arrival time, Dry rock is shown in red, and brine is shown in green. Oil is missing from this experiment. Readings were taken at 1.25MHz frequency. All at 2000lbs compressive stress.

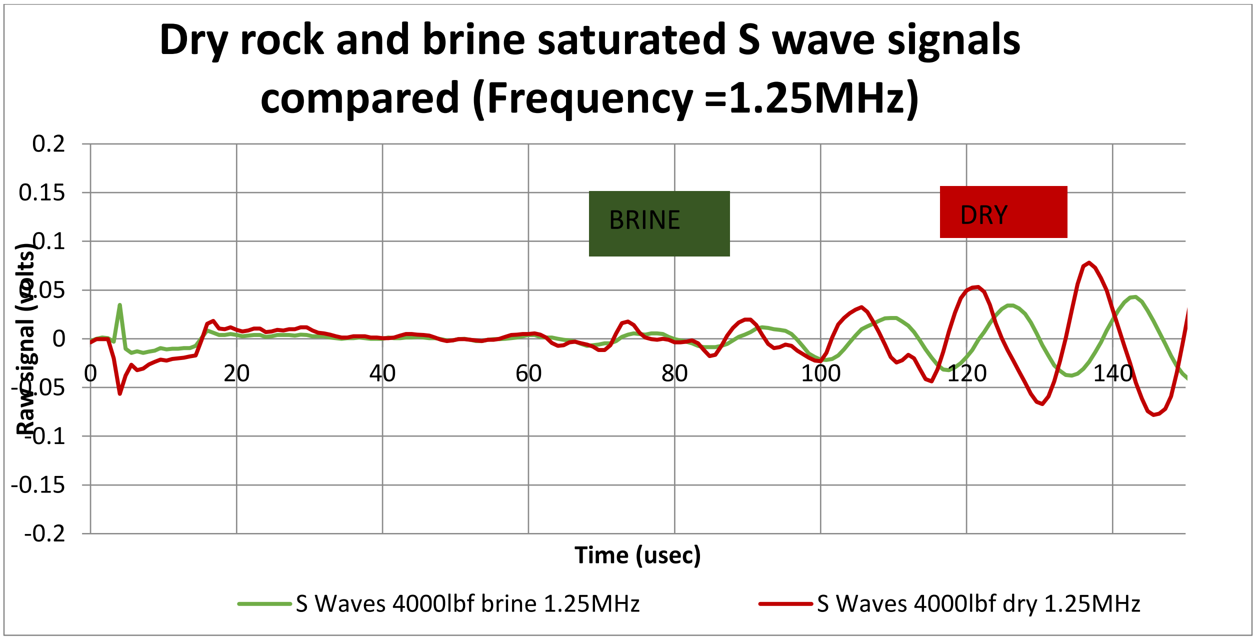

Figure 5.6 Comparison between S wave velocity for sample from depth 5820ft against arrival time, Dry rock is shown in red, oil is represented in purple, and brine is shown in green. Oil is

missing from this experiment. Readings were taken at 1.25MHz frequency. All at 4000lbs compressive stress.

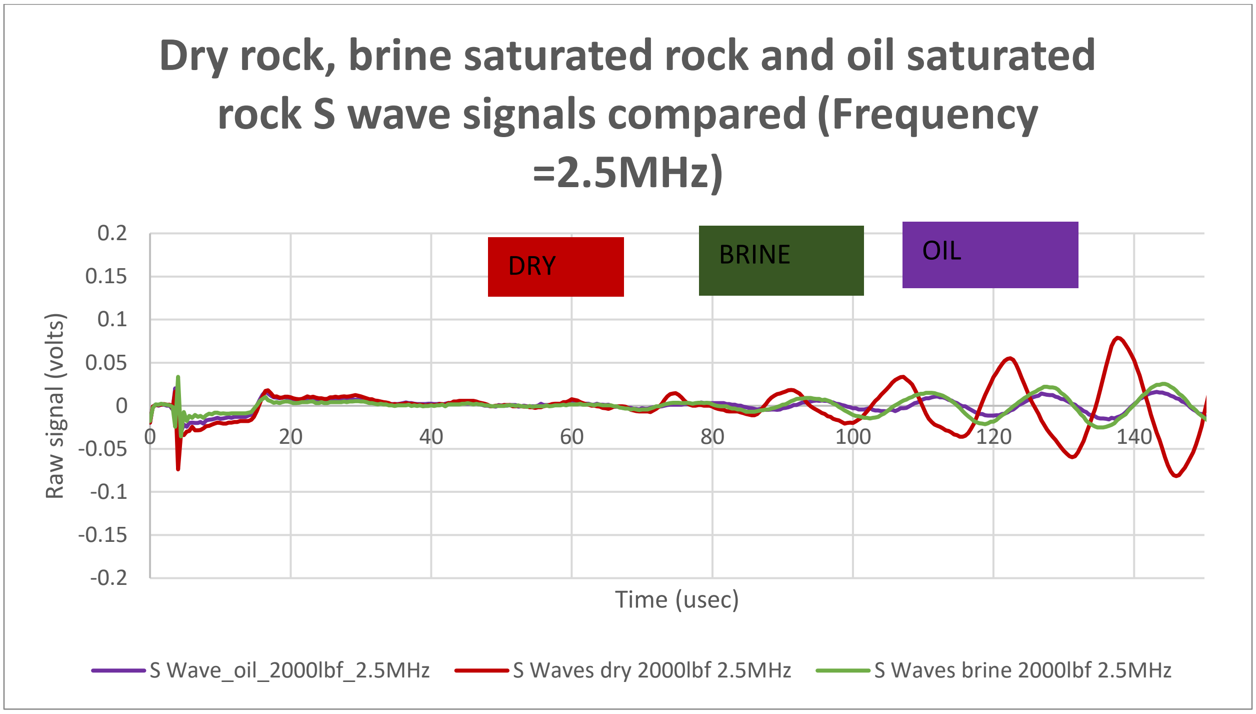

Figure 5.7 Comparison between S wave velocity for sample from depth 5820ft against arrival time, Dry rock is shown in red, oil is represented in purple, and brine is shown in green. Readings were taken at 2.5MHz frequency. All at 2000lbs compressive stress.

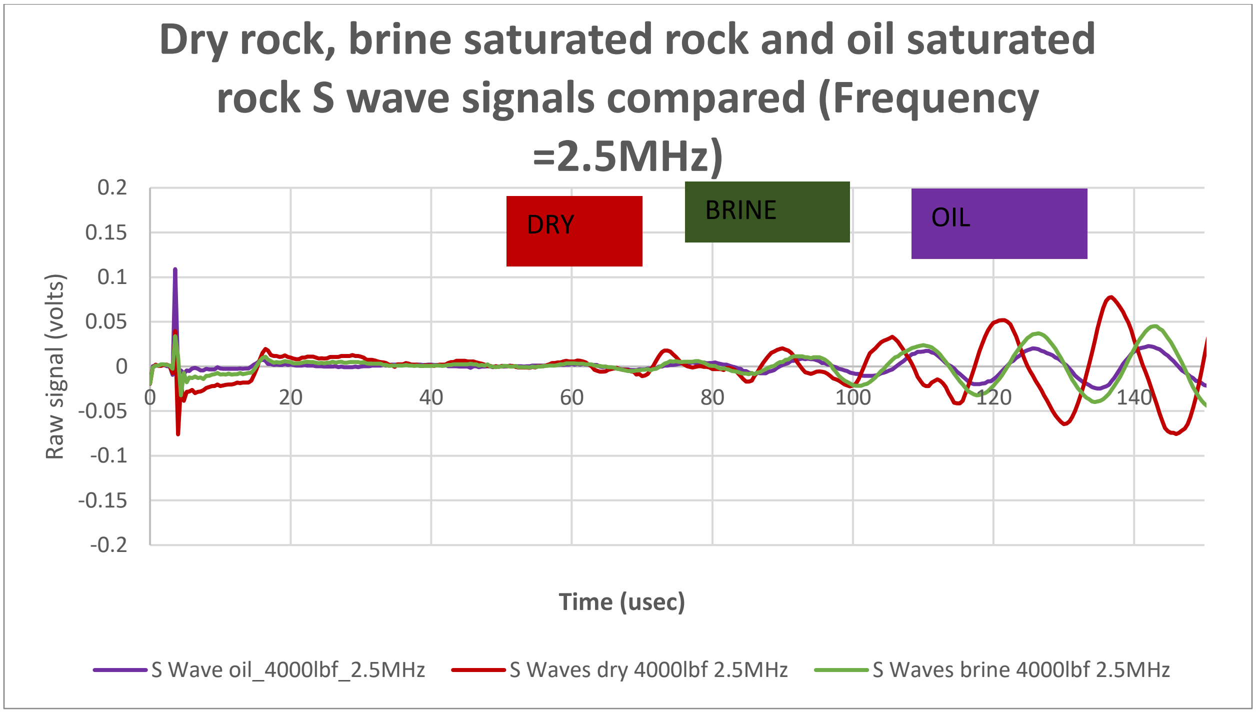

Figure 5.8 Comparison between S wave velocity for sample from depth 5820ft against arrival time, Dry rock is shown in red, oil is represented in purple, and brine is shown in green. Readings were taken at 2.5MHz frequency. All at 4000lbs compressive stress.

5.1 Comparisons across different frequencies

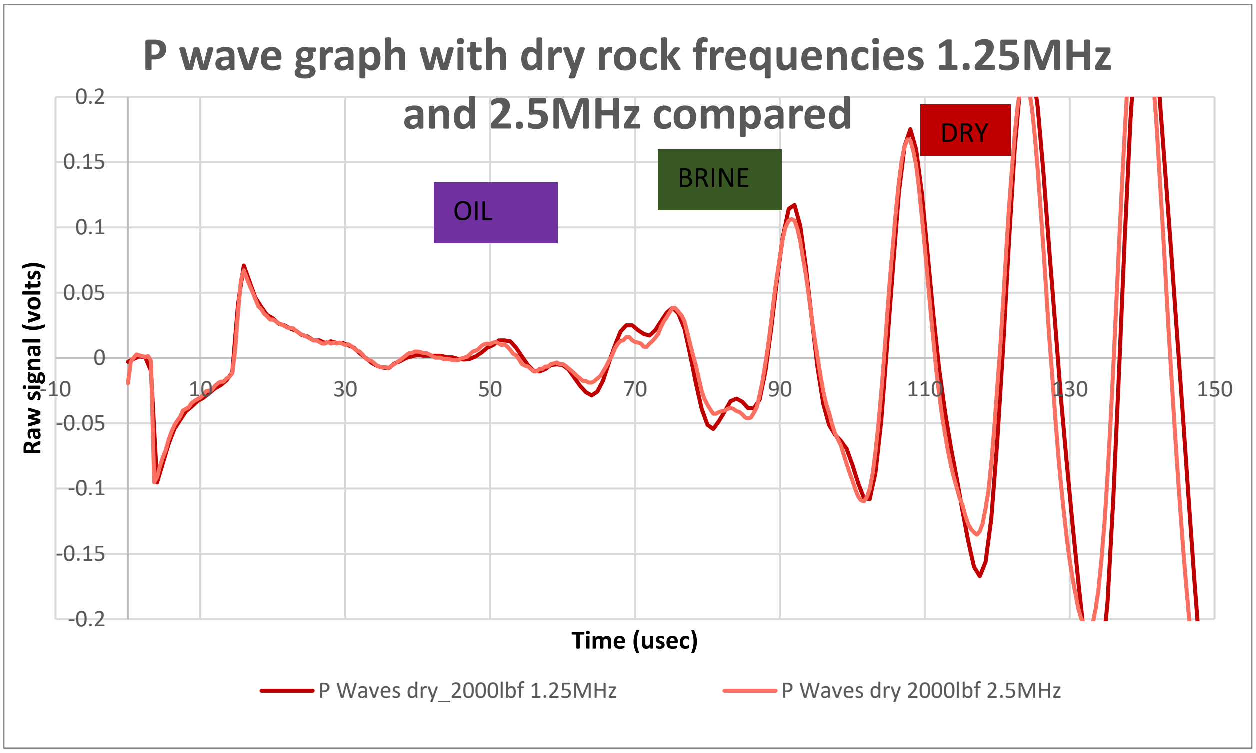

Figure 5.9 Comparison between P wave graph for dry rock sample at frequencies 1.25MHz and 2.5MHz. Measurements are taken at 2000lbf compressive strength. The lighter color represents the higher frequency 2.5MHz, and the darker color represents 1.25MHz

Comparing the P wave graphs for dry rocks at different frequencies (1.25MHz and 2.5MHz) at the same compressive strength shows that the different signals all vibrate at the same phase (Figure 5.9). Laboratory measurements on dry rocks are usually independent of frequency (Simm and Bacon, p. 159), so we did not expect to see much change in the output. Although, a slight difference can be noticed in the amplitudes with higher amplitudes associated with a lower frequency and vice versa.

Figure 5.10 shows a comparison of the different dry rock experiments for two different frequencies (1.25MHz and 2.5MHz) and two different compressive stresses (200lbf and 4000lbf). All signals look very similar and only a small difference between the two.

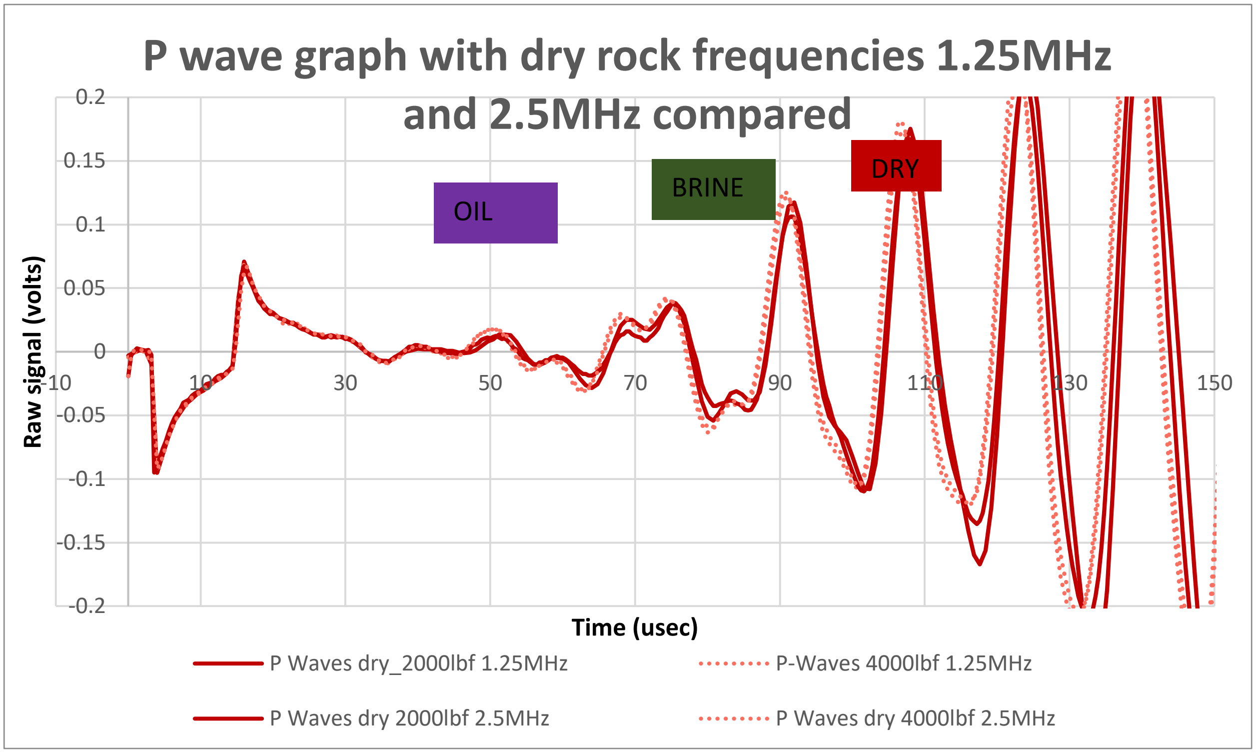

Figure 5.10 Comparison between P wave graph for dry rock sample at frequencies 1.25MHz and 2.5MHz. Measurements are taken at 2000lbf and 4000lbf compressive strength. The lighter color represents the higher frequency 2.5MHz, and the darker color represents 1.25MHz. The solid line represents 2000lbf and the dashed line represents 4000lbf

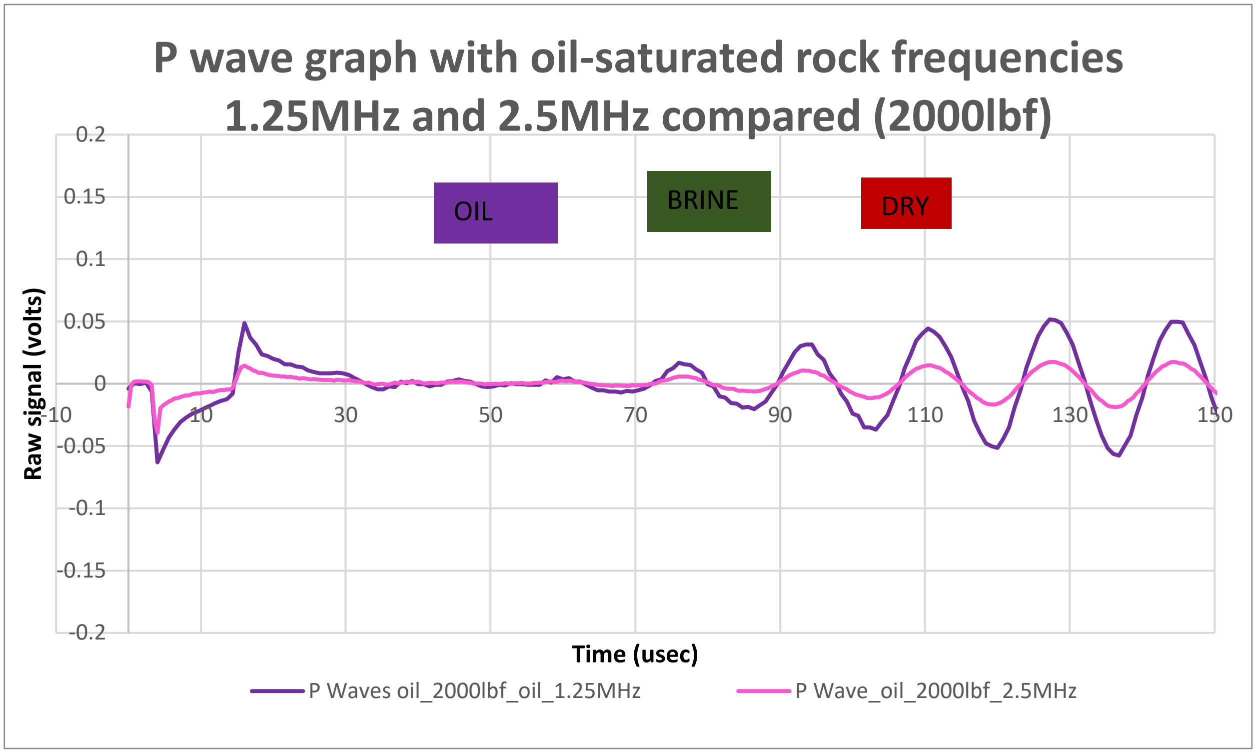

Figure 5.11 Comparison between P wave graph for oil-saturated sample at frequencies 1.25MHz and 2.5MHz. Measurements are taken at 2000lbf compressive strength. The lighter color represents the higher frequency 2.5MHz, and the darker color represents 1.25MHz

Figure 5.11 shows a comparison between oil-saturated rock sampled at different frequencies. Higher amplitudes are associated with lower frequencies and lower amplitudes are associated with higher frequencies. All signals are in the same phase.

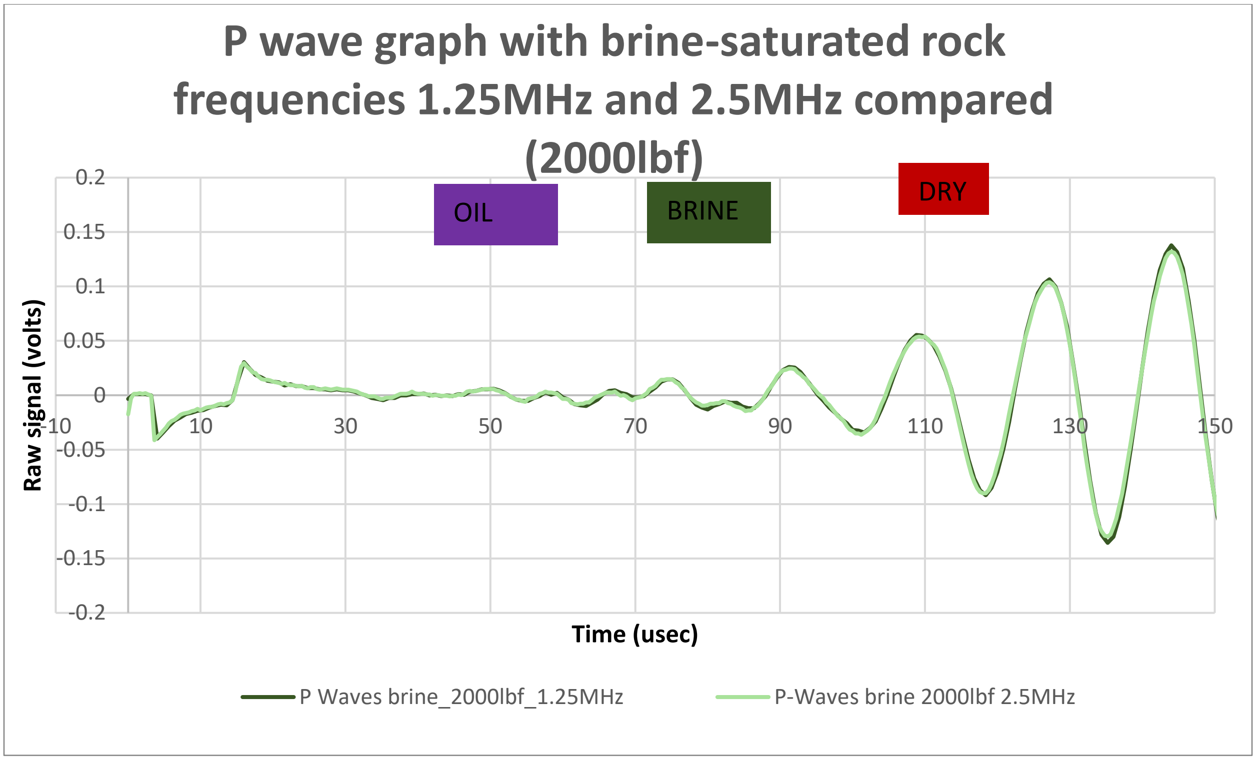

Figure 5.12 Comparison between P wave graph for brine-saturated sample at frequencies 1.25MHz and 2.5MHz. Measurements are taken at 2000lbf compressive strength. The lighter color represents the higher frequency 2.5MHz, and the darker color represents 1.25MHz

Figure 5.12 which shows a comparison between the P wave signal for brine saturated rock sample at different frequencies (1.25MHz and 2.5MHz), shows a different output from the previous figures 5.10 and 5.11. Here it is difficult to distinguish between higher and lower frequencies for the oil-saturated sample, but all signals remain in the same phase.

5.2 Amplitude and Attribute Effects of the Viola Limestone Formation

Analysis of the P and S wave data from the ultrasonic velocity experiments carried out on the Viola carbonate rocks from the Rich C 7 well in Comanche County, Kansas shows that lower amplitudes are associated with fluid-saturated rocks (Figures 5.1 to 5.8), while higher amplitudes were associated with the dry rock. These experimental results suggest that fluid-bearing wells containing oil, brine, and/or water will show higher amplitudes than those associated with dry rock, Vohs (2016) made similar observations from the seismic data taken from the Viola in a nearby county. He found lower amplitudes corresponding to the top of the Viola in the interval associated with the productive facies. Lower amplitudes were associated with producing wells and higher amplitudes corresponded with dry holes and uneconomical wells Vohs (2016). Vohs (2016) shows that amplitude analysis can assist in discriminating between dry uneconomical wells and potential locations for hydrocarbon extraction. Figures 5.1 to 5.12 in this study show corresponding results, with higher amplitudes associated with dry rocks and lower amplitudes associated with brine-saturated and oil-saturated rock samples. This shows that amplitude is an important attribute that should be considered in any oil exploration project whether for lab studies or field studies.

Unlike amplitude variation, which does not robustly distinguish brine- from oil-saturated rock, lithofacies (dolomitization induced porosity) can be used in addition to amplitude analysis for characterizing the carbonate reservoir. Therefore, lithofacies variations should be another property considered in identifying productive zones (higher porosity, higher dolomitization, lower calcite ratio) in the Viola. Similar results were observed by Cimino (2020), especially in comparing Gassmann fluid replacement modeling with lithologic variations in the Viola and its elastic parameters. Results from the brine saturation experiment (Table 4.5) and the oil saturation experiment (Table 4.6) show that lower P and S wave velocities were observed for oil-bearing rocks. This is in accordance with Cimino’s observed results from Gassmann fluid replacement modeling where there was a negative percent change with the increase in oil saturation in either 100% dolomite, calcite, or chert rock (Figures 5.13 to 5.15). A similar observation was made by

Raef et al. (2019) where higher porosity zones, especially when filled with hydrocarbon, caused seismic velocities to decrease.

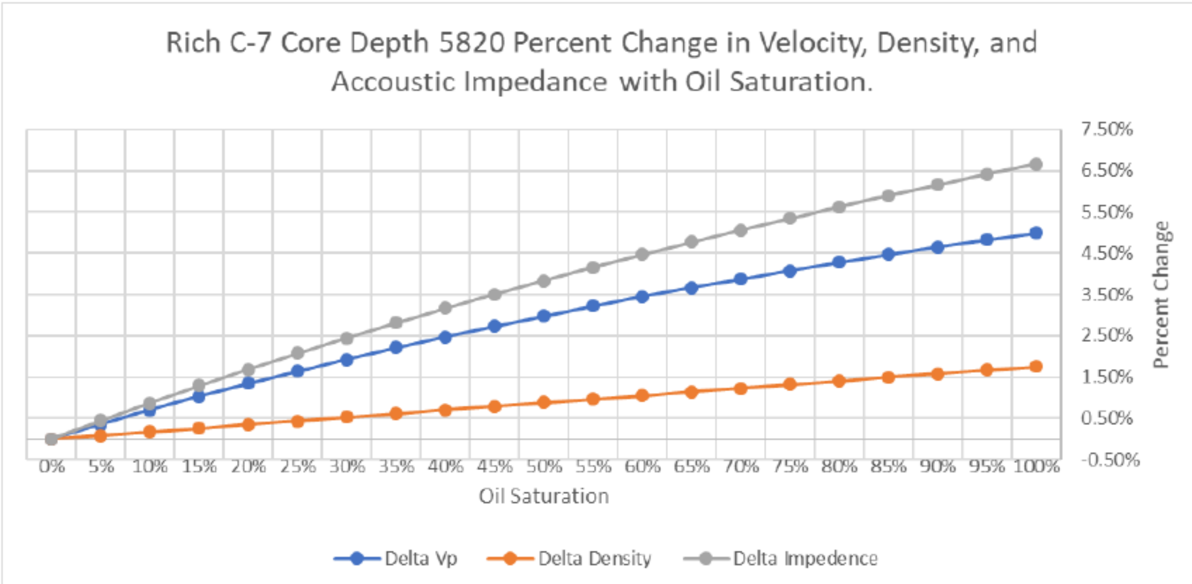

Figure 5.13 Gassmann Fluid Replacement results at 100% dolomite composition and 17% porosity (in-situ). Figure from Vohs (2020).

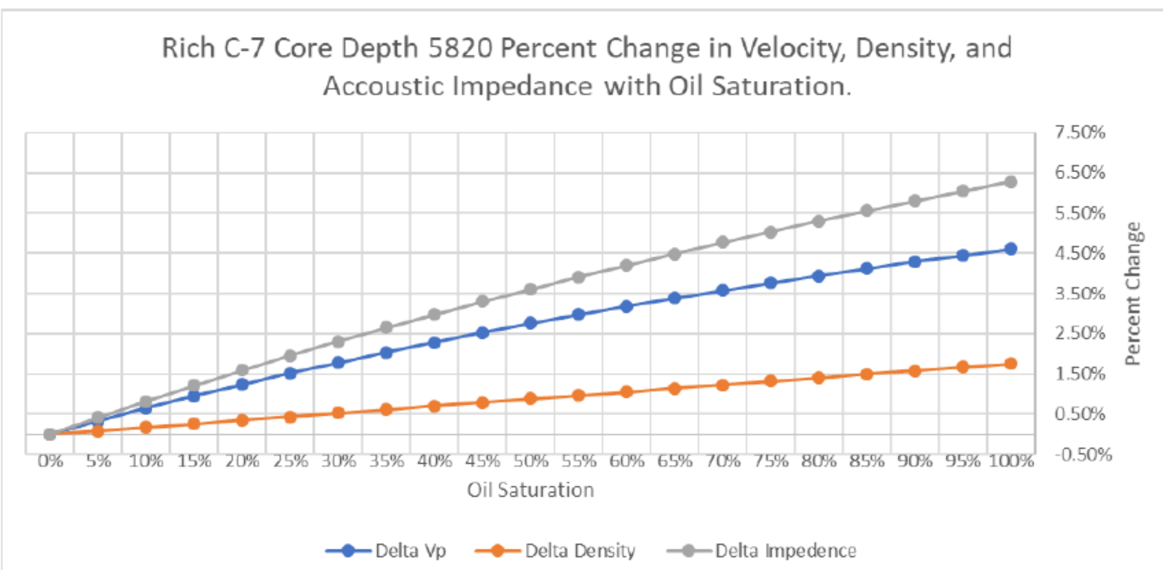

Figure 5.14 Gassmann Fluid Replacement results at 100% calcite composition and 17% porosity (in-situ). Figure from Vohs (2020).

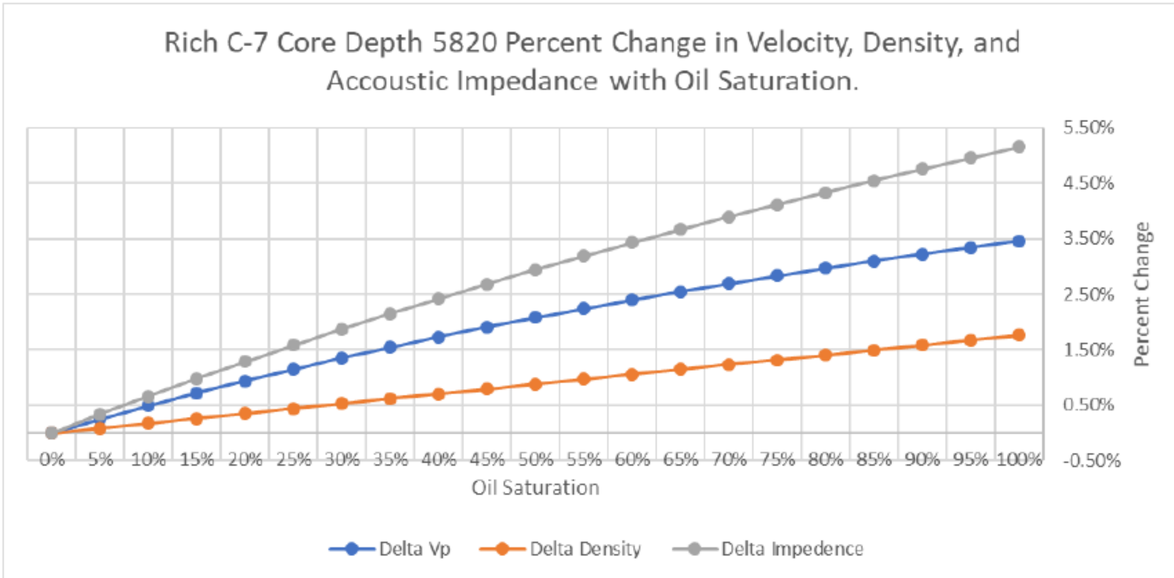

Figure 5.15 Gassmann Fluid Replacement results at 100% chert composition and 17% porosity (in-situ). Figure from Vohs (2020).

Combined with amplitude analysis, other methods found to indicate hydrocarbon presence in the Viola limestone reservoir from previous studies (Vohs, 2016; Raef et al. 2019) include attribute analysis; analysis of instantaneous frequency, instantaneous phase and acoustic impedance, thin-bed tracking, degree of dolomitization, and porosity. Amplitude shows a consensus in distinguishing between dry rock and oil-bearing rocks both from this experiment and Vohs (2016) experiment (Figure 5.16).

Considering the ultrasonic velocity experiments and fluid replacement modeling results and the sonic and density logs, the prolific zones are mainly controlled by lithofacies and porosity and identifiable as lower amplitude seismic response, which is also associated with tuning effects when the pay zone is below seismic resolution. The producing beds in the Viola are thin layers (Vohs, 2016), which might be below seismic resolution. As a result, overlying beds could boost the signal of the producing bed which originally would have been missed due to its thinness.

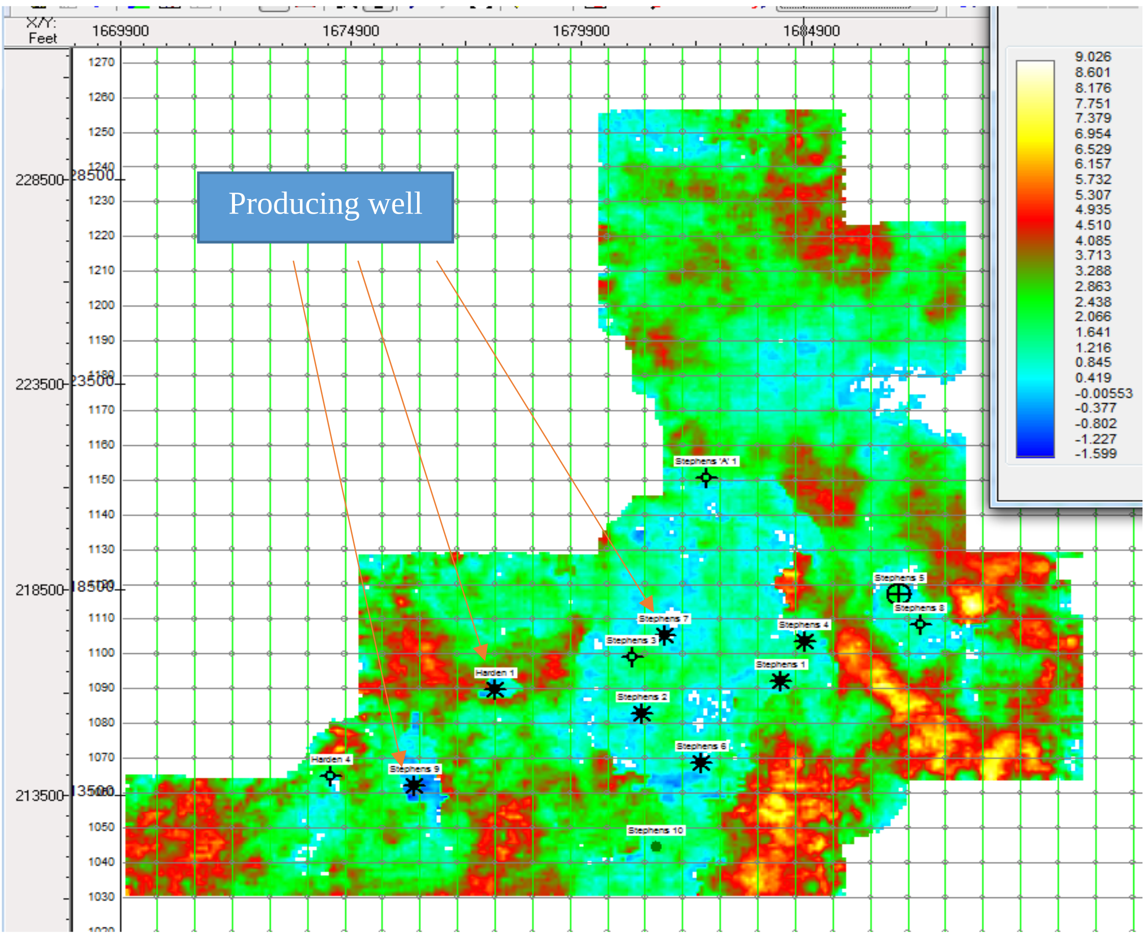

Figure 5.16 Amplitude map of the Viola top showing producing wells linked to lower amplitudes. A few of the producing wells are highlighted with the orange arrows pointing towards them. Figure form Vohs (2016).

Chapter 6 - Conclusion

This study finds that attenuation is an important phenomenon in the case of propagation of ultrasonic waves through carbonate rock and can be a useful phenomenon to be considered during hydrocarbon exploration. Oil bearing rocks are more likely to show more attenuation of the wave signal compared to water or brine bearing rocks or even dry rocks. Future research should consider examining the effects of attenuation in greater detail. Impedance and velocity also seem to be reliable in distinguishing between oil-bearing rocks and non-oil-bearing rocks. Lower impedance (lower velocity values of wave signal and lower density of fluid present) strongly indicate the presence of hydrocarbons in the Viola.

The main findings of this study, namely amplitude sensitivity to pore-fluid composition, and the subtle velocity dependence on pore-fluid composition, emphasizes the significant potential of utilizing amplitude “low” anomalies in development decisions of fields targeting the Viola. Shadow zones created by differential attenuation effects are a dependable hydrocarbon indicator; higher attenuation combined velocity lag correlates with the presence of hydrocarbon pore fluid. Even though velocity differences as a result of different fluid-saturation types are subtle, the confluence of higher porosity due to dolomitization, and lower effective stresses, cause the velocity variation observed in prolific reservoir facies to be pronounced. This is particularly apparent in the form of lower seismic amplitudes areas on amplitude horizon maps.

References

Adkison, W.L., 1972, Stratigraphy and structure of Middle and Upper Ordovician rocks in the Sedgwick basin and adjacent areas, south-central Kansas. U.S. Geological Survey Professional Paper 702.

Ahr, W.M., 2008, A new genetic classification of carbonate porosity and its application to reservoir characterization: American Association of Petroleum Geology Annual convention, San Antonio, TX, Abstracts, Apr. 20–23, p. 20–23: http://www.searchanddiscovery.com/documents/2008/08177ahr/ahr-40308.pdf

Bornemann, E., Doveton, J. H., and St. Clair, P. N., 1982, Lithofacies analysis of the Viola Limestone in South-central Kansas, Kansas Geological Survey, Petrophysical Series 3, http://www.kgs.ku.edu/Publications/Bulletins/PS3/index.html

Besheli, S.A., Hendi, S.S., Vali, J., 1998, Reservoir characterization by seismic attributes with Vp & Vs measurement of core samples (a “rock physics” study): Geophysics Department, RIPI-NIOC.

Blakey, R., 2016, Paleogeography Maps- Teaching Material Images*:* Professor Emeritus, Northern Arizona University, NAU.edu.

Choquette, P.W., and Pray, L.C., 1970, Geological nomenclature and classification of porosity in sedimentary carbonates: American Association of Petroleum Geologists Bulletin, v. 54, p. 207-250

Cimino, V., 2020, A rock physics modeling approach in analysis and integration of well logs and ultrasonic velocities for characterizing the reservoir facies of the Viola Limestone in southwestern Kansas

Cole, V, 1975, Subsurface Ordovician-Cambrian Rocks in Kansas, Kansas Geological Survey, subsurface geology series 2, KGS online, http://www.kgs.ku.edu/Publications/Bulletins/Sub2/index.html (accessed December 2020)

Grochau, M., & Gurevich, B., 2009, Testing Gassmann fluid substitution: sonic logs versus ultrasonic core measurements. Geophysical Prospecting, v. 57(1), 75-79, doi: 10.1111/j.1365-2478.2008.00726.x

Hagood, W. K., 2019, Detailed core and log analysis of a producing Viola dolomite well in Comanche county [Master’s Thesis]: Kansas State University.

Hagood, W. K., Cimino, V., Totten, M., & Raef A., 2018, Analysis and integration of well logs and ultrasonic velocities of productive facies in the upper Viola formation in south-west Kansas, AAPG ACE conference poster 2018.

Henry, M.E., & Hester, T.C., 1995, Viola Oil and Gas—Summary, KGS Digital Petroleum Atlas: from U.S Geological Survey 1995 National Assessment of United States Oil and Gas Resources, CD-ROM, Digital Data Series DDS-30, Release 2, http://www.kgs.ku.edu/DPA/frontEnd/Anadarko/Viola/provSum.html (accessed October 2020).

IHS Global Inc., 2012, Rock Solid Attributes, Version 8.7.

Isham, R., 2012, Integration of in situ and laboratory velocity measurements analysis and calibration for rock formation characterization [Master's Thesis]: Kansas State University.

Jensik, C., 2013, Geologic controls on reservoir quality of the Viola limestone in soldier field, Jackson County, Kansas [Master's Thesis]: Kansas State University.

Kansas Geological Survey (KGS), 2020, Comanche County -- Oil and Gas Production, http://www.kgs.ku.edu/PRS/County/abc/comanche.html (accessed October 2020).

Kansas Geological Survey (KGS), 2019, Oil and Gas Wells, Specific Well, 15-033-21305, https://chasm.kgs.ku.edu/ords/qualified.well_page.DisplayWell?f_kid=1024491665 (accessed February 2020)

Linares, A., 2016, Petrographic Analysis and diagenetic history of the Viola limestone at Stephen's ranch, in the Morrison Northeast field of Clark County, Kansas [Master's Thesis]: Kansas State University

Lueck, A., 2017, Characterizing two carbonate formations for CO_2-EOR and carbon geosequestration applicability of existing rock physics models and implications for feasibility of a time lapse monitoring program in the Wellington Oil Field, Sumner County, Kansas [Master's Thesis]: Kansas State University.

Madonna, C., Almqvist, B. S. G., Saenger, E. H., 2012, Digital rock physics: numerical prediction of pressure-dependent ultrasonic velocities using micro-CT imaging, Geophysical Journal International, v. 189, Issue 3, p. 1475–1482, https://doi.org/10.1111/j.1365-246X.2012.05437.x

Merriam, D.F., 1963, KGS--Geologic History of Kansas—Tectonic Framework: Kansas Geological Survey Bulletin 162, p. 317.

Misaghi, A., Negahban, S., Landro, M., Javaherian, A., 2010, A Comparison of Rock Physics Models for Fluid Substitution in Carbonate Rocks, Exploration Geophysics, 10.1071/EG09035, v. 41, p. 146 – 154.

Mukerji, T., Avseth, P., Mavko, G., Takahashi, I., & Ezequiel F. González., 2001, Statistical rock physics: Combining rock physics, information theory, and geostatistics to reduce uncertainty in seismic reservoir characterization, The Leading Edge, v. 20, issue 3, p. 313-319. doi:10.1190/1.1438938

Raef, A. E., Totten, M. W., Linares, A., & Kamari, A., 2019, Lithofacies control on reservoir quality of the viola limestone in southwest Kansas and unsupervised machine learning approach of seismic attributes facies-classification, Pure and Applied Geophysics, doi:10.1007/s00024-019-02205-4

Raef, A., Totten, M., Vohs, A., & Linares, A., 2017, 3D Seismic Reflection Amplitude and Instantaneous Frequency Attributes in Mapping Thin Hydrocarbon Reservoir Lithofacies: Morrison NE Field and Morrison Field, Clark County, KS. Pure and Applied Geophysics, 174(12), 4379-4394.

Reservoir Characterization, n.d., in Schlumberger oilfield glossary online, https://www.glossary.oilfield.slb.com/en/Terms/r/reservoir_characterization.aspx (accessed December 2020).

Richardson, L. J., 2013, The Herd Viola Trend, Comanche County, Kansas: AAPGG Mid-Continent Section Meeting 20220th ser., p. 1 – 32

Sayers, C., & Chopra, S., 2009, Introduction to this special section - rock physics, The Leading Edge, v. 28, Issue 1, https://doi.org/10.1190/1.3064140

Silvia, M. T., & Robinson, E. A., 1979, Chapter 1- Geophysical modeling, *in* Developments in Petroleum Science, Elsevier, v. 10(C), p. 21–45. https://doi.org/10.1016/S0376-7361(08)70134-1

Simm, R., & Bacon M., 2014, Seismic Amplitude: An Interpreter's Handbook. Cambridge University Press, Cambridge., p. 7-10, p. 10-19, p.158-162.

Smith, T., Sondergeld, C. H., Rai, C. S., 2003, Gassmann fluid substitutions: A tutorial, Geophysics, v. 68 (2), p. 430-440, doi:10.1190/1.1567211

Sonic log, n.d., in Schlumberger oilfield glossary online, https://www.glossary.oilfield.slb.com/Terms/s/sonic_log.aspx (accessed September 2020).

Toksöz M. N., Johnston D. H., & Timur A., 1979, Attenuation of seismic waves in dry and saturated rocks; I, Laboratory measurements, Geophysics, v. 44 (4), p. 681-690, doi: 10.1190/1.1440969.

Vernengo, L., Trinchero, E., Torrejon, M. G., & Rovira I., 2017, Attributes at your fingertips, AAPG Explorer, November 2017, https://explorer.aapg.org/story/articleid/42728

Vohs, A. B., 2016, 3D Seismic Attributes Analysis in Reservoir Characterization: The Morrison

NE Field & Morrison Field, Clark County, Kansas [Master's Thesis]: Kansas State University.

Wang, Z, & Nur, A., 1992, Elastic wave velocities in porous media: A theoretical recipe, in seismic and acoustic velocities in reservoir rocks, v. 2, SEG Geophysics reprint series no. 10.

Wang, Z.Z., 2001, Fundamentals of seismic rock physics, Geophysics, v. 66, issue 2, p. 398 – 412.

Wang, Z., Wang, H., & Cates, M.E., 2001, Effective elastic properties of solid clays, Geophysics, v. 66, p. 428 – 440.

Witzke, B.J., 1980, Middle and Upper Ordovician paleogeography of the region bordering the Transcontinental arch; *in*, Paleozoic paleogeography of west-central United States, T.D. Fouch and E. R. Magathan, eds.: Society of. Economic Paleontologists and Mineralogists, Rocky Mountain Paleogeography Symposium 1, p. 1-18.

Xu, S., & Payne, M., 2009, Modeling elastic properties in carbonate rocks, The Leading Edge, v. 28. issue 1, p. 66-74, doi: 10.1190/1.3064148.

Zeller, D. E., ed., 1968, The stratigraphic succession in Kansas: Kansas Geological Survey, Bulletin 189, p. 81

Appendix A - Preliminary data from the Viola formation cores

Table 6.1 Preliminary data taken from the Viola formation cores which were inputted into the Ultrasonic software to calculate P and S wave velocity.

Sample depth	Dry Mass (g)	Height (cm)	Volume (ml)
5808	1704.9	12.4	650
5809	1263.9	10.9	490
5816	1316	20.7	-
5819	691.7	16.8	655.3
5820	2082.2	19.4	940.8
5821	1096.8	9	500
5824	1827.2	11.5	-
5825	1582	11.6	-
5826	-	15.2	-
5827	-	15.7	-
5829	1632	11.5	620
5832	1477.4	11.2	560
5838	2089.5	14.1	800
5839	1831.3	13.5	690
5842	1515.4	10.7	600
5846	1793.9	13.8	740
5848	1249.4	10.2	520
5857	1598.6	12.5	650
5858	1962.2	15.7	640
5859	1086.5	8	785.8
5862	1950.1	13.8	760
5865	1859.3	15.3	750
5866	1377.3	10.6	550

Appendix B - Description of Fluid Replacement Experiment Process

Instruments and Items used

1. Vacuum Pump
2. Thin flexible clear connector pipe
3. Desiccator
4. Scale balance
5. Honey, Neogen mineral oil, Morton All-Natural Canning, and Pickling salt
6. Saran wrap

Setting up the desiccator

A glass desiccator was used during this experiment. To prepare the desiccator for the experiment, it was connected to the vacuum pump using a thin flexible clear connector pipe. Before the desiccator was used for the experiment, the porcelain plate which came with it was removed to carry out the experiment.

Setting up the vacuum pump

A vacuum was used during the course of the experiment. The oil in the vacuum was checked to ensure that it remains free of water or any other contaminant. The oil had to be changed because of the air bubbles found in the one originally in the machine. Without changing the contaminated oil, the vacuum exhibits a weird dissonant sound.

Water

Tap water was used to carry out the water saturation experiment.

- Collect tap water in 2 1000ml beakers at room temperature.
- Pour water from beakers into the prepared desiccator.

- Select core sample on which measurement will be carried out.
- Take the initial weight of the core on the scale.
- Place core sample on which experiment is going to be run inside the desiccator either longitudinally or laterally. For a longer sample, place laterally for the water to fully cover the sample. Just as long as the sample is fully submerged in water, the experiment is ready to be run. If the sample is not fully submerged in water, then more tap water can be added to the desiccator to cover the sample.
- Plug in the vacuum pump, make sure the connector pipe is properly connected between the vacuum pump and the desiccator (Fig. 1), then turn the vacuum pump on and run it for a while until most of the air bubbles within the carbonate sample is gone.
- At this point, quickly remove the rock and place it on the scale to take the final reading. If a plastic shrinkable jacket or plastic wrap is available, this can be placed around the sample and vacuum sealed. This process was tested on a few samples, but there wasn't any significant change between using a plastic wrap and just carrying the sample about.
- Once the weight reading is taken, the sample can then be placed between the cores on the hydraulic press for the ultrasonic velocity experiment.

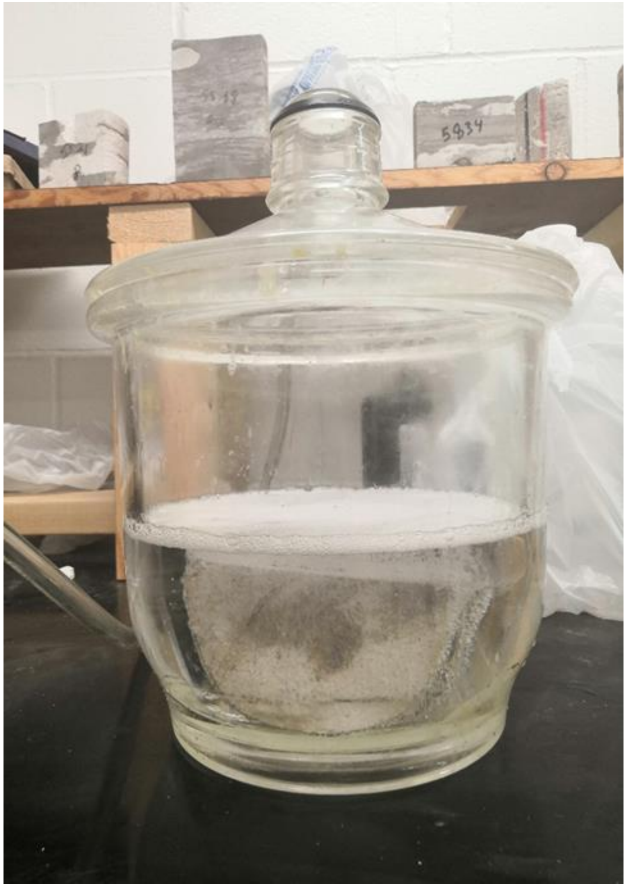

Figure 6.1 Beginning of saturating fluid with water, with most of the air bubbles being ejected from the rock and water filling the empty pores.

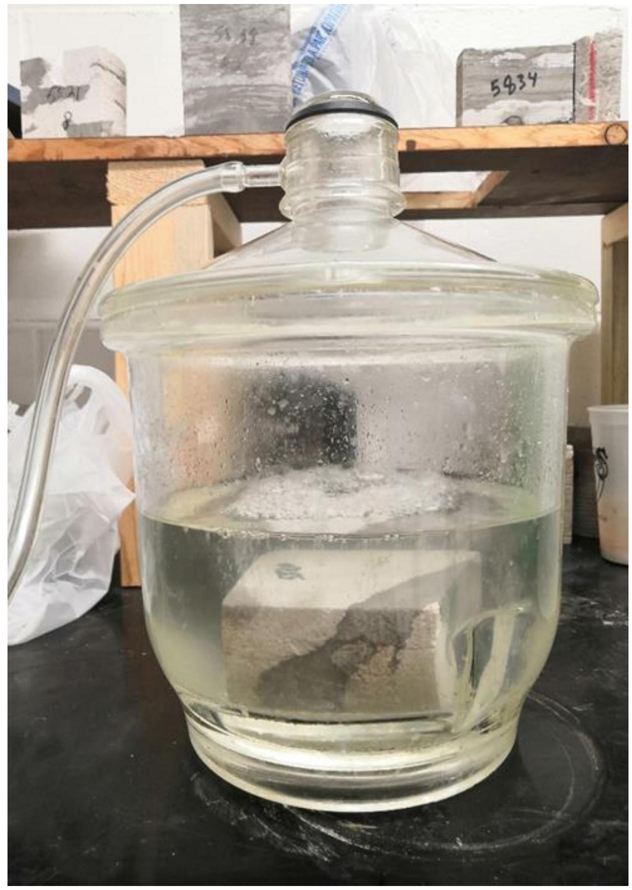

Figure 6.2 Midpoint in saturating rock with water. Most of the air bubbles have been removed, but not all of it.

Brine

- To create the brine solution, salt mixed with tap water was used for the experiment.
- We created our brine solution based on data of the brine found in the Comanche County Viola formation. The composition of the Viola formation brine is:
    - Calcium, Ca = 8910mg/l or 8.9g/l
    - Magnesium, Mg = 2260mg/l or 2.260g/l
    - Chloride, Cl = 88900mg/l or 88.9g/l

- Bicarbonate, HCO_3^- = 504mg/l = 0.5g/l
- Sulfate, SO_4^{2-} = 20mg/l or 0.02g/l

- Our prepared brine mix consisted of the basic and commonly found materials, bicarbonate and chloride in the proportion of the original formation. 88.9g/l of chloride was equivalent to 266.7g of Morton All-Natural Canning & Pickling Sal, which contains 590mg of sodium to 1.5g of salt. With sodium having a one-to-one ratio with Cl, the adequate amount of salt (266.7g was mixed with 1L of tap water and the brine solution was made.
- 2L of the brine solution is created and then poured into the desiccator glass container.
- The initial weight of the core sample to be measured is taken and the core is placed in the desiccator. Once the vacuum pump is run and most of the air bubbles are gone from the rock and replaced with oil, the sample is removed, and the final weight is taken before carrying out the ultrasonic velocity experiment.

Oil

- Neogen light mineral oil was used for this experiment.
- Mineral oil was used instead of crude oil taken directly from the Viola in order to preserve the sample for further testing. Using crude oil would have caused staining of the Viola core and would have been harder to extract.
- 2L of the mineral oil is measured out using the beakers and then poured into the desiccator glass container.
- The initial weight of the core sample to be measured is taken and the core is placed in the desiccator. Once the vacuum pump is run and most of the air bubbles are gone from the

rock and replaced with oil, the sample is removed, and the final weight is taken before carrying out the ultrasonic velocity experiment.

Appendix C - P Wave and S Wave Graphs Generated from Ultrasonic Velocity Testing on Viola Cores

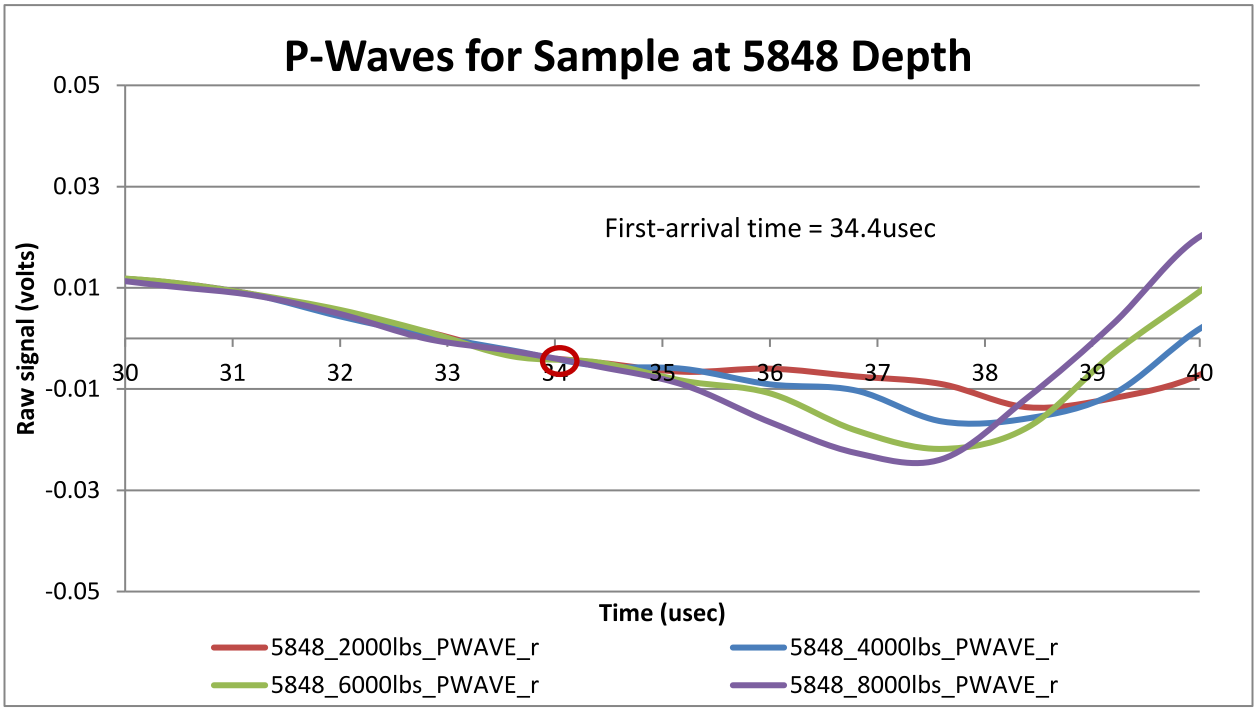

Figure 6.3 Closer look at a P wave graph showing amplitude versus time for different compressive stresses for sample taken at depth 5839ft. Dry rock. Red circle represents first arrival time pick. First arrival time = 34usec. It is easier to see where the first-arrival point of the wave signal begins.

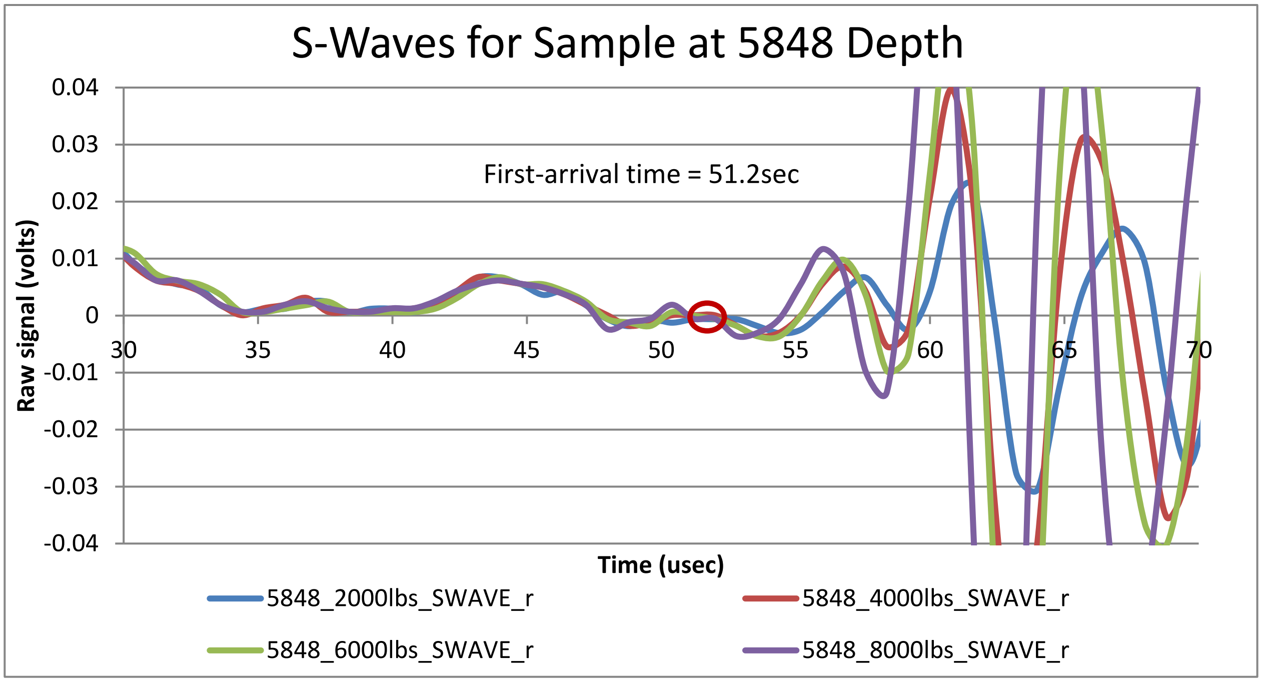

Figure 6.5 Closer look at S wave graph showing amplitude versus time for different compressive stresses for sample taken at depth 5848ft. Dry rock. Red circle represents first arrival time pick. First-arrival time = 51.2usec.

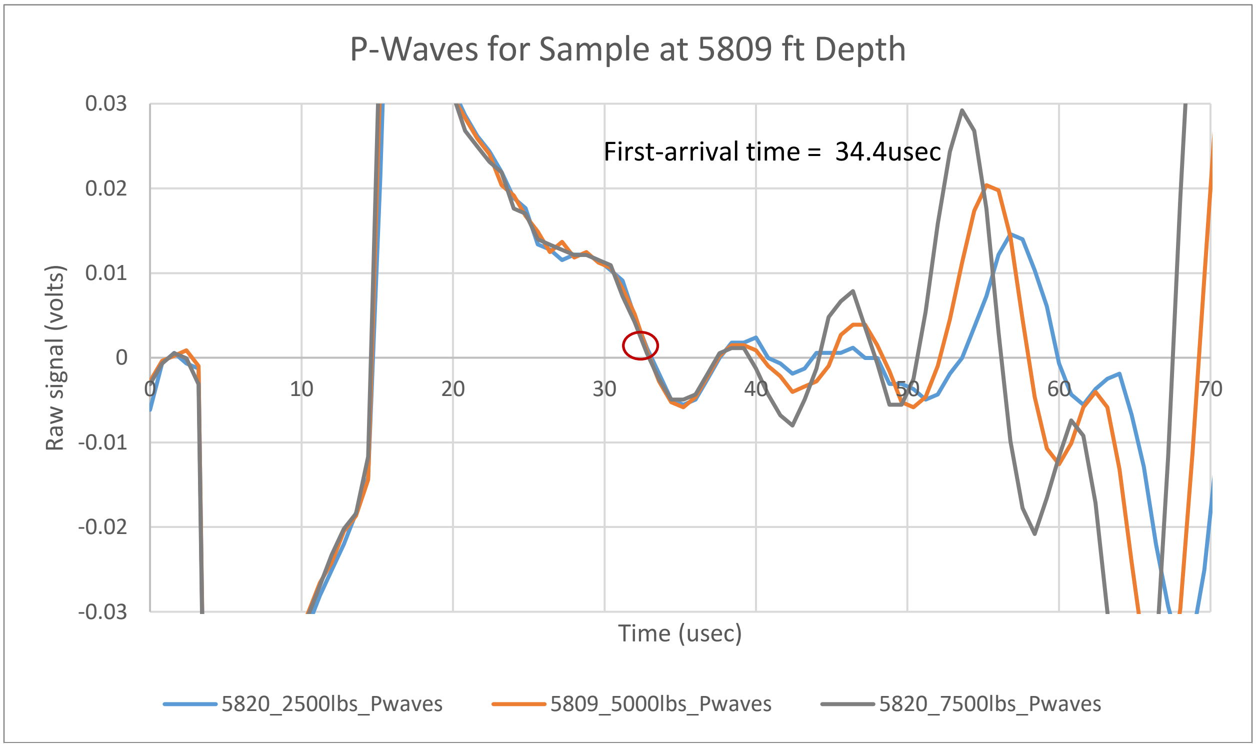

Figure 6.4 P wave graph showing amplitude versus time for different compressive stresses for sample taken at depth 5809ft. Dry rock. Red circle represents first arrival time pick. First-arrival time = 34.4usec.

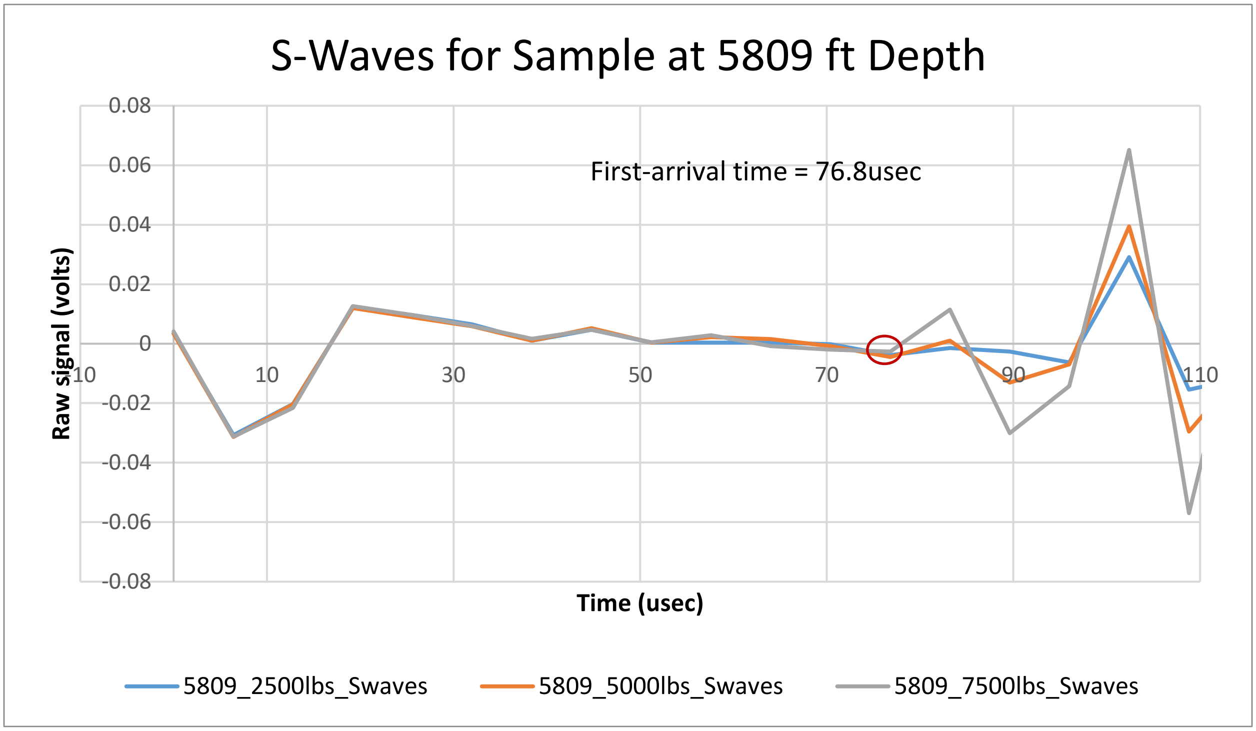

Figure 6.6 S wave graph showing amplitude versus time for different compressive stresses for sample taken at depth 5809ft. Dry rock. Red circle represents first arrival time pick. First-arrival time = 76.8usec